REPORT DOCUMENTATION PAGE

Form Approved OMB NO. 0704-0188

1. REPORT DATE (DD-MM-YYYY)
25-04-2019

2. REPORT TYPE
Final Report

3. DATES COVERED (From - To)
13-Sep-2010 - 12-Sep-2015

4. TITLE AND SUBTITLE
Interim Report: Advanced Optical fibers for High Power Fiber Lasers

5a. CONTRACT NUMBER
W911NF-10-1-0423

5b. GRANT NUMBER

5c. PROGRAM ELEMENT NUMBER

5d. PROJECT NUMBER

5e. TASK NUMBER

5f. WORK UNIT NUMBER

6. AUTHORS
Liang Dong, John Ballato, Bryce Samson, Joshua E. Rothenberg

7. PERFORMING ORGANIZATION NAMES AND ADDRESSES
Clemson University Research Foundation
Office of Sponsored Programs
Clemson University Research Foundation
Clemson, SC 29631 -0946

8. PERFORMING ORGANIZATION REPORT NUMBER

9. SPONSORING/MONITORING AGENCY NAME(S) AND ADDRESS (ES)
U.S. Army Research Office
P.O. Box 12211
Research Triangle Park, NC 27709-2211

10. SPONSOR/MONITOR'S ACRONYM(S)
ARO

11. SPONSOR/MONITOR'S REPORT NUMBER(S)
58391-EL-HEL.46

12. DISTRIBUTION AVAILIBILITY STATEMENT
Approved for public release; distribution is unlimited.

13. SUPPLEMENTARY NOTES
The views, opinions and/or findings contained in this report are those of the author(s) and should not contrued as an official Department of the Army position, policy or decision, unless so designated by other documentation.

14. ABSTRACT
The project is to develop large mode area optical fibers based on all-solid photonic bandgap designs (Thrust I) and a SBS suppression technique based on hydrogen loading (Thrust II), both for power scaling of fiber lasers to well beyond kW. Major objectives of this period are to improve refractive index control of highly-uniform and silica-index-matched ytterbium-doped active core glass and to characterize active 50µm all-solid photonic bandgap fibers in Thrust I, and to demonstrate SBS suppression in amplifiers using the hydrogen loading and UV exposure technique in Thrust II. In Thrust I. Major achievements are demonstrations of 50µm core active fibers with robust

15. SUBJECT TERMS
Specialty optical fibers, optical fiber lasers

16. SECURITY CLASSIFICATION OF: a. REPORT	b. ABSTRACT	c. THIS PAGE	17. LIMITATION OF ABSTRACT	15. NUMBER OF PAGES	19a. NAME OF RESPONSIBLE PERSON
UU	UU	UU	UU		Liang Dong
					19b. TELEPHONE NUMBER
					864-656-5915

RPPR Final Report
as of 25-Apr-2019

Agency Code:

Proposal Number: 58391ELHEL

Agreement Number: W911NF-10-1-0423

INVESTIGATOR(S):

Name: Liang Dong
Email: dong4@clemson.edu
Phone Number: 8646565915
Principal: Y

Organization: **Clemson University Research Foundation**
Address: Office of Sponsored Programs, Clemson, SC 296310946
Country: USA
DUNS Number: 159952407
EIN: 84600545

Report Date: 12-Dec-2014
Date Received: 25-Apr-2019
Final Report for Period Beginning 13-Sep-2010 and Ending 12-Sep-2015
Title: Advanced Optical fibers for High Power Fiber Lasers
Begin Performance Period: 13-Sep-2010
End Performance Period: 12-Dec-2018
Report Term: 0-Other
Submitted By: Liang Dong
Email: dong4@clemson.edu
Phone: (864) 656-5915
Distribution Statement: 1-Approved for public release; distribution is unlimited.

STEM Degrees: 5
STEM Participants: 8

Major Goals: The primary thrust of this research is to develop mode area scaling solutions with all-solid photonic bandgap fibers by exploiting strong differential mode loss from photonic bandgap guidance. More specifically, we will demonstrate ytterbium-doped single-mode all-solid photonic bandgap fibers with core diameters of 50?m and coil diameter of ~50cm and investigate the feasibility of fabricating an all-solid photonic bandgap fiber with a core diameter of 100?m.
The second thrust of this research is to demonstrate over >20dB SBS suppression by longitudinally varying acoustic velocity profile. More specifically, we will investigate the feasibility of diffusing gases such as hydrogen or deuterium into fabricated optical fibers and then locking the gas molecules to the glass lattice by UV exposure. The UV exposure is varied longitudinally along the fiber to create the desired acoustic velocity profile.

Accomplishments: i. Discovery of theoretical evidence for strong higher order mode filtering property of all solid photonic bandgap fibers in large core designs. This class of designs has been found to have the highest differential mode losses, enabling large core optical fibers with potentially very high quality single mode operation. This technique can provide the key for power scaling of single mode fiber lasers.
ii. First experimental demonstration of all solid photonic bandgap fibers operating in robust single mode in 50?m cores.
iii. First demonstration of significant SBS suppression using H2/UV treatment.
iv. Demonstration of record 13dB SBS suppression capability using fiber design/treatments.
v. Establish analytical mode for mode instability
vi. Record demonstration of 50μm-core all-solid photonic bandgap fiber lasers and amplifiers with robust single mode and high efficiency
vii. Record multimode 600W from an all-solid photonic bandgap fiber
viii. Record demonstration of passive 100μm-core all-solid photonic bandgap fiber with robust single-mode operation using innovative multiple resonance design
ix. Demonstrate record single-mode/single-frequency power of >400W in all-solid photonic bandgap fibers
x. Demonstrate active PM all-solid photonic bandgap fibers operating in robust single mode in record 50μm cores.
xi. First measurement of stimulated thermal Rayleigh scattering gain
xii. Records ~1kW single-mode output power from 50?m-core fiber.
xiii. Analysis of thermal lensing in optical fibers
xiv. Fabrication of 25/400 all solid photonic bandgap fiber with potential TMI threshold of ~4kW

Training Opportunities: Nothing to Report

RPPR Final Report
as of 25-Apr-2019

Results Dissemination: Nothing to Report

Honors and Awards: 1. Featured in “Clemson University researcher making lasers more powerful” GSA Business, 2015
2. Liang Dong, OSA fellow, 2014
3. Christopher Dunn, DEPS scholarship in 2014 and 2015
4. Guancheng Gu, OSA Incubic Milton travel grant in 2014
5. Guancheng Gu, Clemson Professional Enrichment Grant Application (PEGAS) grant in 2014
6. SPIE fellow, 2017
7. IEEE senior member 2017
8. University Research, Scholarship, and Artistic Achievement award, May 2018
9. Dean’s Distinguished Professor Award in the Department of Electrical and Computer Engineering, 4/16/2019 to 4/15/2022

Protocol Activity Status:

Technology Transfer: Nothing to Report

PARTICIPANTS:

Participant Type: Faculty
Participant: Liang Dong
Person Months Worked: **Funding Support:**
Project Contribution:
International Collaboration:
International Travel:
National Academy Member:
Other Collaborators:

Participant Type: Graduate Student (research assistant)
Participant: Guancheng Gu
Person Months Worked: **Funding Support:**
Project Contribution:
International Collaboration:
International Travel:
National Academy Member:
Other Collaborators:

Participant Type: Graduate Student (research assistant)
Participant: Thomas Hawkins
Person Months Worked: **Funding Support:**
Project Contribution:
International Collaboration:
International Travel:
National Academy Member:
Other Collaborators:

Participant Type: Graduate Student (research assistant)
Participant: Christopher Dunn
Person Months Worked: **Funding Support:**
Project Contribution:
International Collaboration:
International Travel:
National Academy Member:
Other Collaborators:

Participant Type: Postdoctoral (scholar, fellow or other postdoctoral position)
Participant: Fanting Kong
Person Months Worked: **Funding Support:**
Project Contribution:
International Collaboration:
International Travel:
National Academy Member:
Other Collaborators:

Participant Type: Postdoctoral (scholar, fellow or other postdoctoral position)
Participant: Monica T. Kalichevsky-Dong
Person Months Worked: **Funding Support:**
Project Contribution:
International Collaboration:
International Travel:
National Academy Member:
Other Collaborators:

Participant Type: Graduate Student (research assistant)
Participant: Turghun Matniyaz
Person Months Worked: 12.00 **Funding Support:**
Project Contribution:
International Collaboration:
International Travel:
National Academy Member: N
Other Collaborators:

ARTICLES:

Publication Type: Journal Article Peer Reviewed: N **Publication Status:** 1-Published
Journal: IEEE Journal of Lightwave Technology
Publication Identifier Type: Publication Identifier:
Volume: 0 Issue: 0 First Page #: 0
Date Submitted: Date Published:
Publication Location:
Article Title: Formulation of a complex mode solver for arbitrary circular acoustic waveguides
Authors:
Keywords: Optical fiber amplifiers, optical fiber lasers, Brillouin scattering, optical fiber
Abstract: There has been a resurgence of interests in stimulated Brillouin scattering (SBS) in optical fibers recently. This is largely due to the need to overcome SBS for power scaling of single frequency fiber lasers. Complex acoustic waveguide designs have been proposed for SBS suppression in optical fibers. There is, therefore, a strong need for finding acoustic modes in complex acoustic waveguides. Furthermore, leaky acoustic modes are often ignored in recent works on SBS in optical fiber. Many leaky acoustic modes involved in SBS in optical fibers often have comparable losses to guided acoustic modes. The losses of both guided acoustic modes and many leaky acoustic modes are dominated by the extremely high material loss of acoustic waves in the GHz region in optical fibers. Therefore, it is very important to consider these leaky acoustic modes in SBS in optical fibers, especially for acoustic anti-guide designs used for SBS suppressions, where those leaky acoustic modes are often responsib
Distribution Statement: 1-Approved for public release; distribution is unlimited.
Acknowledged Federal Support:

Publication Type: Journal Article Peer Reviewed: N **Publication Status:** 1-Published
Journal: IEEE Journal of Lightwave Technology
Publication Identifier Type: Publication Identifier:
Volume: 0 Issue: 0 First Page #: 0
Date Submitted: Date Published:
Publication Location:
Article Title: Limits of stimulated Brillouin scattering suppression in optical fibers with transverse acoustic waveguide designs
Authors:
Keywords: Optical fiber amplifiers, optical fiber lasers, Brillouin scattering, optical fiber
Abstract: A major approach investigated recently for stimulated Brillouin scattering (SBS) suppression in fiber amplifiers for high power single frequency fiber lasers is to explore designs of acoustic waveguide in optical fibers. This acoustic waveguide can be implemented to some extent independent of the optical waveguide by using a combination of dopants which modify the host glass by varying levels in acoustic and optical properties. Although this approach provides some SBS suppressions, the new analysis described in this work, considering the often omitted leaky acoustic modes, demonstrates its limit. A complex acoustic mode solver, reported in details elsewhere, was recently developed to find solutions for simultaneous longitudinal and shear acoustic wave equations which satisfy rigorous boundary conditions in an arbitrary circular acoustic waveguide. By taking advantage of this new tool, it is possible to find the leaky acoustic modes for acoustic waveguides designed for SBS suppressions.
Distribution Statement: 1-Approved for public release; distribution is unlimited.
Acknowledged Federal Support:

Publication Type: Journal Article Peer Reviewed: N **Publication Status:** 1-Published
Journal: Optics Express
Publication Identifier Type: Publication Identifier:
Volume: 0 Issue: 0 First Page #: 0
Date Submitted: Date Published:
Publication Location:
Article Title: A vector boundary matching technique for efficient and accurate determination of photonic bandgaps in photonic bandgap fibers
Authors:
Keywords: Fiber optics and optical communications; Fiber design and fabrication; Photonic crystal fibers.
Abstract: A vector boundary matching technique has been proposed and demonstrated for finding photonic bandgaps in photonic bandgap fibers with circular nodes. Much improved accuracy, comparing to earlier works, comes mostly from using more accurate cell boundaries for each mode at the upper and lower edges of the band of modes. It is recognized that the unit cell boundary used for finding each mode at band edges of the 2D cladding lattice is not only dependent on whether it is a mode at upper or lower band edge, but also on the azimuthal mode number and lattice arrangements. Unit cell boundaries for these modes are determined by mode symmetries which are governed by the azimuthal mode number as well as lattice arrangement due to mostly geometrical constrains. Unit cell boundaries are determined for modes at both upper and lower edges of bands of modes dominated by m=1 and m=2 terms in their longitudinal field Fourier-Bessel expansion series, equivalent to LP0s and LP1s modes in the approximate
Distribution Statement: 1-Approved for public release; distribution is unlimited.
Acknowledged Federal Support:

Publication Type: Journal Article Peer Reviewed: Y **Publication Status:** 1-Published
Journal: Optics Express
Publication Identifier Type: Publication Identifier:
Volume: 19 Issue: 13 First Page #: 12582
Date Submitted: Date Published:
Publication Location:
Article Title: A vector boundary matching technique for efficient and accurate determination of photonic bandgaps in photonic bandgap fibers
Authors:
Keywords: : (060.0060) Fiber optics and optical communications; (060.2280) Fiber design and fabrication; (060.5295) Photonic crystal fibers.
Abstract: A vector boundary matching technique has been proposed and demonstrated for finding photonic bandgaps in photonic bandgap fibers with circular nodes. Much improved accuracy, comparing to earlier works, comes mostly from using more accurate cell boundaries for each mode at the upper and lower boundaries edges of the band of modes. It is recognized that the unit cell boundary used for finding each mode at band boundaries edges of the 2D cladding lattice is not only dependent on whether it is a mode at upper or lower band boundary modeedge, but also on the azimuthal mode number and lattice arrangements. Unit cell boundariesy forof these modes areis determined by mode symmetriesy which areis governed by the azimuthal mode number as well as lattice arrangement due to mostly geometrical constrains. Unit cell boundaries are determined for modes at both upper and lower boundaries edges of bands of modes dominated by m=1 and m=2 terms in their longitudinal field Fourier-Bessel expansion series,
Distribution Statement: 1-Approved for public release; distribution is unlimited.
Acknowledged Federal Support:

Publication Type: Journal Article Peer Reviewed: Y **Publication Status:** 1-Published
Journal: IEEE Journal of Lightwave Technology
Publication Identifier Type: Publication Identifier:
Volume: 28 Issue: 21 First Page #: 3162
Date Submitted: Date Published:
Publication Location:
Article Title: Formulation of a Complex Mode Solver for Arbitrary Circular Acoustic Waveguides
Authors:
Keywords: Optical fiber amplifiers, optical fiber lasers, Brillouin scattering, optical fiber
Abstract: There has been a resurgence of interests in stimulated Brillouin scattering (SBS) in optical fibers recently. This is largely due to the need to overcome SBS for power scaling of single frequency fiber lasers. Complex acoustic waveguide designs have been proposed for SBS suppression in optical fibers. There is, therefore, a strong need for finding acoustic modes in complex acoustic waveguides. Furthermore, leaky acoustic modes are often ignored in recent works on SBS in optical fiber. Many leaky acoustic modes involved in SBS in optical fibers often have comparable losses to guided acoustic modes. The losses of both guided acoustic modes and many leaky acoustic modes are dominated by the extremely high material loss of acoustic waves in the GHz region in optical fibers. Therefore, it is very important to consider these leaky acoustic modes in SBS in optical fibers, especially for acoustic anti-guide designs used for SBS suppressions, where those leaky acoustic modes are often responsib
Distribution Statement: 1-Approved for public release; distribution is unlimited.
Acknowledged Federal Support:

Publication Type: Journal Article Peer Reviewed: Y **Publication Status:** 1-Published
Journal: IEEE Journal of Lightwave Technology
Publication Identifier Type: Publication Identifier:
Volume: 28 Issue: 21 First Page #: 3156
Date Submitted: Date Published:
Publication Location:
Article Title: Limits of Stimulated Brillouin Scattering Suppressionin Optical Fibers With Transverse AcousticWaveguide Designs
Authors:
Keywords: Brillouin scattering, optical fiber amplifiers, opticalfiber lasers, optical fiber.
Abstract: A major approach investigated recently for stimulated Brillouin scattering (SBS) suppression in fiber amplifiers for high power single frequency fiber lasers is to explore designs of acoustic waveguide in optical fibers. This acoustic waveguide can be implemented to some extent independent of the optical waveguide by using a combination of dopants which modify the host glass by varying levels in acoustic and optical properties. Although this approach provides some SBS suppressions, the new analysis described in this work, considering the often omitted leaky acoustic modes, demonstrates its limit. A complex acoustic mode solver, reported in details elsewhere, was recently developed to find solutions for simultaneous longitudinal and shear acoustic wave equations which satisfy rigorous boundary conditions in an arbitrary circular acoustic waveguide. By taking advantage of this new tool, it is possible to find the leaky acoustic modes for acoustic waveguides designed for SBS suppressions.
Distribution Statement: 1-Approved for public release; distribution is unlimited.
Acknowledged Federal Support:

Publication Type: Journal Article Peer Reviewed: N **Publication Status:** 1-Published
Journal: Optics Express
Publication Identifier Type: Publication Identifier:
Volume: 0 Issue: 0 First Page #: 0
Date Submitted: Date Published:
Publication Location:
Article Title: Mode Area Scaling with All-solid Photonic Bandgap Fibers
Authors:
Keywords: Optical fibers, fiber lasers
Abstract: There are still very strong interests for power scaling in high power fiber lasers for a wide range of applications in medical, industry, defense and science. In many of these lasers, fiber nonlinearities are the main limits to further scaling. Although numerous specific techniques have studied for the suppression of a wide range of nonlinearities, the fundamental solution is to scale mode areas in fibers while maintaining sufficient single mode operation. Here the key problem is that more modes are supported once physical dimensions of waveguides are increased. The key to solve this problem is to look for fiber designs with significant higher order mode suppression. In conventional waveguides, all modes are increasingly guided in the center of the waveguides when waveguide dimensions are increased. It is hard to couple a mode out in order to suppress its propagation, which severely limits their scalability. In an all-solid photonic bandgap fiber, modes are guided due to anti-resonance
Distribution Statement: 1-Approved for public release; distribution is unlimited.
Acknowledged Federal Support:

Publication Type: Journal Article Peer Reviewed: N **Publication Status:** 1-Published
Journal: IEEE Photonics Technology Letters
Publication Identifier Type: Publication Identifier:
Volume: 0 Issue: 0 First Page #: 0
Date Submitted: Date Published:
Publication Location:
Article Title: Observation of Delocalization of Higher Order Modes in All-solid Photonic Bandgap Fiber
Authors:
Keywords: Optical fibers, fiber lasers
Abstract: The needs for mode area scaling of optical fibers has led to the development of large core all-solid photonic bandgap fibers with significant built-in higher order mode suppressions. Higher order modes in these fibers are no longer localized in the core. Using S2 measurements, we have observed, for the first time, that index of each higher order mode covers a continuous band, much like the bands of non-localized modes in the cladding photonics lattice. This observation will help better understanding of photonic bnadgap fibers and has interesting implications in designs of those fibers for single-mode operations.
Distribution Statement: 1-Approved for public release; distribution is unlimited.
Acknowledged Federal Support:

Publication Type: Journal Article Peer Reviewed: N **Publication Status:** 1-Published
Journal: Nature Photonics
Publication Identifier Type: Publication Identifier:
Volume: 0 Issue: 0 First Page #: 0
Date Submitted: Date Published:
Publication Location:
Article Title: Precise and Significant Tailoring of Acoustic Velocity in Optical Fibers by Hydrogenation and UV Exposure
Authors:
Keywords: nonlinear effect, optical fibers, stimulated brillouin scattering
Abstract: Tailoring of acoustic properties in solids has many potential applications in both acoustics, i.e. acoustic gratings and waveguides, and photon-phonon interactions, i.e. stimulated Brillouin scattering (SBS). One immediate application is in the area of SBS suppression in optical fibers. Further power scaling of single-frequency fiber lasers is of significant interests for many scientific and defense applications. It is currently limited by SBS. In recent years, a variety of techniques have been investigated for the suppression of SBS in optical fibers. A notable example is to design transverse acoustic velocity of optical fibers in order to minimize optical and acoustic mode overlap. It was pointed out recently that SBS suppression from such transverse acoustic tailoring is limited when considering the existence of acoustic leaky modes. We demonstrate, for the first time, a post-processing technique where hydrogen is diffused in to a fiber core and then locally bonded to core glass by
Distribution Statement: 1-Approved for public release; distribution is unlimited.
Acknowledged Federal Support:

Publication Type: Journal Article Peer Reviewed: N **Publication Status:** 1-Published
Journal: Optics Express
Publication Identifier Type: Publication Identifier:
Volume: 21 Issue: 3 First Page #: 2643
Date Submitted: Date Published:
Publication Location:
Article Title: Stimulated thermal Rayleigh scattering inoptical fibers
Authors:
Keywords: Fiber lasers, stimulated Rayleigh scattering
Abstract: Recently, mode instability was observed in optical fiber lasers at high powers, severely limiting power scaling for single-mode outputs. Some progress has been made towards understanding the underlying physics. A thorough understanding of the effect is critical for continued progress of this very important technology area. Mode instability in optical fibers is, in fact, a manifestation of stimulated thermal Rayleigh scattering. In this work, a quasi-closed-form solution for the nonlinear coupling coefficient is found for stimulated thermal Rayleigh scattering in optical fibers. The results help to significantly improve understanding of mode instability.
Distribution Statement: 1-Approved for public release; distribution is unlimited.
Acknowledged Federal Support:

Publication Type: Journal Article Peer Reviewed: N **Publication Status:** 1-Published
Journal: Optics Express
Publication Identifier Type: Publication Identifier:
Volume: 20 Issue: 24 First Page #: 26363
Date Submitted: Date Published:
Publication Location:
Article Title: Mode area scaling with all-solid photonicbandgap fibers
Authors:
Keywords: Optica fibers, photonic bandgap fibers,fiber lasers
Abstract: There are still very strong interests for power scaling in high power fiber lasers for a wide range of applications in medical, industry, defense and science. In many of these lasers, fiber nonlinearities are the main limits to further scaling. Although numerous specific techniques have studied for the suppression of a wide range of nonlinearities, the fundamental solution is to scale mode areas in fibers while maintaining sufficient single mode operation. Here the key problem is that more modes are supported once physical dimensions of waveguides are increased. The key to solve this problem is to look for fiber designs with significant higher order mode suppression. In conventional waveguides, all modes are increasingly guided in the center of the waveguides when waveguide dimensions are increased. It is hard to couple a mode out in order to suppress its propagation, which severely limits their scalability. In an allsolid photonic bandgap fiber, modes are only guided due to anti-reson
Distribution Statement: 1-Approved for public release; distribution is unlimited.
Acknowledged Federal Support:

Publication Type: Journal Article Peer Reviewed: N **Publication Status:** 1-Published
Journal: Optics Express
Publication Identifier Type: Publication Identifier:
Volume: 20 Issue: 25 First Page #: 27810
Date Submitted: Date Published:
Publication Location:
Article Title: Precise tailoring of acoustic velocity in opticalfibers by hydrogenation and UV exposure
Authors:
Keywords: Stimulated Brillouin scattering,fiber lasers
Abstract: Tailoring of acoustic properties in solids has many potential applications in both acoustics, i.e. acoustic gratings and waveguides, and photon-phonon interactions, i.e. stimulated Brillouin scattering (SBS). One immediate application is in the area of SBS suppression in optical fibers. We demonstrate, for the first time, a post-processing technique where hydrogen is diffused in to a fiber core and then locally and permanently bonded to core glass by a subsequent UV exposure. It is discovered that local acoustic velocity can be altered by as much as ~2% this way, with strong potential for much further improvements with an increased hydrogen pressure. It is also found that the large change in acoustic velocity is primarily due to a reduction in bulk modulus, possibly as a result of network bonds being broken up by the addition of OH bonds. It is possible to use this technique to precisely tailor acoustic velocity along a fiber for more optimized SBS suppression in a fiber amplifier. Cha
Distribution Statement: 1-Approved for public release; distribution is unlimited.
Acknowledged Federal Support:

Publication Type: Journal Article Peer Reviewed: Y **Publication Status:** 1-Published
Journal: Journal of Lightwave Technology
Publication Identifier Type: Publication Identifier:
Volume: 32 Issue: 3 First Page #: 440
Date Submitted: Date Published:
Publication Location:
Article Title: Design Optimization of Large-Mode-Area All-Solid Photonic Bandgap Fibers for High-Power Laser Applications
Authors:
Keywords: specialty optical fibers, photonic bandgap fibers, fiber lasers
Abstract: We optimized the structural parameters of largemode- area all-solid photonic bandgap fibers for high-power laser applications with numerical simulations. We obtained an effective mode area of greater than 1000 ?m2 in bending condition while maintaining single-mode operation and realizing compact packaging for both 7- and 19-cell core fibers.We also found out that a core diameter of larger than 115 ?m could be achieved for the 19-cell core fibers.
Distribution Statement: 1-Approved for public release; distribution is unlimited.
Acknowledged Federal Support:

Publication Type: Journal Article Peer Reviewed: Y **Publication Status:** 1-Published
Journal: Optics Express
Publication Identifier Type: Publication Identifier:
Volume: 22 Issue: 11 First Page #: 13962
Date Submitted: Date Published:
Publication Location:
Article Title: Ytterbium-doped large-mode-area all-solid photonic bandgap fiber lasers
Authors:
Keywords: Lasers, ytterbium; Lasers, fiber; Laser beam characterization
Abstract: Single-mode operation in a large-mode-area fiber laser is highly desired for power scaling. We have, for the first time, demonstrated a 50?m-core-diameter Yb-doped all-solid photonic bandgap fiber laser with a mode area over 4 times that of the previous demonstration. 75W output power has been generated with a diffraction-limited beam and an efficiency of 70% relative to the launched pump power. We have also experimentally confirmed that a robust single-mode regime exists near the high frequency edge of the bandgap. These fibers only guide light within the bandgap over a narrow spectral range, which is essential for lasing far from the gain peak and suppression of stimulated Raman scattering. This work demonstrates the strong potential for mode area scaling of in single-mode all-solid photonic bandgap fibers.
Distribution Statement: 1-Approved for public release; distribution is unlimited.
Acknowledged Federal Support:

BOOKS:

Publication Type: Book Peer Reviewed: Y **Publication Status:** 1-Published
Publication Identifier Type: ISBN Publication Identifier: 1498725546
Book Edition: Volume: Publication Year: 2016 Date Received: 01-Aug-2018
Publication Location: Boca Raton, London, New York
Publisher: CRC Press
Book Title: Fiber Lasers: Basics, Technology and Applications
Authors: 6. Liang Dong and Bryce Samson
Editor:
Acknowledged Federal Support: Y

CONFERENCE PAPERS:

Publication Type: Conference Paper or Presentation **Publication Status:** 1-Published
Conference Name: SPIE Denfense, Sensors and Security
Date Received: 01-Aug-2018 Conference Date: 25-Apr-2012 Date Published: 25-Apr-2018
Conference Location: Baltimore, Maryland
Paper Title: Mode Area Scaling for High Power Fiber Lasers with All Solid Photonic Bandgap Fibers
Authors: Liang Dong
Acknowledged Federal Support: **Y**

Publication Type: Conference Paper or Presentation **Publication Status:** 1-Published
Conference Name: Workshop on Specialty Optical Fibers
Date Received: 01-Aug-2018 Conference Date: 29-Aug-2013 Date Published: 29-Aug-2013
Conference Location: Sigtuna, Sweden
Paper Title: Large-mode-area Fibers Enabled by Significant Differential Mode Losses
Authors: Liang Dong, Fanting Kong, Thomas W. Hawkins, Guancheng Gu, Paul Foy, Kunimasa Saitoh, Kanxian
Acknowledged Federal Support: **Y**

Publication Type: Conference Paper or Presentation **Publication Status:** 1-Published
Conference Name: DEPS Solid State and Diode Laser Review
Date Received: 01-Aug-2018 Conference Date: 25-Jun-2013 Date Published: 25-Jun-2013
Conference Location: Santa Fe
Paper Title: Quasi-analytical Solution for Mode Instability Thresholds
Authors: Liang Dong, Fanting Kong, Thomas W. Hawkins, Guancheng Gu, Paul Foy, Kunimasa Saitoh Kanxian W
Acknowledged Federal Support: **Y**

Publication Type: Conference Paper or Presentation **Publication Status:** 1-Published
Conference Name: Specialty Optical Fiber Conference
Date Received: 01-Aug-2018 Conference Date: 17-Jun-2012 Date Published: 17-Jun-2012
Conference Location: Colorado Springs
Paper Title: Large-core Single-mode Solid Photonic Bandgap Fibers
Authors: Liang Dong, Kunimasa Saitoh, Fanting Kong, Paul Foy, Thomas Hawkins, and Devon Mcclane
Acknowledged Federal Support: **Y**

Publication Type: Conference Paper or Presentation **Publication Status:** 1-Published
Conference Name: Photonics Global Conference
Date Received: 01-Aug-2018 Conference Date: 13-Dec-2012 Date Published: 13-Dec-2012
Conference Location: Singapore
Paper Title: Advanced Optical Fibers and Their Applications in Fiber Lasers
Authors: Liang Dong, Fanting Kong, Thomas Hawkins, Devon Mcclane, Guancheng Gu, Kunimasa Saitoh
Acknowledged Federal Support: **Y**

Publication Type: Conference Paper or Presentation **Publication Status:** 1-Published
Conference Name: PhotonicsWest
Date Received: 01-Aug-2018 Conference Date: 03-Feb-2013 Date Published: 03-Feb-2013
Conference Location: San Francisco
Paper Title: Robust Single-mode All Solid Photonic Bandgap Fibers with Core Diameter of 50?m
Authors: Liang Dong, Kunimasa Saitoh, Fanting Kong, Thomas Hawkins, Devon Mcclane,and Guancheng Gu
Acknowledged Federal Support: **Y**

Publication Type: Conference Paper or Presentation **Publication Status:** 1-Published
Conference Name: PhotonicsWest
Date Received: 01-Aug-2018 Conference Date: 03-Feb-2013 Date Published: 03-Feb-2013
Conference Location: San Francisco
Paper Title: Stimulated Brillouin Scattering Suppression in Optical Fibers by Hydrogen-loading Technique
Authors: Fanting Kong and Liang Dong
Acknowledged Federal Support: **Y**

Publication Type: Conference Paper or Presentation **Publication Status:** 1-Published
Conference Name: SPIE European Security and Defence Conference
Date Received: 01-Aug-2018 Conference Date: 22-Sep-2012 Date Published: 22-Sep-2012
Conference Location: Edinburg
Paper Title: All-Solid Photonic Bandgap Fibers for High Power Lasers
Authors: Liang Dong, Kunimasa Saitoh, Fanting Kong, Paul Foy, Thomas Hawkins, Devon Mcclane, and Guanch
Acknowledged Federal Support: **Y**

Publication Type: Conference Paper or Presentation **Publication Status:** 1-Published
Conference Name: Optical Fiber Communications Conference
Date Received: 01-Aug-2018 Conference Date: 17-Feb-2013 Date Published: 17-Feb-2013
Conference Location: Anaheim
Paper Title: All-solid Photonic Bandgap Fiber with Record Mode Area
Authors: Fanting Kong, Kunimasa Saitoh, Devon Mcclane, Thomas Hawkins, Paul Foy, Guancheng Gu and Lian
Acknowledged Federal Support: **Y**

Publication Type: Conference Paper or Presentation **Publication Status:** 1-Published
Conference Name: CLEO and OECC
Date Received: 01-Aug-2018 Conference Date: 30-Jun-2013 Date Published: 30-Jun-2013
Conference Location: Kyoto, Japan
Paper Title: All-Solid Photonic Bandgap Fibersfor Fiber Laser Applications
Authors: Kunimasa Saitoh, Shota Saitoh, Masahiro Kashiwagi, Shoichiro Matsuo, and Liang Dong
Acknowledged Federal Support: **Y**

Publication Type: Conference Paper or Presentation **Publication Status:** 1-Published
Conference Name: European Conference on Optical Communications
Date Received: 01-Aug-2018 Conference Date: 22-Sep-2013 Date Published: 22-Sep-2013
Conference Location: London
Paper Title: Precise Tailoring of Acoustical Properties of Optical Fibers by Hydrogen-loading Technique
Authors: Liang Dong, Fanting Kong and Thomas Hawkins
Acknowledged Federal Support: **Y**

Publication Type: Conference Paper or Presentation **Publication Status:** 1-Published
Conference Name: SPIE Defence and Secuirity Conference
Date Received: 01-Aug-2018 Conference Date: 23-Apr-2012 Date Published: 23-Apr-2012
Conference Location: Baltimore
Paper Title: Mode Area Scaling for High Power Fiber Lasers with All-Solid Photonic Bandgap Fibers
Authors: Liang Dong, Kunimasa Saitoh, Fanting Kong, Paul Foy, Thomas Hawkins, Devon Mcclane
Acknowledged Federal Support: **Y**

Publication Type: Conference Paper or Presentation **Publication Status:** 1-Published
Conference Name: Frontier in Optics
Date Received: 01-Aug-2018 Conference Date: 17-Oct-2012 Date Published: 17-Oct-2012
Conference Location: Rochester
Paper Title: Advanced Optical Fibers and Their Applications in Fiber Lasers
Authors: Liang Dong, Kunimasa Saitoh, Fanting Kong, Thomas Hawkins, Guancheng Gu, and Yaobin Dong
Acknowledged Federal Support: **Y**

Publication Type: Conference Paper or Presentation **Publication Status:** 1-Published
Conference Name: SPIE Security and Sensing
Date Received: 01-Aug-2018 Conference Date: 13-Oct-2010 Date Published: 13-Oct-2010
Conference Location: Orlando
Paper Title: Path for Significant SBS Suppression in Fiber Amplifiers
Authors: Liang Dong
Acknowledged Federal Support: **Y**

Publication Type: Conference Paper or Presentation **Publication Status:** 1-Published
Conference Name: Advanced Solid State Photonics
Date Received: 01-Aug-2018 Conference Date: 06-Feb-2011 Date Published: 06-Feb-2011
Conference Location: Istanbul, Turkey
Paper Title: Specialty Optical Fibers for Applications in Fiber Lasers
Authors: Liang Dong
Acknowledged Federal Support: **Y**

Publication Type: Conference Paper or Presentation **Publication Status:** 1-Published
Conference Name: European Conference on Optical Communications
Date Received: 01-Aug-2018 Conference Date: 22-Sep-2013 Date Published:
Conference Location: London
Paper Title: Precise Tailoring of Longitudinal Acoustic Property of Optical Fibers by a Hydrogen-loading Technique
Authors: Fanting Kong and Liang Dong
Acknowledged Federal Support: **Y**

Publication Type: Conference Paper or Presentation **Publication Status:** 1-Published
Conference Name: Conference on Lasers and Electro-Optics
Date Received: 01-Aug-2018 Conference Date: 08-Jun-2014 Date Published: 08-Jun-2014
Conference Location: San Jose
Paper Title: Yb Doped Photonic Bandgap Fiber Lasers with Record Core Diameter
Authors: Guancheng Gu, Fanting Kong, Thomas Hawkins, Joshua Parsons, Maxwell Jones, Christopher Dunn, M
Acknowledged Federal Support: **Y**

Publication Type: Conference Paper or Presentation **Publication Status:** 1-Published
Conference Name: Workshop on Specialty Optical Fibers
Date Received: 01-Aug-2018 Conference Date: 28-Aug-2013 Date Published: 28-Aug-2013
Conference Location: Sigtuna, Sweden
Paper Title: Large-mode-area Fibers Enabled by Significant Differential Mode Losses
Authors: Liang Dong, Fanting Kong, Thomas W. Hawkins, Guancheng Gu, Paul Foy, Kunimasa Saitoh Kanxian W
Acknowledged Federal Support: **Y**

Publication Type: Conference Paper or Presentation **Publication Status:** 1-Published
Conference Name: International Photonics and OptoElectronics (POEM)
Date Received: 01-Aug-2018 Conference Date: 18-Jun-2014 Date Published: 18-Jun-2014
Conference Location: Wuahn, China
Paper Title: Yb-Doped All Solid Photonic Bandgap Fiber Lasers
Authors: Guancheng Gu, Fanting Kong, Thomas Hawkins, Joshua Parsons, Maxwell Jones, Christopher Dunn, M
Acknowledged Federal Support: **Y**

Publication Type: Conference Paper or Presentation **Publication Status:** 1-Published
Conference Name: Advanced Photonics Congress
Date Received: 01-Aug-2018 Conference Date: 28-Jul-2014 Date Published: 28-Jul-2014
Conference Location: Barcelona, Spain
Paper Title: Large Mode Area Yb Doped Photonic Bandgap Fiber Laser
Authors: Guancheng Gu, Fanting Kong, Thomas Hawkins, Joshua Parsons, Maxwell Jones, Christopher Dunn, M
Acknowledged Federal Support: **Y**

Publication Type: Conference Paper or Presentation **Publication Status:** 1-Published
Conference Name: PhotonicsWest
Date Received: 01-Aug-2018 Conference Date: 08-Feb-2015 Date Published: 08-Feb-2015
Conference Location: San Francisco
Paper Title: Large mode area Yb doped photonic bandgap fiber lasers
Authors: Liang Dong1 , Fanting Kong1 , Guancheng Gu1 , Thomas Hawkins1 , Joshua Parsons1 , Maxwell Jones
Acknowledged Federal Support: **Y**

Publication Type: Conference Paper or Presentation **Publication Status:** 1-Published
Conference Name: PhotonicsWest
Date Received: 01-Aug-2018 Conference Date: 08-Feb-2015 Date Published: 08-Feb-2015
Conference Location: San Francisco
Paper Title: Polarizing 50μm core Yb doped photonic bandgap fiber
Authors: Fanting Kong , Guancheng Gu, Thomas Hawkins, Joshua Parsons, Maxwell Jones, Christopher Dunn,
Acknowledged Federal Support: **Y**

Publication Type: Conference Paper or Presentation **Publication Status:** 1-Published
Conference Name: PhotonicsWest
Date Received: 01-Aug-2018 Conference Date: 08-Feb-2015 Date Published: 08-Feb-2015
Conference Location: San Francisco
Paper Title: Polarizing 50μm core Yb doped photonic bandgap fiber
Authors: Fanting Kong , Guancheng Gu , Thomas Hawkins , Joshua Parsons, Maxwell Jones , Christopher Dunn
Acknowledged Federal Support: **Y**

Publication Type: Conference Paper or Presentation **Publication Status:** 1-Published
Conference Name: PhotonicsWest
Date Received: 01-Aug-2018 Conference Date: 08-Feb-2015 Date Published: 08-Feb-2015
Conference Location: San Fancisco
Paper Title: High power narrow linewidth large mode area photonic bandgap fiber amplifier
Authors: Benjamin Pulforda , Iyad Dajania , Thomas Ehrenreicha , Roger Holtena , Christopher Vergiena , Nader
Acknowledged Federal Support: **Y**

Publication Type: Conference Paper or Presentation **Publication Status:** 1-Published
Conference Name: 17th Annual Directed Energy Symposium, Anaheim
Date Received: 01-Aug-2018 Conference Date: 02-Mar-2015 Date Published: 02-Mar-2015
Conference Location: Anaheim
Paper Title: High Power All solid Photonic Bandgap Fiber Lasers
Authors: Liang Dong, Fanting Kong, Guancheng Gu, Thomas Hawkins, Joshua Parsons, Maxwell Jones, Christo
Acknowledged Federal Support: **Y**

Publication Type: Conference Paper or Presentation **Publication Status:** 1-Published
Conference Name: Conference on Lasers and Electro-Optics
Date Received: 01-Aug-2018 Conference Date: 05-Jun-2015 Date Published: 05-Jun-2015
Conference Location: San Jose
Paper Title: Multiple Cladding-Resonance All Solid Photonic Bandgap Fibers with Large Mode Area
Authors: Guancheng Gu, Fanting Kong, Thomas W. Hawkins, Maxwell Jones, and Liang Dong
Acknowledged Federal Support: **Y**

Publication Type: Conference Paper or Presentation **Publication Status:** 1-Published
Conference Name: 4th Photonics Global Conference
Date Received: 24-Aug-2016 Conference Date: 28-Jun-2015 Date Published: 28-Jun-2015
Conference Location: Singapore
Paper Title: Challenges and Solutions for Further Power Scaling of Single-Mode Fiber Lasers
Authors: L. Dong, F. Kong, G. Gu, T.W. Hawkins, and M.T. Kalichevsky-Dong,
Acknowledged Federal Support: **Y**

Publication Type: Conference Paper or Presentation **Publication Status:** 1-Published
Conference Name: Advanced Solid State Lasers
Date Received: 24-Aug-2016 Conference Date: 04-Oct-2015 Date Published: 04-Oct-2015
Conference Location: Berlin, Germany
Paper Title: Challenges for Further Power Scaling of Single-Mode Fiber Lasers
Authors: L. Dong, F. Kong, G. Gu, T.W. Hawkins, M. Jones, J. Parsons, M.T. Kalichevsky-Dong, K. Saitoh, B. Pu
Acknowledged Federal Support: **Y**

Publication Type: Conference Paper or Presentation **Publication Status:** 1-Published
Conference Name: Frontier In Optics
Date Received: 24-Aug-2016 Conference Date: 17-Oct-2015 Date Published: 17-Oct-2015
Conference Location: San Jose, CA
Paper Title: Large Mode Area All-Solid Photonic Bandgap Fibers for High Power Fiber Lasers
Authors: L. Dong, F. Kong, G. Gu, T.W. Hawkins, M. Jones, J. Parsons, M.T. Kalichevsky-Dong, K. Saitoh, B. Pu
Acknowledged Federal Support: **Y**

Publication Type: Conference Paper or Presentation **Publication Status:** 1-Published
Conference Name: Stuttgart Technology Forum
Date Received: 24-Aug-2016 Conference Date: 31-May-2016 Date Published: 31-May-2016
Conference Location: Stuttgart, Germany
Paper Title: Opportunities and challenges of power scaling of single-mode fiber lasers
Authors: Liang Dong
Acknowledged Federal Support: **Y**

Publication Type: Conference Paper or Presentation **Publication Status:** 1-Published
Conference Name: Conference on Lasers and Electro-Optics
Date Received: 24-Aug-2016 Conference Date: 05-Jun-2016 Date Published: 05-Jun-2016
Conference Location: San Jose, 2016
Paper Title: Quantum-defect-assisted Polarization Mode Coupling in a Fiber Amplifier
Authors: Fanting Kong, Roger Stolen, and Liang Dong
Acknowledged Federal Support: **Y**

Publication Type: Conference Paper or Presentation **Publication Status:** 1-Published
Conference Name: Specialty Optical Fiber Conference
Date Received: 24-Aug-2016 Conference Date: 17-Jul-2016 Date Published: 17-Jul-2016
Conference Location: Vancouver, Canada
Paper Title: Observation of Quantum-defect-assisted Polarization Mode Coupling in a Fiber Amplifier
Authors: Fanting Kong, Roger Stolen, and Liang Dong
Acknowledged Federal Support: **Y**

Publication Type: Conference Paper or Presentation **Publication Status:** 1-Published
Conference Name: OSA Frontiers in Optics
Date Received: 02-Aug-2017 Conference Date: 17-Oct-2016 Date Published: 21-Oct-2016
Conference Location: Rochester, NY
Paper Title: ~900W Single-mode CW Power From an 60?m-core Ytterbium-doped All-solid Photonic Bandgap Fiber Laser
Authors: 30. Fanting Kong, Guancheng Gu, Thomas W. Hawkins, Maxwell Jones, Joshua Parsons, Monica T. K
Acknowledged Federal Support: **Y**

Publication Type: Conference Paper or Presentation **Publication Status:** 1-Published
Conference Name: Asia communications and Photonics Conference
Date Received: 01-Aug-2018 Conference Date: 02-Nov-2016 Date Published: 05-Nov-2016
Conference Location: Wuhan, China
Paper Title: Progress and challenges in further power scaling of single mode fiber lasers
Authors: Liang Dong, Fanting Kong, Guancheng Gu, Thomas W. Hawkins, Maxwell Jones, Joshua Parsons, Mor
Acknowledged Federal Support: **Y**

Publication Type: Conference Paper or Presentation **Publication Status:** 1-Published
Conference Name: PhotonicsWest
Date Received: 01-Aug-2018 Conference Date: 28-Jan-2017 Date Published: 02-Feb-2017
Conference Location: San Francisco
Paper Title: 1 kilowatt Ytterbium doped all solid photonic bandgap fiber laser
Authors: anting Kong, Guancheng Gu, Wade Hawkins, Maxwell Jones, Joshua Parsons, Monica T. Kalichevsky-I
Acknowledged Federal Support: **Y**

Publication Type: Conference Paper or Presentation **Publication Status:** 1-Published
Conference Name: Conference on Lasers and Electro_optics
Date Received: 01-Aug-2018 Conference Date: 14-May-2017 Date Published: 19-May-2017
Conference Location: San Jose, CA
Paper Title: Single mode 60μm core multiple cladding resonance photonic bandgap fiber laser with 1kW output power
Authors: Guancheng Gu, Fanting Kong, Thomas Hawkins, Maxwell Jones, Joshua Parsons, Monica T. Kalichevs
Acknowledged Federal Support: **Y**

Publication Type: Conference Paper or Presentation **Publication Status:** 1-Published
Conference Name: Workshop on Specialty Optical Fibers
Date Received: 01-Aug-2018 Conference Date: 27-Jan-2018 Date Published: 01-Feb-2018
Conference Location: Cyprus
Paper Title: Single mode Ytterbium Fiber Laser with Record 220W Output Power at 1018nm
Authors: Fanting Kong, Guancheng Gu, Thomas W. Hawkins, Maxwell Jones, Joshua Parsons, Monica T. Kalich
Acknowledged Federal Support: **Y**

Publication Type: Conference Paper or Presentation **Publication Status:** 1-Published
Conference Name: PhotonicsWest
Date Received: 01-Aug-2018 Conference Date: 29-Jan-2018 Date Published: 01-Jun-2018
Conference Location: San Francisco
Paper Title: Single-mode 240W Output Power at 1018nm from an Ytterbium Fiber Laser
Authors: Fanting Kong, Guancheng Gu, Thomas W. Hawkins, Maxwell Jones, Joshua Parsons, Monica T. Kalich
Acknowledged Federal Support: **Y**

Publication Type: Conference Paper or Presentation **Publication Status:** 1-Published
Conference Name: OptoElectronic Communications Conference
Date Received: 01-Aug-2018 Conference Date: 02-Jul-2018 Date Published: 05-Jul-2018
Conference Location: South Korea
Paper Title: Advanced Specialty Optical Fibers and Their Applications in High Power Fiber Lasers
Authors: Liang Dong
Acknowledged Federal Support: **Y**

INVENTIONS:

Intellectual Property Type: Invention
Invention Title: All solid large core photonic bandgap fibers for use in optical fiber lasers
Description:
Inventors:
Employer Name:
Employer Address:
Confirmatory Instrument:

PATENTS:

Intellectual Property Type: Patent Date Received: **01-Aug-2018**
Patent Title: High Power Optical Fibers
Patent Abstract: Photonic bandgap fibers are described that can be solid across the core and clad and have a la
Patent Number: US 9146345 B1
Patent Country: USA
Application Date: 18-Jan-2013 Application Status: 3
Date Issued: 29-Sep-2015

REPORT DOCUMENTATION PAGE

Form Approved
OMB No. 0704-0188

1. REPORT DATE *(DD-MM-YYYY)*	**2. REPORT TYPE**	**3. DATES COVERED** *(From - To)*
3-25-2019	Final report	From 8-1-2010 to 3-25-2019

4. TITLE AND SUBTITLE Advanced Optical Fibers for High Power Fiber Laser	**5a. CONTRACT NUMBER**
	5b. GRANT NUMBER W911NF-10-1-0423
	5c. PROGRAM ELEMENT NUMBER
6. AUTHOR(S) Liang Dong, John Ballato, Bryce Samson, Joshua E. Rothenberg	**5d. PROJECT NUMBER**
	5e. TASK NUMBER
	5f. WORK UNIT NUMBER
7. PERFORMING ORGANIZATION NAME(S) AND ADDRESS(ES) Clemson University Office of Sponsored Programs P.O.Box 946 Clemson, SC 39631	**8. PERFORMING ORGANIZATION REPORT NUMBER**
9. SPONSORING/MONITORING AGENCY NAME(S) AND ADDRESS(ES) Michael D. Gerhold Army Reseach Office P.O.Box 12211 Research Triangle Park, NC27709-2211	**10. SPONSOR/MONITOR'S ACRONYM(S)** 58391-EL-HEL
	11. SPONSORING/MONITORING AGENCY REPORT NUMBER

12. DISTRIBUTION AVAILABILITY STATEMENT

13. SUPPLEMENTARY NOTES

14. ABSTRACT
The project is to develop large mode area optical fibers based on all-solid photonic bandgap designs (Thrust I) and a SBS suppression technique based on hydrogen loading (Thrust II). A major achievement has been to fabricate silica-index-matched ytterbium-doped active core glass and to demonstrate significant SBS suppression using the hydrogen loading and UV exposure technique. We demonstrated 50μm core active fibers with robust single-mode operation and high slope efficiencies relative to launched power at >80% and absorbed power at >90%. In collaboration with AFRL, single-frequency single-mode >400W output was demonstrated. We also demonstrated passive record-breaking 100μm-core all-solid photonic bandgap fibers and SBS suppression of one order of magnitude using the hydrogen loading and UV exposure technique. We have focused on further HOM suppression in all-solid photonic bandgap fibers to further improve mode instability threshold in this period. Multiple resonant cladding design has been incorporated into 50μm core active all-solid photonic bandgap fibers. We have achieved record near kW single-mode output from this new fiber, a record for micro-structured fibers and LMA fibers at this core diameter. We have also directly measured mode-coupling due to stimulated thermal Rayleigh scattering, providing first direct evidence for its role in mode instability. We have also fabricated all-solid photonic bandgap fibers with ~25μm with projected TMI threshold of several kW. Test is being conducted at AFRL.

15. SUBJECT TERMS
Specialty optical fibers, optical fiber lasers

16. SECURITY CLASSIFICATION OF:			**17. LIMITATION OF ABSTRACT**	**18. NUMBER OF PAGES**	**19a. NAME OF RESPONSIBLE PERSON**
a. REPORT	**b. ABSTRACT**	**c. THIS PAGE**		20	Liang Dong
UNCLASSIFIED	UNCLASSIFIED	UNCLASSIFIED			**19b. TELEPONE NUMBER (*Include area code*)** 864 656 5915

1. REPORT DATE. Full publication date, including day, month, if available. Must cite at lest the year and be Year 2000 compliant, e.g., 30-06-1998; xx-08-1998; xx-xx-1998.

2. REPORT TYPE. State the type of report, such as final, technical, interim, memorandum, master's thesis, progress, quarterly, research, special, group study, etc.

3. DATES COVERED. Indicate the time during which the work was performed and the report was written, e.g., Jun 1997 - Jun 1998; 1-10 Jun 1996; May - Nov 1998; Nov 1998.

4. TITLE. Enter title and subtitle with volume number and part number, if applicable. On classified documents, enter the title classification in parentheses.

5a. CONTRACT NUMBER. Enter all contract numbers as they appear in the report, e.g. F33615-86-C-5169.

5b. GRANT NUMBER. Enter all grant numbers as they appear in the report, e.g. 1F665702D1257.

5c. PROGRAM ELEMENT NUMBER. Enter all program element numbers as they appear in the report, e.g. AFOSR-82-1234.

5d. PROJECT NUMBER. Enter al project numbers as they appear in the report, e.g. 1F665702D1257; ILIR.

5e. TASK NUMBER. Enter all task numbers as they appear in the report, e.g. 05; RF0330201; T4112.

5f. WORK UNIT NUMBER. Enter all work unit numbers as they appear in the report, e.g. 001; AFAPL30480105.

6. AUTHOR(S). Enter name(s) of person(s) responsible for writing the report, performing the research, or credited with the content of the report. The form of entry is the last name, first name, middle initial, and additional qualifiers separated by commas, e.g. Smith, Richard, Jr.

7. PERFORMING ORGANIZATION NAME(S) AND ADDRESS(ES). Self-explanatory.

8. PERFORMING ORGANIZATION REPORT NUMBER. Enter all unique alphanumeric report numbers assigned by the performing organization, e.g. BRL-1234; AFWL-TR-85-4017-Vol-21-PT-2.

9. SPONSORING/MONITORS AGENCY NAME(S) AND ADDRESS(ES). Enter the name and address of the organization(s) financially responsible for and monitoring the work.

10. SPONSOR/MONITOR'S ACRONYM(S). Enter, if available, e.g. BRL, ARDEC, NADC.

11. SPONSOR/MONITOR'S REPORT NUMBER(S). Enter report number as assigned by the sponsoring/ monitoring agency, if available, e.g. BRL-TR-829; -215.

12. DISTRIBUTION/AVAILABILITY STATEMENT. Use agency-mandated availability statements to indicate the public availability or distribution limitations of the report. If additional limitations/restrictions or special markings are indicated, follow agency authorization procedures, e.g. RD/FRD, PROPIN, ITAR, etc. Include copyright information.

13. SUPPLEMENTARY NOTES. Enter information not included elsewhere such as: prepared in cooperation with; translation of; report supersedes; old edition number, etc.

14. ABSTRACT. A brief (approximately 200 words) factual summary of the most significant information.

15. SUBJECT TERMS. Key words or phrases identifying major concepts in the report.

16. SECURITY CLASSIFICATION. Enter security classification in accordance with security classification regulations, e.g. U, C, S, etc. If this form contains classified information, stamp classification level on the top and bottom of this page.

17. LIMITATION OF ABSTRACT. This block must be completed to assign a distribution limitation to the abstract. Enter UU (Unclassified Unlimited) or SAR (Same as Report). An entry in this block is necessary if the abstract is to be limited.

1. Executive Summary

1.1. Introduction

There has been significant progress in the development of fiber lasers in the past decade. Fiber lasers have been gaining market shares in many commercial applications. They are compact, robust and excellent at thermal management. Solid-state lasers still lead in high peak-powers and large pulse-energies. Power-scaling of fiber lasers, currently limited by nonlinear effects, is critical for a wide range of applications in industry, defense and science. Effective-mode-area-scaling of fibers is the key for further power-scaling of fiber lasers.

This project investigates mode-area-scaling with effectively single-mode all-solid photonic bandgap fibers (PBF) in the first thrust. To optimize the large mode-area designs, we exploit the strong mode-dependent loss to mitigate the waveguide-tendency to supports more modes at large core diameters. In the second thrust, the project investigates the feasibility of diffusing gases (e.g. hydrogen or deuterium) into fibers and then bonding them to a glass network by UV exposure. This technique can potentially be performed in a highly controlled manner and can be combined with other techniques to achieve significant SBS suppression, enabling >10kW lasers with sub-MHz line-width.

1.2. Project Status

In the first thrust, major breakthrough was made previously by demonstrating highly efficient and robust single-mode 50μm-core all-solid photonic bandgap fibers in both laser and amplifier configurations, culminating in the recent demonstration of >400W single-frequency single-mode output in one of our all-solid photonic bandgap fibers. This feat was enabled by the fabrication of ytterbium-doped glass with highly uniform and accurate refractive index control achieved in the second iteration of active core glass fabrication completed in June 2013. The tests result indicates that the refractive index is ~2×10^{-4} below silica. This is sufficient for 50μm-core fibers, but not for 100μm-core fibers. The third iteration of ytterbium-doped glass fabrication started in December 2013 and completed in March 2015. Its refractive index is ~2.3×10^{-4} above silica, higher than the target. We have made a 4th iteration glass by mixing the 2nd and 3rd iteration of ytterbium-doped glass at 1:1 ratio in March 2016. Previously we have also demonstrated 50μm-core polarizing ytterbium-doped all-solid photonic bandgap fibers and efficiency single-polarization fiber lasers based on the polarizing fiber. We have also directly measured mode-coupling due to stimulated thermal Rayleigh scattering, providing first direct evidence for its role in mode instability. In the second thrust, we have demonstrated SBS suppression of over an order of magnitude in germanium-doping fibers with UV exposure at 266nm.

We have been focusing on further HOM suppression in all-solid photonic bandgap fibers to further improve mode instability threshold in this period. Multiple resonant cladding design has been incorporated into 50μm core active all-solid photonic bandgap fibers. Several fiber iterations have been made and tested in the period. Progress has been made in how to characterize and fine tune the bandgap of the fibers. We have achieved record kW single-mode output, a record for micro-structured fibers and LMA fibers at this core diameter. In this period, we have incorporated all the latest advances in an all-solid photonic bandgap fiber with a core diameter of ~25μm. This fiber is estimated to have ~4kW threshold for both TMI and SBS at 2GHz linewidth.

1.3. List of Publications/Reports

(a) Papers published in peer-reviewed journals

1. F. Kong, K. Saitoh, D. Mcclane,T. Hawkins, P. Foy, G.C. Gu, and L. Dong, "Mode Area Scaling with All-solid Photonic Bandgap Fibers,", Optics Express, **20**, 26363-26372(2012).
2. F. Kong and L. Dong, "Precise and Significant Tailoring of Acoustic Velocity in Optical Fibers by Hydrogenation and UV Exposure," Optics Express, **20**, 27810-27819(2012).
3. L. Dong, "Stimulated thermal Rayleigh scattering in optical fibers," Optics Express **21**, 2642–2656 (2013).
4. S. Saitoh, K. Saitoh, M. Kashiwagi, S. Matsuo, and L. Dong, "Design Optimization of Large-Mode-Area All-Solid Photonic Bandgap Fibers for High-Power Laser Applications," Journal of Lightwave Technology **32**, 440-449 (2014).
5. G. Gu, F. Kong, T. Hawkins, J. Parsons, M. Jones, C. Dunn, M.T. Kalichevsky-Dong, K. Saitoh, and L. Dong, "Ytterbium-doped large-mode-area all-solid photonic bandgap fiber lasers," Optics Express **22**, 13962-13968(2014).
6. F. Kong, G. Gu, T.W. Hawkins, J. Parsons, M. Jones, C. Dunn, M.T. Kalichevsky-Dong, B. Pulford, I. Dajani, K. Saitoh, S.P. Palese, E. Cheung, and L. Dong, "Polarizing ytterbium-doped all-solid photonic bandgap fiber with ~1150μm^2 effective mode area," Optics Express **23**, 4307-4312 (2015).
7. G. Gu, F. Kong, T.W. Hawkins, M. Jones, and L. Dong, "Extending Mode Areas of Single-mode All-solid Photonic Bandgap Fibers," Optics Express **23**, 9147-9156 (2015).
8. B. Pulford, T. Ehrenreich, R. Holten, F. Kong, T.W. Hawkins, L. Dong, and I. Dajani, "400 W near diffraction-limited single-frequency all-solid photonic bandgap fiber amplifier," Optics Letters **40**, 2297-2300 (2015).
9. L. Dong, F. Kong, G. Gu, T.W. Hawkins, M. Jones, J. Parsons, M.T. Kalichevsky-Dong, K. Saitoh, B. Pulford, and I. Dajani, "Large-Mode-Area All-Solid Photonic Bandgap Fibers for the Mitigation of Optical Nonlinearities," Journal of Selected Topics in Quantum Electronics **22**, invited paper, 4900207 (2015).
10. F. Kong, J. Xue, R.H. Stolen, and L. Dong, "Experimental Observation of Quantum-defect-assisted Polarization Mode Coupling in a Fiber Amplifier," Optica **3**(9), 975-978(2016).
11. L. Dong, "Thermal Lensing in Optical Fibers," Optical Express **24**(17), 19841-19852(2016).
12. F. Kong, G. Gu, T.W. Hawkins, M. Jones, J, Parsons, M.T. Kalichevsky-Dong, S.P. Palese, E. Cheung, and L. Dong, "Efficient 240W single-mode 1018nm laser from an Ytterbium-doped 50/400μm all-solid photonic bandgap fiber," Optics Express **26**(3), 3138-3144 (2018).
13. T. Matniyaz, W. Li, M.T. Kalichevsky-Dong, T.W. Hwakins, J. Parsons, G. Gu, and L. Dong, "Highly efficient cladding-pumped single-mode three-level Yb all-solid photonic bandgap fiber lasers," Optics Letters **44**, 807-810 (2019).

(b) Papers published in non-peer-reviewed journals or in conference proceedings

1. L. Dong, K. Saitoh, F. Kong, P. Foy, T. Hawkins, D. Mcclane, G. Gu, and Y. Dong, "All-Solid Photonic Bandgap Fibers for High Power Lasers," SPIE Security and Defense, invited paper, September 2012, Edinburg, Scotland.
2. L. Dong, K. Saitoh, F. Kong, T. Hawkins, G. Gu, and Y. Dong, "Advanced Optical Fibers and Their Applications in Fiber Lasers," Frontier in Optics, paper FTh3C.4, invited paper, October 2012, Rochester, New York.
3. L. Dong, K. Saitoh, F. Kong, T. Hawkins, D. Mcclane and G.C. Gu, "Advanced Optical Fibers and Their Applications in Fiber Lasers," Photonics Global Conference, invited paper, December 2012 in Singapore.

4. L. Dong, K. Saitoh, F. Kong, T. Hawkins, D. Mcclane, and G.C. Gu, “Robust Single-mode All Solid Photonic Bandgap Fibers with Core Diameter of 50μm,” PhotonicsWest, paper 8601-64, 2013.
5. F. Kong and L. Dong, “Stimulated Brillouin Scattering suppression in Optical Fibers by Hydrogen-loading Technique,” PhotonicsWest, paper 8601-31, 2013.
6. J. Ballato, A. Evert, T.W. Hawkins, P.D. Dragic, P. Foy, L. Dong. R.H. Stolen, R.R. Rice, “Longitudinally-graded optical fibers,” PhotonicsWest, paper 8601-18, 2013.
7. F. Kong, K. Saitoh, D. Mcclane, T.W. Hawkins, P. Foy, G.C. Gu and L. Dong, “All-solid photonic bandgap fiber with record mode area,” Optical Communications Conference, paper OTh1J2, 2013.
8. G.C. Gu, F. Kong, T.W. Hawkins, L. Dong, K. Wei, and B. Samson “Mode-dependent Losses in 50micron Core Leakage Channel Fibers,” DEPS Solid State and Diode Laser Review, paper 13-SSDLTR 004, 2013.
9. L. Dong, “Quasi-analytical Solution for Mode Instability Thresholds ,” DEPS Solid State and Diode Laser Review, paper 13-SSDLTR-002, 2013.
10. K. Saitoh, S. Saitoh, M. Kashiwagi, S. Matsuo, and L. Dong, “All-Solid Photonic Bandgap Fibers for Fiber Laser Applications,” Lasers and Electro-Optics Pacific Rim (CLEO-PR), paper TuA3-2, July 2013.
11. L. Dong, F. Kong, T. Hawkins; G. Gu, P. Foy, K. Saitoh, K. Wei; B. Samson, “Large-mode-area Fibers Enabled by Significant Differential Mode Losses,” Workshop on Specialty Optical Fibers, invited talk, Sigtuna Sweden, August 2013.
12. L. Dong, F. Kong and T. Hawkins, “Precise Tailoring of Longitudinal Acoustic Property of Optical Fibers by a Hydrogen-loading Technique,” European Conference on Optical Communications, invited talk, paper Tu3.A.1 London, September 2013.
13. G. Gu, F. Kong, T. Hawkings, J. Parsons, M. Jones, C. Dunn; M. Kalichevsky-Dong; K. Saitoh, and L. Dong, “High power, large core ytterbium-doped photonic bandgap fiber laser,” DEPS Advanced High Power Lasers, paper 14-SSDLTR-009, May 2014.
14. G. Gu, F. Kong, T. Hawkings, J. Parsons, M. Jones, C. Dunn, M. Kalichevsky-Dong, K. Saitoh, and L. Dong, “ Yb-Doped Photonic Bandgap Fiber Lasers with Record Core Diameter,” CLEO, paper SF1N.2, June 2014.
15. G. Gu, F. Kong, T. Hawkins, J. Parsons, M. Jones, C. Dunn, M.T. Kalichevsky-Dong, K. Saitoh, and L. Dong, “Yb-Doped All-Solid Photonic Bandgap Fiber Lasers,” International Photonics and OptoElectronics (POEM), paper FTh4F.5 June 2014.
16. G. Gu, F. Kong, T. Hawkins, J. Parsons, M. Jones, C. Dunn, M.T. Kalichevsky-Dong, K. Saitoh, and L. Dong, “Large-Mode-Area Yb-Doped Photonic Bandgap Fiber Laser,” Advanced Photonics Congress, paper SoTu4B.3, August 2014.
17. L. Dong, “Control of light flow in optical fibers,” 5th International Conference on Photonics, keynote speaker, September 2014, Kuala Lumpur.
18. L. Dong, F. Kong, G. Gu, T.W. Hawkins, J. Parsons, M. Jones, C. Dunn, M.T. Kalichevsky-Dong, K. Saitoh, B. Pulford, and I. Dajani, “Large mode area Yb-doped photonic bandgap fiber lasers,” SPIE PhotonicsWest, invited talk, paper 9344-1, San Francisco, February 2015.
19. F. Kong, G. Gu, T.W. Hawkins, J. Parsons, M. Jones, C.D. Dunn, M.T. Kalichevsky-Dong, B. Pulford, I. Dajani, K. Saitoh, L. Dong, “Polarizing 50μm core Yb-doped photonic bandgap fiber,” SPIE PhotonicsWest, paper 9344-2, San Francisco, February 2015.
20. B. Pulford, I. Dajani, T. Ehrenreich, R.H. Holten, C.L. Vergien, N. Naderi, C. Mart, G. Gu, F. Kong, T.W. Hawkins, and L. Dong, “High-power narrow-linewidth large mode area photonic bandgap fiber amplifier,” SPIE PhotonicsWest, paper 9344-5, San Francisco, February 2015.

21. L. Dong, F. Kong, G. Gu, T.W. Hawkins, J. Parsons, M. Jones, C. Dunn, M.T. Kalichevsky-Dong, K. Saitoh, B. Pulford, and I. Dajani, “High-Power All-solid Photonic Bandgap Fiber Lasers,” 17th Annual Directed Energy Symposium, Anaheim, CA, March 2015.
22. G. Gu, F. Kong, T.W. Hawkins, M. Jones, and L. Dong, “Large Mode Area, All-Solid Photonic Bandgap Fiber with Resonant Cladding Cores,” 17th Annual Directed Energy Symposium, Anaheim, CA, March 2015.
23. G. Gu; F. Kong, T. Hawkins, M. Jones, and L Dong, “Multiple Cladding-Resonance All-Solid Photonic Bandgap Fibers with Large Mode Area,” CLEO, SM2L.1, San Jose, CA, May 10-15 2015.
24. L. Dong, F. Kong, G. Gu, T.W. Hawkins, and M.T. Kalichevsky-Dong, “Challenges and Solutions for Further Power Scaling of Single-Mode Fiber Lasers,” 4th Photonics Global Conference, invited paper, ICMAT15-A-4343, Singapore June-July 2015.
25. L. Dong, F. Kong, G. Gu, T.W. Hawkins, M. Jones, J. Parsons, M.T. Kalichevsky-Dong, K. Saitoh, B. Pulford and I. Dajani, “Challenges for Further Power Scaling of Single-Mode Fiber Lasers,” Advanced Solid State Lasers, invited talk, Berlin, October 4-7, 2015.
26. L. Dong, F. Kong, G. Gu, T.W. Hawkins, M. Jones, J. Parsons, M.T. Kalichevsky-Dong, K. Saitoh, B. Pulford and I. Dajani, “Large Mode Area All-Solid Photonic Bandgap Fibers for High Power Fiber Lasers,” Frontier in Optics, invited talk, San Jose, October 17-21, 2015.
27. L. Dong, “Opportunities and challenges of power scaling of single-mode fiber lasers,” Stuttgart Laser Technology Forum, invited talk, Stuttgart, May 31st and June 1st, 2016.
28. Fanting Kong, Roger Stolen, and Liang Dong, “Quantum-defect-assisted Polarization Mode Coupling in a Fiber Amplifier,” Conference on Lasers and Electro Optics, SM2Q.1, San Jose, June 2016.
29. Fanting Kong, Roger Stolen, and Liang Dong, “Observation of Quantum-defect-assisted Polarization Mode Coupling in a Fiber Amplifier,” Advanced Photonics Congress, SoW2H.3, Vancouver, Canada, July 2016.
30. Fanting Kong, Guancheng Gu, Thomas W. Hawkins, Maxwell Jones, Joshua Parsons, Monica T. Kalichevsky-Dong, Benjamin Pulford, Iyad Dajani, and Liang Dong, “~900W Single-mode CW Power From an 60μm-core Ytterbium-doped All-solid Photonic Bandgap Fiber Laser,” OSA Frontiers in Optics, paper FW5B.3, Rochester, October 17-21, 2016.
31. Cody Mart, Benjamin Ward, Benjamin Pulford, Iyad Dajani, Liang Dong and Khanh Kieu, “Brillouin gain spectroscopy on LMA Yb-doped photonic bandgap fiber,” OSA Frontiers in Optics, paper FW5B.4, Rochester, October 17-21, 2016.
32. Liang Dong, Fanting Kong, Guancheng Gu, Thomas W. Hawkins, Maxwell Jones, Joshua Parsons, Monica Kalichevsky-Dong, and Christopher Dunn, “Progress and challenges in further power scaling of single-mode fiber lasers” ***invited talk***, Asia communications and Photonics Conference, paper AF4A, Wuhan, China , November 2-5, 2016.
33. Fanting Kong, Guancheng Gu, Wade Hawkins, Maxwell Jones, Joshua Parsons, Monica T. Kalichevsky-Dong, Benjamin Pulford, Iyad Dajani, and Liang Dong, “~ 1 kilowatt Ytterbium-doped all-solid photonic bandgap fiber laser,” PhotonicsWest, paper 10083-36, San Francisco, January 28 to February 2nd, 2017.
34. C. Mart, B. Pulford, B. Ward, I. Dajani, L. Dong, K. Kieu, and A. Sanchez, “SBS Investigation of an All-solid Ytterbium-doped Photonic Bandgap Fiber Amplifier”, Nineteenth Annual Directed Energy Symposium, Huntsville, Alabama, 13-17 February 2017.
35. Guancheng Gu, Fanting Kong, Thomas Hawkins, Maxwell Jones, Joshua Parsons, Monica T. Kalichevsky-Dong, Benjamin Pulford, Iyad Dajani, Stephen Palese, Eric Cheung, and Liang Dong, “Single-mode 60μm-core multiple-

cladding-resonance photonic bandgap fiber laser with ~1kW output power; ” CLEO, SM1L.5 San Jose, June 2017.

36. Fanting Kong, Guancheng Gu, Thomas W. Hawkins, Maxwell Jones, Joshua Parsons, Monica T. Kalichevsky-Dong, and Liang Dong, “Single-mode Ytterbium Fiber Laser with Record 220W Output Power at 1018nm,” Workshop on Specialty Optical Fibers, October 11-13, 2017, Limassol, Cyprus.
37. Fanting Kong, Guancheng Gu, Thomas W. Hawkins, Maxwell Jones, Joshua Parsons, Monica T. Kalichevsky-Dong, and Liang Dong, “Single-mode Ytterbium Fiber Laser with Record 240W Output Power at 1018nm,” PhotonicsWest, paper 10512-16 (PW18L-LA102-92), January 27 - February 1, 2018, San Francisco.
38. Liang Dong, “Advanced specialty optical fibers and their applications in high-power fiber lasers,“ The 23rd OptoElecronics and Communications Conference (OECC2018), tutorial, 2-6 July, 2018, Jeju, Korea.
39. Turghun Matniyaz, Monica T. Kalichevsky-Dong, Thomas W. Hawkins, Joshua Parsons, Guancheng Gu, Wensong Li, Max Faykus, Bradley Selee, Jonathan A. Dong, and Liang Dong, “Single-mode Yb-doped Double-clad All-solid Photonic Bandgap Fiber Laser Generating 27.8W at 976nm,” OSA Laser Congress, Boston, November 4 2018.
40. Zhimeng Huang, Shankar Pidishety, Thomas Hawkins, Yujun Feng, Yutong Feng, Sheng Zhu, Liang Dong, and Johan Nilsson, “Low-birefringence 120 W Yb fiber amplifier producing linearly polarized pulses with 69-GHz linewidth at 1083 nm,”, OSA Laser Congress, Boston, November 4 2018.
41. Turghun Matniyaz, Monica T. Kalichevsky-Dong, Thomas W. Hawkins, Joshua Parsons, Guancheng Gu, Wensong Li, Max Faykus, Bradley Selee, Jonathan A. Dong, and Liang Dong, “Diffraction-limited Yb-doped Double-clad All-solid Photonic Bandgap Fiber Laser at 976nm,” PhotonicsWest, invited talk, San Francisco, February 2 2019.
42. Liang Dong, “Challenges and potential solutions in further power scaling of single-mode fiber lasers,” Oasis 7 - International Conference and Exhibition on Optics and Electro-Optics, invited talk, April 1-2, 2019, Tel Aviv, Israel.
43. Turghun Matniyaz, Wensong Li, Monica T. Kalichevsky-Dong, Thomas W. Hawkins, Joshua Parsons, Guancheng Gu, and Liang Dong, “Efficient High-power Single-mode Yb Three-level Cladding-pumped All-solid Photonic Bandgap Fiber Lasers at ~978nm,” CLEO, 3160577, San Jose, May 2019.
44. Turghun Matniyaz, Wensong Li, Saddam Gafsi, Monica T. Kalichevsky-Dong, Thomas W. Hawkins, Joshua Parsons, Guancheng Gu, and Liang Dong, “A monolithic single-mode Yb three-level fiber laser at ~978nm with a record power of ~150W,” CLEO, postdeadline paper, 3212958, San Jose, May 2019.

(c) Papers presented at meetings, but not published in conference proceedings

1.4. Scientific Personnel Supported by This Project and Honors/Wards/Degree Received

Personnel Supported by This Project:
Prof. Liang Dong, PI, Clemson University
Dr. Paul Foy, director of fiber fabrication, Clemson University
Dr. Monica T. Kalichevsky-Dong, characterization, Clemson University
Mr. Thomas Hawkins, associate director of fiber fabrication, Clemson University
Mr. Joshua Parsons, staff, fiber fabrication, Clemson University
Dr. Fanting Kong, research associate, optics, Clemson University
Mr. Matthew Vanoverstraeten, ECE undergraduate student, micro-lathe development
Mr. Andrew Rennion, ECE undergraduate student, fiber taper and fiber lasers
Mr. Turghun Matniyaz, PhD student
Mr. Kenneth Peters, undergraduate student
Mr. Nikhil Gandhi, undergraduate student

Mr. Jonathan Drake, undergraduate student
Mr. Bailey Meehan, undergraduate student
Mr. Max Faykus, undergraduate student
Mr. Bradley Selee, undergraduate student

PhD degree received:
Guancheng Gu, ECE, August 2016

MSc degree received:
Christopher Dunn, August 2016

BSc degree received:
Mr. Devon Mcclane, MSE
Mr. Christopher Dunn, MSE
Mr. Tyler Hughes, MSE
Mr. Matthew Vanoverstraeten, ECE
Mr. Andrew Rennion, ECE
Mr. Maxwell Jones, MSE
Mr. Alex Gay, ECE
Mr. Camden Griggs, MSE
Mr. Jonathan Drake, ECE

Honors/Awards:
Guancheng Gu, OSA Incubic Milton travel grant, 2015
Guancheng Gu, Clemson Professional Enrichment Grant Application (PEGAS) grant. 2015
Christopher Dunn, DEPS graduate student fellowship (2014, 2015)
Liang Dong, Fellow of Optical Society of America, 2014
Liang Dong, Fellow of SPIE, 2017
Liang Dong, University Research, Scholarship, and Artistic Achievement award, 2018

1.5. Reports of Inventions

1. Granted patent "High power optical fibers", US9146345 B1.
2. Invention disclosure to Clemson University "A post-processing method for the suppression of stimulated Brillouin scattering in optical fibers

1.6. Scientific Progress and Accomplishments

i. Discovery of theoretical evidence for strong higher order mode filtering property of all solid photonic bandgap fibers in large core designs. This class of designs has been found to have the highest differential mode losses, enabling large core optical fibers with potentially very high quality single mode operation. This technique can provide the key for power scaling of single mode fiber lasers.
ii. First experimental demonstration of all solid photonic bandgap fibers operating in robust single mode in 50μm cores.
iii. First demonstration of significant SBS suppression using H_2/UV treatment.
iv. Demonstration of record 13dB SBS suppression capability using fiber design/treatments.
v. Establish analytical mode for mode instability

vi. Record demonstration of 50μm-core all-solid photonic bandgap fiber lasers and amplifiers with robust single mode and high efficiency
vii. Record multimode 600W from an all-solid photonic bandgap fiber
viii. Record demonstration of passive 100μm-core all-solid photonic bandgap fiber with robust single-mode operation using innovative multiple resonance design
ix. Demonstrate record single-mode/single-frequency power of >400W in all-solid photonic bandgap fibers
x. Demonstrate active PM all-solid photonic bandgap fibers operating in robust single mode in record 50μm cores.
xi. First measurement of stimulated thermal Rayleigh scattering gain
xii. Records ~1kW single-mode output power from 50μm-core fiber.
xiii. Analysis of thermal lensing in optical fibers
xiv. Fabrication of 25/400 all solid photonic bandgap fiber with potential TMI threshold of ~4kW

1.7. Technology Transfer, several fibers to AFRL.

1.8. Copies of Technical Reports, None

2. Introduction to the Project

2.1 Statements of Objectives

The primary thrust of this research is to develop mode area scaling solutions with all-solid photonic bandgap fibers by exploiting strong differential mode loss from photonic bandgap guidance. More specifically, we will demonstrate ytterbium-doped single-mode all-solid photonic bandgap fibers with core diameters of 50μm and coil diameter of ~50cm and investigate the feasibility of fabricating an all-solid photonic bandgap fiber with a core diameter of 100μm.

The second thrust of this research is to demonstrate over >20dB SBS suppression by longitudinally varying acoustic velocity profile. More specifically, we will investigate the feasibility of diffusing gases such as hydrogen or deuterium into fabricated optical fibers and then locking the gas molecules to the glass lattice by UV exposure. The UV exposure is varied longitudinally along the fiber to create the desired acoustic velocity profile.

Thrust I: to demonstrate efficient ytterbium-doped single-mode all-solid photonic bandgap fibers of 50μm core diameters and coil diameter of ~50cm and to investigate the feasibility of all-solid photonic bandgap fibers of 100μm core diameter. More specifically:

i) Establish and refine simulation tools for designing an all-solid photonic bandgap fiber (PBF).
ii) Investigate and optimize designs for mode area scaling beyond 50μm by exploiting mode-dependent leakage loss in all-solid PBFs.
iii) Develop a stack-and-draw fabrication process for all-solid PBFs.
iv) Demonstrate passive single-mode all-solid PBF with a 50μm core diameter.
v) Fabricate a low photo-darkening highly uniform ytterbium-doped silica glass with precisely controlled refractive index, essential for active core diameter scaling beyond 35μm:

a. Ytterbium-doped silica, co-doped with high phosphorus and some aluminum for low photo-darkening, and, fluorine and boron for low refractive index.
b. Refractive index uniformity better than 10^{-4}.
c. Precise refractive index control to be within $\pm 2\times10^{-4}$ of silica

vi) Demonstrate ytterbium-doped single-mode all-solid PBF with 50μm core and coil diameter of ~50cm.
vii) (optional) Investigate feasibility of core diameter scaling to 100μm.

Thrust II: to develop techniques for controlled longitudinal acoustic property variations in fibers and to demonstrate SBS suppression of over two orders of magnitude. The primary approach is based on diffusion of hydrogen or deuterium molecules into LMA fibers. Longitudinally varying UV exposure is then used to bond the gas molecules to the glass lattice and to create permanent composition variation along the fibers. The goal is to modify the glass composition by a few percent and to demonstrate controlled acoustic property profile along the fiber for >20dB SBS suppression. More specifically:

i) Systematically characterize the change of SBS properties of various fibers under different diffusion conditions and UV exposure conditions.
ii) Establish and refine simulation algorithms for accurate predictions of SBS in fibers.
iii) Design and optimize longitudinal acoustic property profiles for maximum SBS suppression in active fiber amplifiers.
iv) Demonstrate SBS suppression over two orders of magnitude.
v) (optional) Demonstrated SBS suppression in fiber amplifers.
vi) (optional) Investigate the feasibility of sub-MHz 10kW fiber lasers.

2.2 Work Plan

	Year 1	Year 2	Year 3	Year 4	Year 5
Clemson	**Thrust I** i) 50μm Design optimizations ii) Develop PBF fabrication process iii) Core glass fabrication **Thrust II** i) Design optimizations ii) Establish SBS characterization iii) Establish hydrogen loading process iii) Establish UV exposure	**Thrust I** i) Develop PBF fabrication process ii) Uniform active core glass development iii) Demonstration of passive fibers **Thrust II** i) Systematical SBS tests for various conditions ii) Optimization of gas loading conditions iii) Optimization of UV exposure conditions	**Thrust I** i) Demonstrate active 50μm fiber ii) Active amplifier tests iii) Full active fiber characterization **Thrust II** i) Demonstration of controlled implementation of longitudinal acoustic profile ii) Demonstration of 20dB SBS suppression	**Thrust I** i) 100μm Design optimizations ii) Demonstration of passive 100μm core fiber ii) Refine active glass **Thrust II** i) Demonstration of potential of SBS suppression in fiber amplifiers	**Thrust I** i) Demonstration of active 100μm fiber ii) Characterization of active 100μm core fiber iii) Amplifier tests of active 100μm core fiber **Thrust II** i) Demonstration of potential of SBS suppression in fiber amplifiers
Nufern			Characterizations and tests	Characterizations and tests	Characterizations and tests
Northrop			Characterizations and tests	Characterizations and tests	Characterizations and tests

2.3 Background of the Project

Though there has been significant progress in developing fiber laser technology, there is still a great need to enhance the power scaling of both CW and pulsed lasers for use in a wide range of industrial, scientific and defense applications for precision material processing, sensors, weapon systems, particle manipulation/acceleration, and many high power nonlinear processes. A significant area of power scaling for CW fiber lasers is in the use of high power single frequency lasers for direct energy weapon development. In this case, stimulated Brillouin scattering (SBS) is a major limit. In pulsed laser systems, stimulated Raman scattering (SRS) is a major limit in peak-power scaling in systems with pulse durations longer than few hundreds of picoseconds. In ultra-short pulse laser systems with pulse duration less than few tens of picoseconds, self-phase modulation (SPM) is the major limit. Four-wave-maxing (FWM) can also be limiting in fiber systems involving multiple wavelengths. All these nonlinearities can be mitigated by effective mode-area scaling of fibers while maintaining single-transverse-mode operation. In addition, effective mode-area scaling can also lead to a high pulse energy desired in many pulse laser systems, due to an increase in the number of active ions involved in the amplification process.

The major obstacle in mode-area scaling of optical waveguides is the tendency of the waveguide to support an increase in the number of modes as the core diameter increases. Many approaches have been intensively studied in the last decade to prevent the waveguide from this increase, including single-mode operation in coiled conventional step-index fibers, chirally-coupled-core fibers, gain-guided index-anti-guided fibers, photonic crystal fibers, higher-order-mode-propagating fibers and leakage channel fibers[1-16]. Thus far, photonic crystal fibers have enabled fiber amplifiers with the largest core diameter of 100μm in a short straight length[6], while leakage channel fibers[9,10,11] and higher-order-mode propagation fibers[8,16] provides the only coiled fiber amplifiers with a core diameter beyond 50μm or an equivalent effective mode area. In general, engineered differential mode loss approaches, with robust and coilable solutions, show the most promise for mode-area scaling. The key here is to provide maximum loss for all higher order modes while maintaining minimum excessive loss for the fundamental mode. Although resonant coupling between modes can be used to increase mode propagation loss[4,15], the scalability of these approaches is limited for core diameters exceeding 35μm. For larger core diameters, it becomes more difficult to find phase-matching conditions so that out-coupling of the large number of undesired higher order modes can occur at the same desired wavelength of use. Furthermore, these higher order modes are increasingly confined to the guiding core and this significantly reduces their out-coupling efficiency and narrows their coupling resonance peaks in wavelength. On the other hand, the leaky waveguides used in gain-guided, index-anti-guided fibers[5] and leakage channel fibers[9,10,11,12] lend themselves intrinsically to high loss for all higher order modes even at very large core diameters. The fact that they do not rely on any resonant effects makes them generally broad band, easy to make and robust to use. The issue now becomes to minimize excessive loss for the fundamental mode, while maximizing all higher order mode propagation loss. Leakage channel fiber designs do a reasonable job in this regard.

In the first thrust of this proposal, we will study and demonstrate the use of all-solid photonic bandgap fibers (PBF) for effective mode-area scaling. Mode guidance in all-solid PBF is provided by the photonic bandgap effect of the cladding lattice. Low loss propagation is only possible over a limited wavelength range and strongly mode-dependent. These factors can be effectively explored for mode-area scaling. All-solid PBFs can also potentially provide much improved bend performance for large core fibers, due to their unique guidance properties. We have found in our initial study that, unlike any other known fiber designs, they do not suffer from bend-induced mode area compression. This is primarily due to the very open core/cladding boundary which easily expands modes into cladding in a bent fiber. Because all-solid PBFs are physically very much like conventional fibers, they can be potentially fabricated and similarly used. Polarization- maintaining and double-clad designs, both used in most high power laser systems, can also be easily incorporated. The unique property of transmission within a narrow wavelength can be optimized to provide strong wavelength-dependent loss. This transmission property has potential use i) for SRS suppression by providing significant loss at the Raman Stoke wavelength, and ii) to make lasers at wavelengths normally dominated by much stronger emissions. One such example is ytterbium fiber lasers at ~980nm made by suppressing the four-level system at longer wavelengths. Single transverse mode ytterbium fibers of a few hundred watts at ~980nm pumped by multiple diodes at ~915nm can potentially provide the high brightness pumps for solid state and fiber lasers. The first thrust will focus on designing and demonstrating large core fiber amplifiers (≥50μm) with solid PBFs.

Currently, SBS is the main factor limiting the further power-scaling of narrow line-width fiber lasers much beyond the 1kW power level. Our new analysis shows that optimized transverse acoustic velocity profiles provide only a limited SBS suppression. However, such approaches alone will not lead to narrow line-width fiber lasers much beyond about 1kW. The second thrust will focus on longitudinally profiling acoustic velocity along the length of fibers, potentially resulting in over two-orders of magnitude improvements in SBS threshold. More specifically, we will investigate novel concepts for achieving a controlled longitudinal compositional variation along fiber amplifiers for SBS suppression.

3. Status of the Project

<u>Thrust 1</u>

3.1.1 Fiber design

3.1.1.1 Relevant design parameters

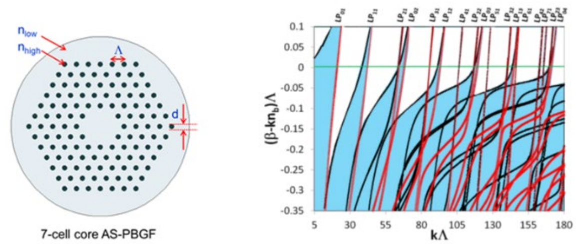

(a) (b)

Figure 1 (a) Illustration of a 7-cell all solid photonic bandgap fiber and (b) typical bandgap diagram for an all solid photonic bandgap fiber.

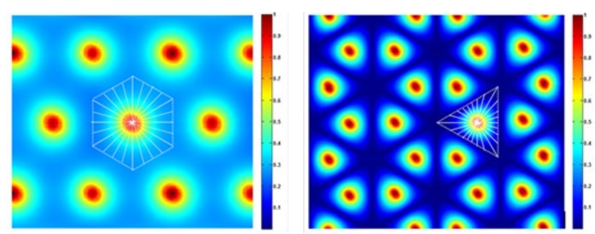

(a) **(b)**

Figure 2 Amplitude of the transverse electric field of the global mode located at (a) the upper edge and (b) lower edge of the first band.

The basic design is illustrated in figure 1. The fiber is made of two transparent glass components. The black nodes are made of higher index material such as germanium-doped silica and lower index background glass is typically made of silica. This is a 7-cell all solid photonic bandgap fiber with core formed by missing seven innermost nodes. The fiber will transmit lights in multiple photonic bandgaps illustrated in the white areas in figure 1(b). The transverse electric field of the mode at the upper edge of the first band, labeled LP_{01} in figure 1 (b), is shown in figure 2 (a) and that at the lower edge of the first band is shown in figure 2 (b). These global modes in the bands can be viewed as arising from the localized mode coupled to its nearest neighbors. Under this program, we have identified that we need to use 7-cell design and to operate in the third bandgap, third from the left in figure 1(b). This is because 7-cell design and wider third band offer better bend resistance. The relevant fiber parameters are listed below.

Λ:	center to center node spacing,
d:	node diameter,
n_{high}:	refractive index of the node glass,
n_{low}:	refractive index of the background glass,
Δ:	relative index contrast, $\Delta = 2\frac{n_{high}-n_{low}}{n_{high}+n_{low}}$
N:	number of hexagonal rings of nodes around central core, N=5 nominally,
ρ:	core radius, core diameter $2\rho = 5\Lambda$-d,
V:	normalized frequency, $V = \frac{\pi}{\lambda} d \sqrt{n_{high}^2 - n_{low}^2}$
R:	bend radius, R=15cm in all our designs,
λ:	optical wavelength, λ=1050nm for all our designs.

The designs are studied with finite element model (FEM) which allows simulation of complex designs when sufficiently mesh size is used.

3.1.1.2 Further design optimization

Design optimization of 50μm-core fibers have mostly completed before this period. This design effort is summarized in figures 2, 3 and 4. Design space is well identified. It is clearly better to operate in the third bandgap. It also shows the difficulty of achieving 100μm core diameter using this basic design. As it will be demonstrated later, an innovative multiple resonance design is both theoretically and experimentally studied in this period.

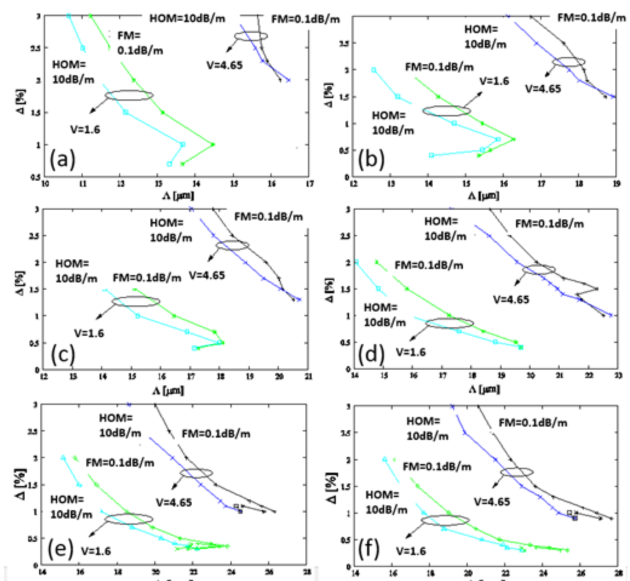

Figure 3 Design defined by maximum FM loss of 0.1dB/m and minimum HOM loss of 10dB/m for the 1st and 3rd bandgaps, 3 layers of cladding nodes, 7-cell core and various bending radius (a) 10cm, (b) 15cm, (c) 20cm, (d) 25cm, (e) 35cm and (f) 40cm.

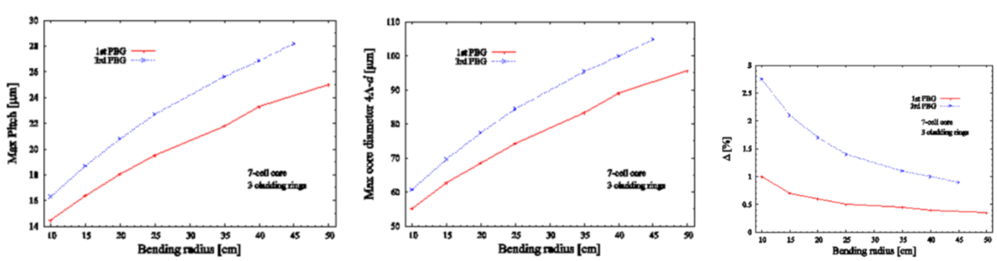

Figure 4 Optimization for maximum core diameters.

3.1.2 Passive 50µm-core Fibers

Multiple of passive 50µm-core fibers were fully characterized in the last period. The fibers have low loss (<0.1dB/m) and well defined bandgap (figure 5). The mode quality at the fiber output was well characterized both qualitatively by adjusting launch conditions (figure 6) and quantitatively by using a S^2 technique (figure 7), demonstrating robust single mode behavior. 6m fiber coiled at 50cm also demonstrate maximum PER of ~14dB (figure 8).

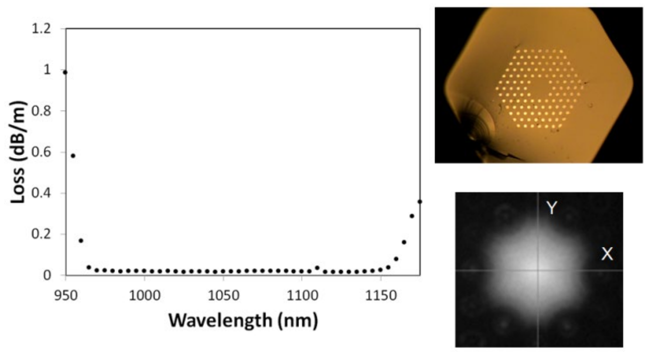

Figure 5 Typical loss measured with fiber in loose coil.

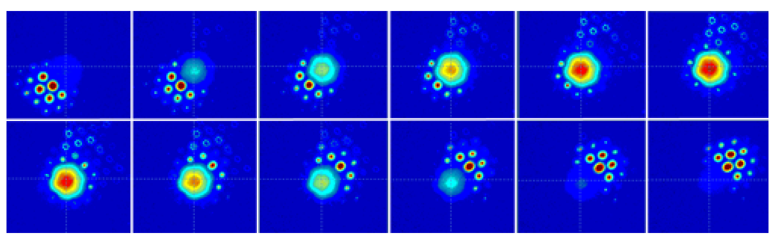

Figure 6. Near field pattern at the output of 2m of Fiber 1 coiled at 30cm while launch beam is moved slowly across the center of the fiber (sequence moving from left to right).

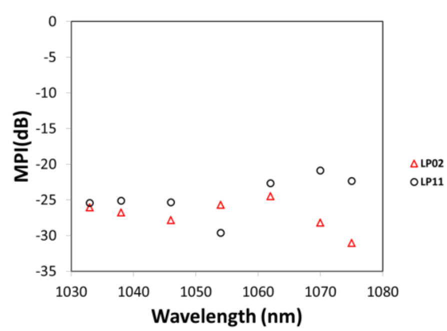

Figure 7 Mode content from 5m fiber 2 coiled at 70cm diameters.

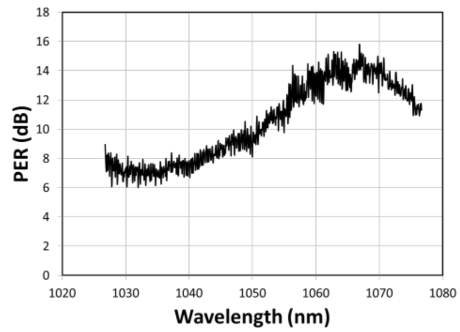

Figure 8 Measured PER in 6m fiber at coiling diameter of 50cm.

3.1.3 Active core glass fabrication

The most critical fabrication challenge of this thrust is to develop a fabrication process to make a rare-earth-doped core glass with good refractive index uniformity and accurate refractive index control appropriate for core diameter scaling towards 100μm. Regardless of the approach used, a good refractive index control of the doped core is critical for core diameter scaling beyond 35μm. As the core size increases, any localized high refractive index region within can provide localized guidance and quickly become the dominant guiding mechanism. It is critical that the active core refractive index uniformity is good enough to prevent such localized guidance. The required peak-to-peak refractive index uniformity clearly depends upon the spatial dimensions of the refractive index fluctuations. Slightly higher peak-to-peak refractive index fluctuations can be tolerated if they have smaller physical dimensions. Accurate average refractive index control of the active core glass is also critical. The requirement for this refractive index accuracy scales inversely with square of the core diameter and becomes quite strict quite quickly at large core diameters, especially for errors leading to an average refractive index slightly higher than that of the background glass, i.e. silica in all-solid photonic bandgap fibers.

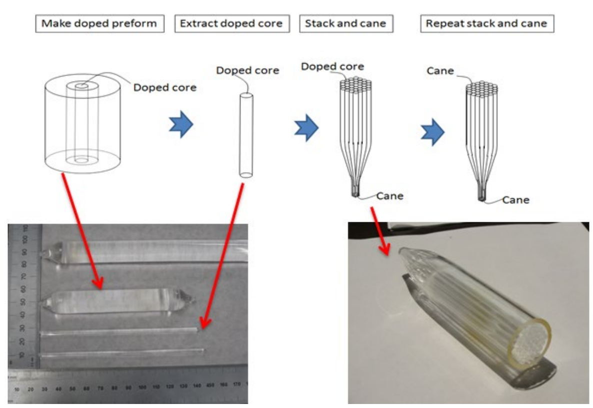

Figure 9 Basic steps for making a uniform rare-earth-doped core glass.

We must make an active core glass with peak-to-peak refractive index fluctuations of less than 1×10^{-4} and with average refractive index within -5×10^{-4} to 1×10^{-4} of silica for core diameter scaling towards 100μm. These core glasses must also be engineered to incorporate a high level of ytterbium ions with minimum clustering and photo-darkening effects. This active core glass is critical for core diameter scaling beyond 35μm.

The first step of our plan is to fabricate ytterbium, phosphorus, aluminum, fluorine and boron doped silica glass with average refractive index matched to that of the silica using a standard modified chemical vapor deposition system (MCVD). We will fabricate many preforms with an active core. The active cores will then be extracted and stacked. The stack of active cores will subsequently be drawn into canes (see figure 9 for an illustration of the process). We can repeat this process many times to reduce the dimension of the original preform cores and to achieve a high degree of averaging. The dimensions of each original preform core will be much smaller than optical wavelength in the final fiber. This smaller dimension, in combination with diffusion during fabrication, renders the often-hard-to-control original refractive index variation over preform cores no longer a problem.

3.1.3.1 1st iteration active core glass fabrication

The first iteration of ytterbium-doped core glass was fabricated in 2012. Detailed measurements indicates that the ytterbium doping level and refractive index are both lower than expected. An active leakage channel fiber was first made with the 1st iteration active core glass (figure 10). The active glass index is too low. This is indicated by the darker color in the center of the cross section image. Guided mode is significantly altered by this low refractive index. The refractive index of the fiber is measured to be $\sim 1\times 10^{-3}$ below that of the silica. An active 50μm core all-solid photonic bandgap fiber was also fabricated using this 1st iteration active core glass (figure 11). The low active glass index also make mode guidance impossible in this fiber.

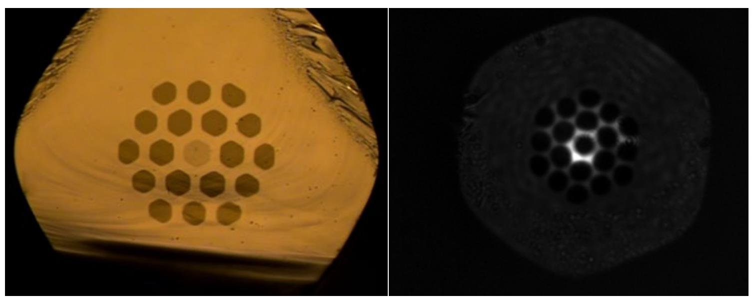

Figure 10 Cross section and mode measurement of an active leakage channel fiber made from the 1st iteration active core glass.

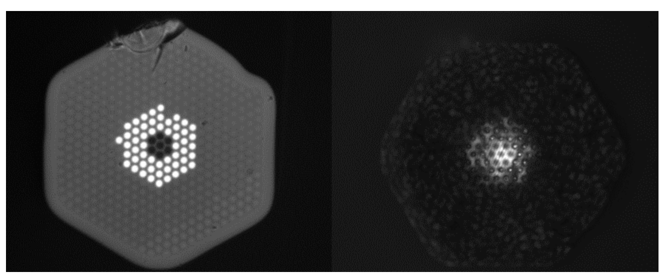

Figure 11 Cross section and mode measurement of an active all-solid photonic bandgap fiber made from the 1st iteration active core glass.

3.1.3.2 2nd iteration active core glass fabrication

The 2nd iteration active core glass fabricated started in fall 2012 once it is realized the issues that we have with the first iteration active core glass. We initially focused on further optimization of preform recipe. Ytterbium-doping level is increased by a factor of two to ~5wt. Collapse process is optimized for high phosphors content and better control. Once we satisfied with the new recipe and fabrication process, the preform fabrication started in December 2012. We have decided to tighten the average refractive index specification by ~5 times from (-5×10-4 to 1×10-4) in 1st iteration to (-1×10-4 to 5×10-5) in the second iteration (see figure 12). We have further increased the number of refractive index scan along the preform from 7 in the 1st iteration to 20 in the 2nd iteration allow capture of finer spatial variations.

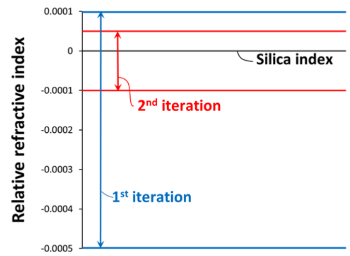

Figure 12 Average refractive index specifications used in the first and second iteration.

Repeated stack-and-draw was performed in May and June 2013. A stacking plan for the phase 1 was first developed, taking into account of both the measured average refractive index and their slope of variation along its length, so that neighbors can be chosen to achieve better average index and uniformity along the stack. The stack was formed in the graphite clamp and was then joined to a rod on the lathe. The clamp was then removed. The stack was then inserted into a clad tube of ID=24mm and OD=28mm for drawing. The stack was first dried at T=1200 ^oC, N_2=5 l/min, feed=50mm/min for 3 passes. Drawing conditions were adjusted and the following drawing parameters were used when optimized: vacuum = 3 inch water, temperature = 1850 ^oC, feed rate= 3mm/min.

Figure 13 Cross section of the phase 2 cane. Magnification increases from left to right.

Over 130 pieces of phase 1 canes were stacked inside a clad tube (ID=19mm, OD=25mm). The assembly was first dried at T=1400 ^oC, N2=5 l/min, feed=50mm/min for 10 passes. The drawing parameters were: vacuum = 4 inch water, temperature = 1950 oC, feed rate= 3mm/min, draw rate=0.81 m/min. The cross section of the phase 2 cane is illustrated in figure 13. The 134 first phase canes are clearly seen as well as the 37 original ground preforms in each first phase cane, making a total of ~5000 original ground preforms in the phase 2 cane. Once drawn into fibers, the size of the original ground preform will be <1μm and the doped glass will appear to be uniform to light.

3.1.3.3 3nd iteration Active core glass fabrication

The 3nd iteration active core glass fabrication started in December 2013 and completed in March 2015 (see figure 14 for final stack arrangement and cross section). The 2nd iteration active core glass is sufficient for 50μm cores, but better refractive index match to silica is required for 100μm. The third iteration aims to further improve absolute refractive index control.

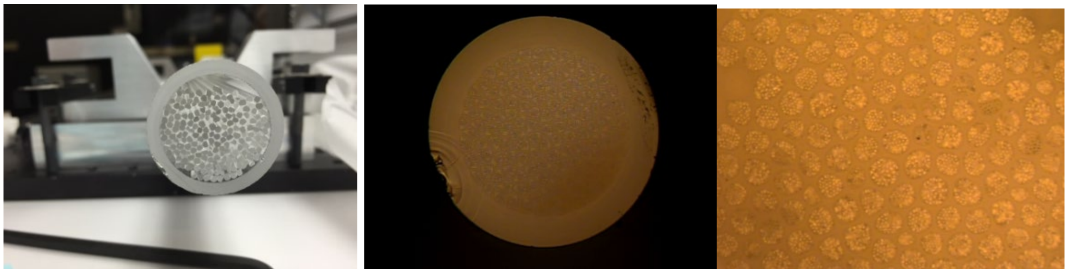

Figure 14 Refractive index target for 3rd iteration.

A step-index fiber was fabricated in order to accurately determine the refractive index. The cross section and refractive index measurements are shown in figure 15. The fabricated glass has an average refractive index of ~2.3×10^{-4}, higher than the target. The NA of this step-index fiber is ~0.026, much lower than commercial LMA fibers. 4th iteration ytterbium-doped glass is planned currently. Since 2nd and 3rd iterations have refractive index of similar magnitude but opposite signs relative to silica, we plan to mix the 2nd and 3rd interactions with a ratio of 1:1. This should get us very close to our target.

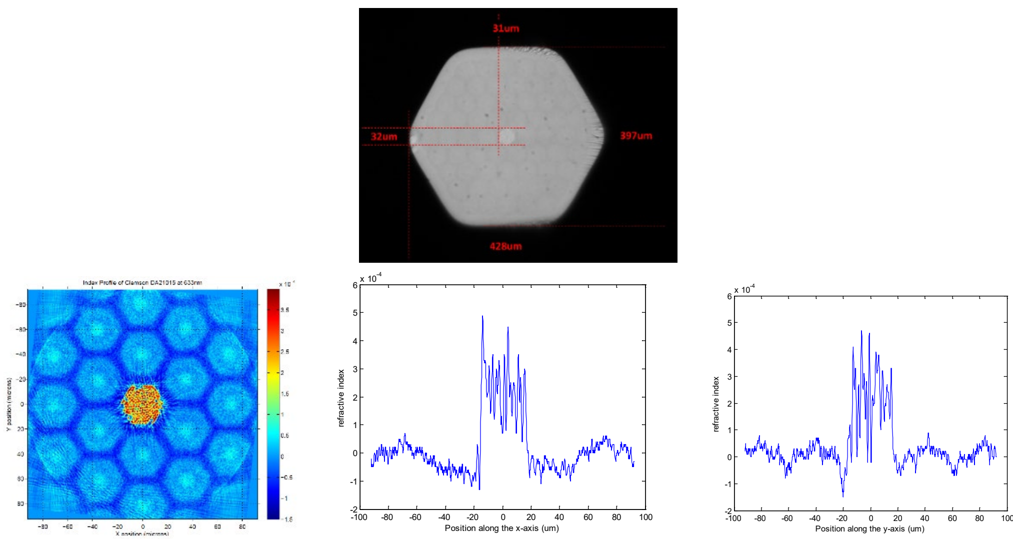

Figure 15 Step-index fiber made with 3rd iteration ytterbium-doped glass, (top) fiber cross section, (right of bottom row) 2D refractive index, (middle of bottom row) refractive index versus x-axis and (right of bottom row) refractive index versus y-axis.

3.1.4 Active 50µm-core all-solid photonic bandgap fibers

The success of the 2nd iteration active core glass fabrication enables us to proceed to demonstrate 50µm-core active all-solid photonic bandgap fibers in both lasers and amplifier configurations.

Three of the fabricated fibers are shown in Table 1. The passive fiber was fabricated for testing bandgaps, which is hard to do in active fibers. Both active fibers were drawn from the same preform while the second active PBF (Active2) was ~4% larger than the first active PBF (Active1) in dimensions. This small increment was calculated to allow true single-mode operation at the lasing wavelength. For all three fibers, the nodes in the cladding were made of germanium-doped silica with graded index profile which has a peak value of 1.48. Both active PBFs were coated with low refractive index polymer coating, providing a numerical aperture (NA) of 0.46 for the guidance of pump light. The cross-section of the Active1 PBF and the dimensions of three fibers are shown in figure 16 and table 1 respectively.

Table.1. Dimensions of Fabricated PBF

PBF	Pitch/Λ (μm)	Node Size/d (μm)	d/Λ	Core size flat to flat (μm)	Core size corner to corner (μm)	OD flat-to-flat (μm)	OD corner-to-corner (μm)
Active1	16.41	6.56	0.4	48.14	56.66	404.52	439.06
Active2	16.96	6.71	0.4	50.07	58.83	417.5	454.3
Passive	16.52	6.37	0.39	49.46	58.08	405.01	440.15

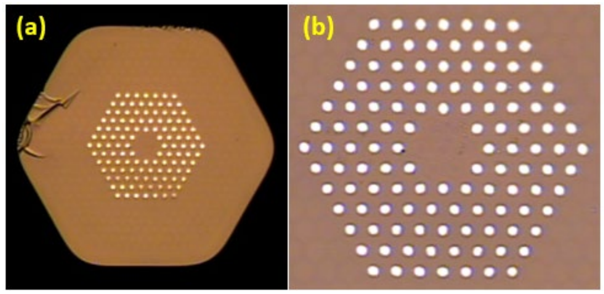

Figure 16 (a) Cross-section of the Active1 PBF; (b) Zoomed-in cross-section of Active1 PBF.

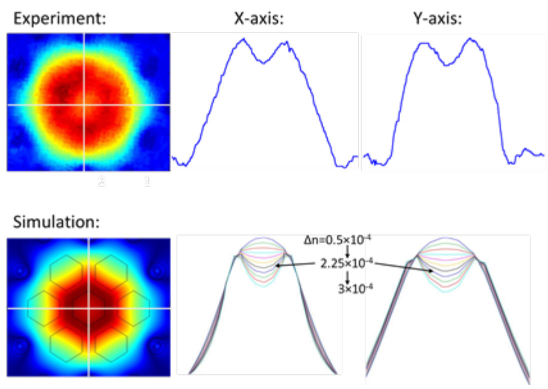

Figure 17 (a) Top: Experimental results of mode profile and intensity distribution using ASE; (b) Below: Simulation of mode profile at $\Delta n=2.25\times10^{-4}$ and intensity distributions at various Δn with 0.25×10^{-4} increments.

The core of the active PBFs consists of 7 Yb-doped rods in the center. Ideally, the refractive index of the active rods should be matched to that of silica background. However, this is very hard to satisfy and our active rods have a small index depression relative to silica. In order to determine the index depression Δn which is defined as the difference of refractive index between the background glass and the active rods, the fiber was cladding pumped well below the lasing threshold and the mode pattern was measured using amplified spontaneous emission (ASE). This was then compared to the simulation. The simulation studied mode profiles at different index depression Δn, ranging from 0.5×10^{-4} to 3×10^{-4} with increment of 0.25×10^{-4}. The mode patterns and the intensity distributions across the white axis are presented in figure 17. A shallow dip at the center of the core was observed during the experiment due to the index depression. The simulation showed this phenomenon clearly. It is estimated that the measurement best matches simulation result when Δn equals 2.25×10^{-4}.

The depressed refractive index of the Yb-doped rods would directly affect the effective mode area of the non-Gaussian-like mode. Figure 18(a) shows the effective mode area with respect to the index depression in a straight fiber. As the difference in refractive index increases, the FM becomes flatter, resulting in a larger effective mode area. At an index depression of 2.25×10^{-4}, the effective mode area reaches ~1450μm^2. On the other hand, the effective mode area at various bending radii when Δn is fixed at 2.25×10^{-4} is plotted in figure 18(b). At a bending radius of 0.25m, which is the designed coil configuration, the effective mode area is estimated to be ~1020μm^2.

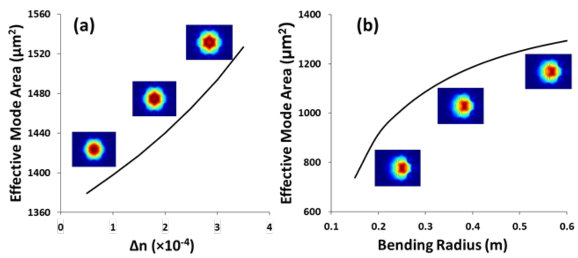

Figure 18 (a) Simulated effective area versus index depression Δn in a straight fiber; (b) Simulated effective area versus bending radius with Δn=2.25×10⁻⁴.

The two active PBFs were subjected to extensive study to determine the power scalability and robustness of single mode operation. In all the characterizations, the fiber had both ends perpendicularly cleaved to form the cavity and was laid in an aluminum groove with a 50cm diameter coil in accordance to the initial design. The metal plate also served to dissipate heat from outside coating. The fiber was cladding pumped by a commercial laser diode emitting at ~976nm (LIMO200-F200-DL980) through a dichroic mirror. The output power at 1030nm and the residual pump light were measured at the other end. The slope efficiency with respect to the absorbed pump power and lasing threshold as a function of bending diameter using 6m Active1 is shown in figure 18(a). The slope efficiency remained above 80% with the threshold below ~6W when bending diameter was kept at and above 50cm. It can be seen that from a bending diameter of 60cm to 50cm, the slope efficiency only dropped 3%, but the mode quality is expected to benefit from a tighter coil size. The optimal coil size was consequently determined to be ~50cm. The Active1 was then repeatedly cut back from its original length. The slope efficiencies versus fiber length are shown in figure 19(b). The dashed blue line indicates the slope efficiency with respect to the launched pump power while the solid red line indicates the slope efficiency with respect to the absorbed pump power. Both efficiencies increased as the fiber length was shortened until they reached maximal values of 72% and 83% at the optimal fiber length of 5.2m.

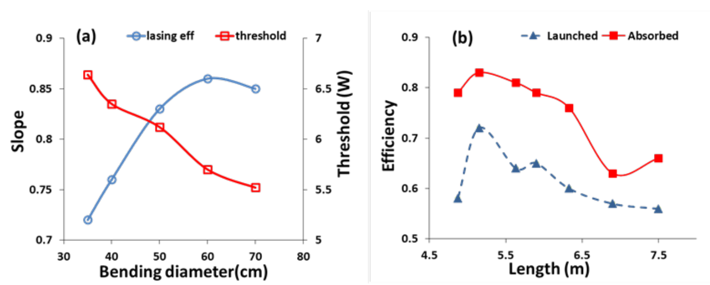

Figure 19 (a) Efficiency relative to the absorbed pump as a function of bending diameter. (b) Measured optimal fiber length to achieve maximal efficiency.

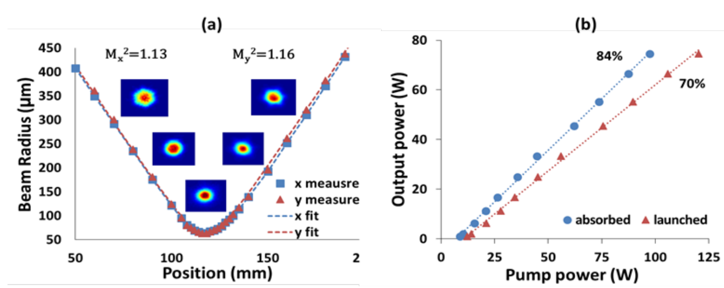

Figure 20 (a) Beam quality measurement of the output signal. Insets along the curve represent mode profiles at near-field, beam waist and other transition phases. (b) Measured slope efficiencies relative to the launched and absorbed pump power. The dotted line represents a linear fit while the solid circles and triangles represent measured values.

However, a closer look shows that Active1 did not provide single-mode operation very well at 50cm coil diameter. This was attributed to the lasing wavelength being too close to the low frequency edge of the bandgap, where the fiber is multimode[24]. The Active2 PBF with 4% increase in dimension was drawn to aim at moving the lasing wavelength of ~1030nm closer to the high frequency edge of the bandgap, where robust single-mode operation is expected. Laser output from a section of 6m Active2 coiled at 50cm in diameter was characterized for beam quality. A CCD camera traced the output beam propagation over 15cm distance. Calculation of the beam size was based on the second-moment method, yielding M^2=1.13 and M^2=1.16 along the horizontal and vertical direction respectively. The fact that M^2 is slightly larger than 1 is attributed to the non-Gaussian-like beam shape. The promising result shown in figure 20(a) implies robust single mode operation. The expected rotation of the hexagonal mode shape from near field to far field can be clearly observed. The slope efficiencies of Active2 were measured subsequently. The slope efficiencies relative to the launched and absorbed pump power were measured to be 70% and 84% respectively, which is close to the maximum efficiencies of Active1. The highest output power achieved in this configuration was ~75W, limited by the pump power available.

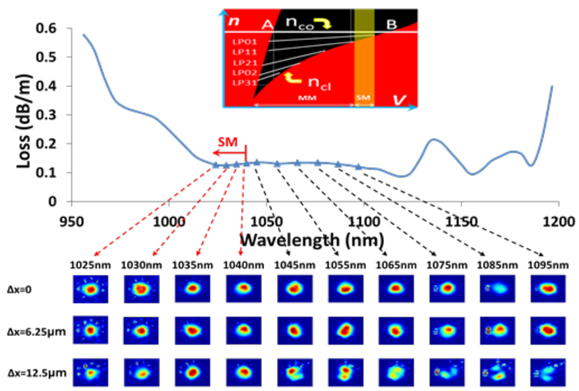

Figure 21 The transmission band measured from the passive PBF and the measured mode profile from Active2 at different wavelengths. Δx is distance of the launch offset. The inset illustrates modes supported within the bandgap of a PBF.

As mentioned before, by bringing the high-frequency bandgap edge closer to the laser wavelength, one can expect more robust single-mode operation. This can be illustrated by the inset in figure 21, as the frequency increases, the HOMs are cut off gradually at the high-frequency badgap edge and only FM is supported at the highest frequency[24]. To test the robustness of the single-mode operation, the light from a tunable laser was launched into a section of Active2 with only a single 50cm coil. The launch beam was first carefully aligned then intentionally moved by 6.25μm and 12.5μm in the transverse plane off the optimal launch condition so that HOM may be excited. Figure 20 shows the scaled transmission band obtained from the passive PBF and mode profile captured from Active2 at various wavelengths from 1025nm-1095nm. Since the index depression of the active fiber is very small, we expect its bandwidth to be only slightly narrower than that of the passive fiber while the overall bandgap structure remains the same. Near the short wavelength edge of the bandgap, i.e. at the high frequency edge of the bandgap, the fiber exhibited a clear robust single-mode regime in Active2. HOM was observed at non-optimal launch conditions above 1040nm.

In summary, we have demonstrated an Yb-doped all-solid PBF laser with a core diameter of ~50μm. The effective area is ~1450μm^2 in a straight fiber and ~1020μm^2 when coiled at 50cm diameter. The large effective mode area will help to mitigate nonlinear effects at high powers. Active1, reached 83% and 72% slope efficiencies against the absorbed and launched power respectively. Active2 reached 84% and 70% slope efficiencies with respect to the absorbed and launched power respectively. We have also confirmed robust single-mode operation in Active2 with M^2 less than 1.2 in both horizontal and vertical axes. We have also experimentally confirmed that the single-mode regime exists at shorter wavelengths close to the edge of transmission window and small fiber diameter adjustments can be used to fine tune the robustness of single mode operation, a feature unique to PBF. This work demonstrates that the significant power scalability and excellent beam quality is possible in all-solid PBF lasers.

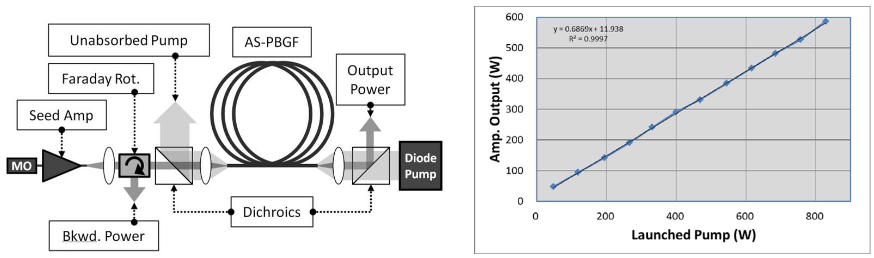

Figure 22 Amplifier demonstration at AFRL.

AFRL has demonstrated record 600W from one of our all-solid photonic bandgap fibers (figure 22). Approximately 11 m of this fiber was mounted on a cold spool possessing a diameter of 53 cm. The PBGF was pumped in a counter-propagating configuration using 976 nm diodes from Laserline. The master oscillator was a non-planar-ring oscillator (NPRO) operating at 1064 nm. The output of the NPRO was then coupled into a phase modulator for stimulated Brillouin scattering (SBS) suppression and then amplified using a multi-stage amplifier system manufactured by IPG. The phase modulation frequency was set at 400 MHz and the modulation depth was chosen such that three equal peaks corresponding to the carrier frequency and the two adjacent sidebands were generated. As much as 20 W were used to seed the PBGF. A plot of the signal power vs. pump power is shown in figure 22. The output signal power obtained was 587 W; which represents to the best of our knowledge the highest power reported to date for a PBGF amplifier. The slope efficiency for this amplifier was ~70%. At the highest output power, there was little sign of SBS.

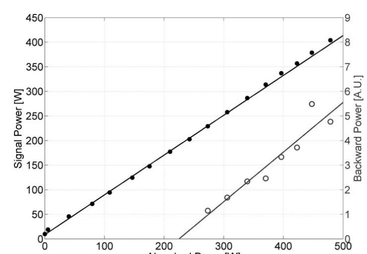

Figure 23 Signal and backward powers versus absorbed pump power for PBGF amplifier. The slope efficiency is 82%.

Very recently, using a refined 50μm-core all-solid photonic bandgap fiber with the operating wavelength moved closer to the low-wavelength edge of the bandgap to improve single-mode performance >400W single-frequency and single-mode output was demonstrated. Slope efficiency with respect to the absorbed pump power was 82% (figure 23). &m fiber was used in 65cm coil diameter. The higher-order mode was seen above 500W and output remained single-mode below ~450W (figure 24). The measured SBS Stokes wave was >20dB below Rayleigh scattering at 409W (figure 24), indicating a SBS threshold well above 400W.

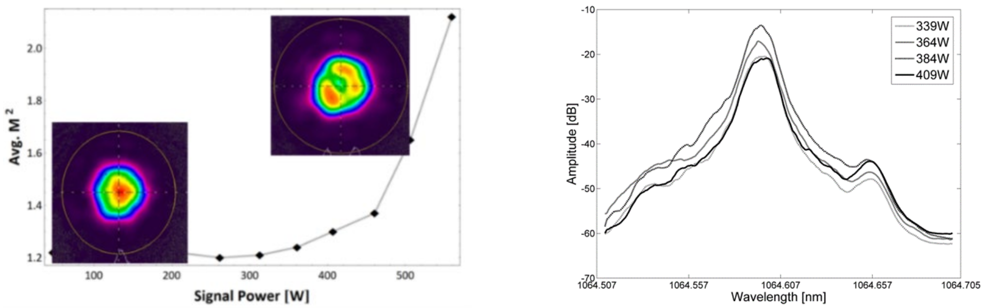

Figuer 24 (left) M² versus output powers and (right) spectra of the counter-propagarting output at various output powers

Recently we also demonstrated a polarizing ytterbium-doped 50µm-core all-solid photonic bandgap fiber (figure 25). This was achieved by introducing stress elements next to the core. The resulting high birefringence of 3.2×10^{-4} was sufficient to lower the effective mode index of the fast axis closer to the bandgap to significantly increase its loss (figure 25). The slope efficiency with respect to the absorbed pump power was 71%and the measured M^2 was ~1.17 (figure 26).

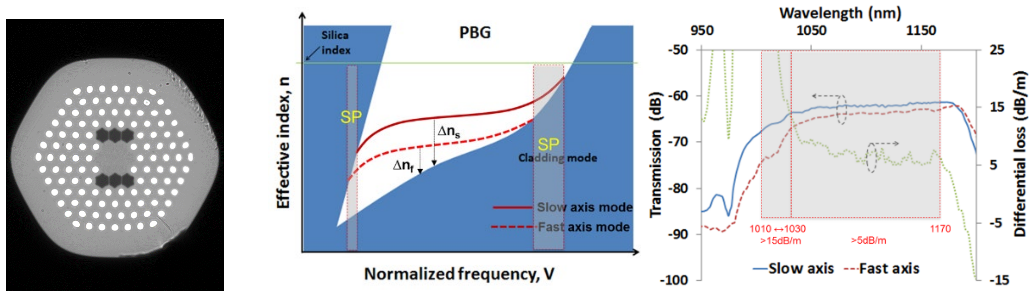

Figure 25 (left) Polarizing ytterbium-doped 50µm-core all-solid photonic bandgap fiber and (middle) operating principle of the polarizing fiber and (right) measured polarization-dependent loss.

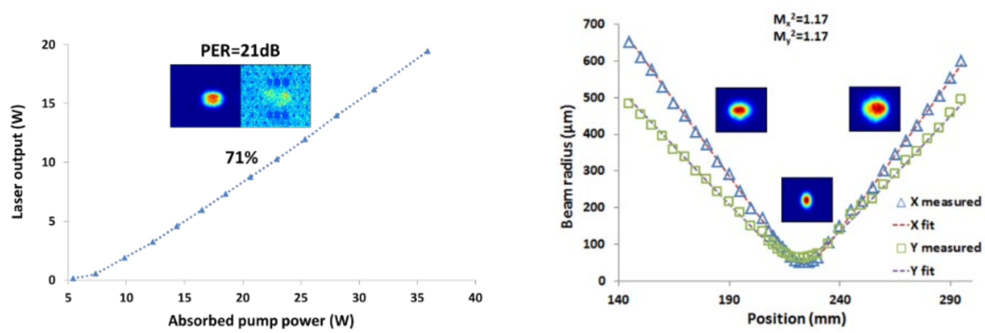

Figure 26 (left) Output power veresus absorbed pump power and (right) measured M².

3.1.5 100µm-core all-solid photonic bandgap fibers

Our first attempt at 100µm-core fiber used conventional all-solid photonic bandgap fiber design similar to those used in the 50µm-core fibers. The fabricated fiber gave poor mode quality. This prompted us to look at more refined design. The design we studied is an innovative multiple resonant fiber (MRF) shown in figure 27. We have developed a theory showing strong resonant mode coupling from higher-order core modes to cladding modes. A FEM simulation was carried to show the much better performance of the MRF (figures 28 and 29) for 100µm core. The conventional design does not show much higher-order-mode suppression at all, while MRF shows significant higher-order-mode suppression even for 100μm core (see figure 28 and 29).

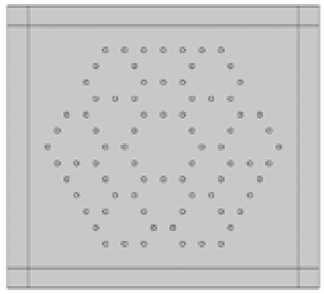

Figure 27 Multiple resonant fiber (MRF).

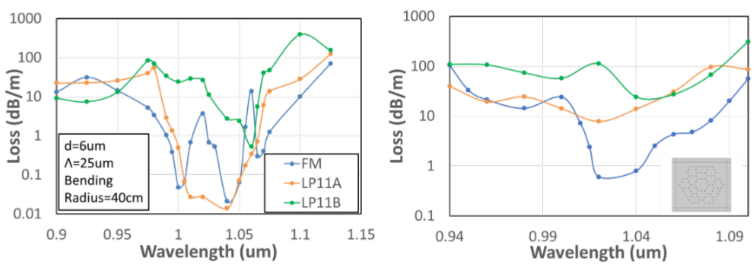

Figure 27 Comparison of 100μm-core designs for R=20cm (left=conventional design, right=MRF).

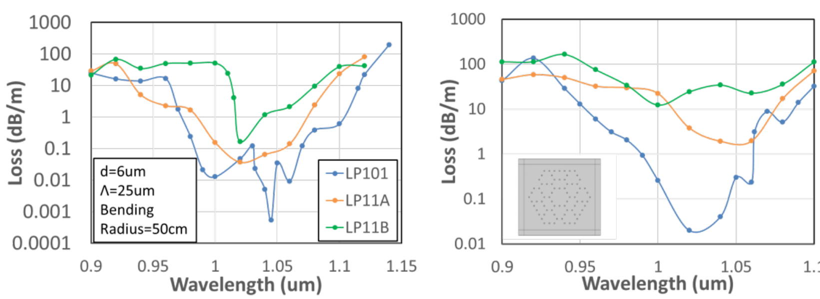

Figure 29 Comparison of 100μm-core designs for R=25cm (left=conventional design, right=MRF).

The fabricated 100μm-core fiber is shown in figure 30 along with its transmission band in figure 31. The qualitative measurement of output mode at various launch condition offset from optimum is shown in figure 32, demonstrating robust single-mode operation except at wavelengths next to the long wavelength band edge as expected.

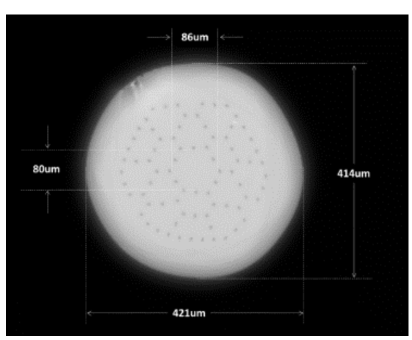

Figure 30 Fabricated MRF.

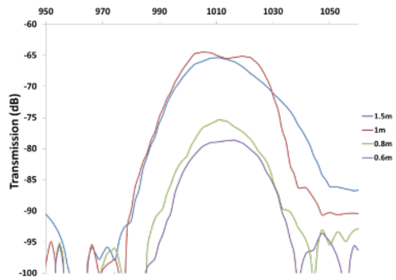

Figure 31 Measured transmission of 3m MRF (legend shows coil diameters).

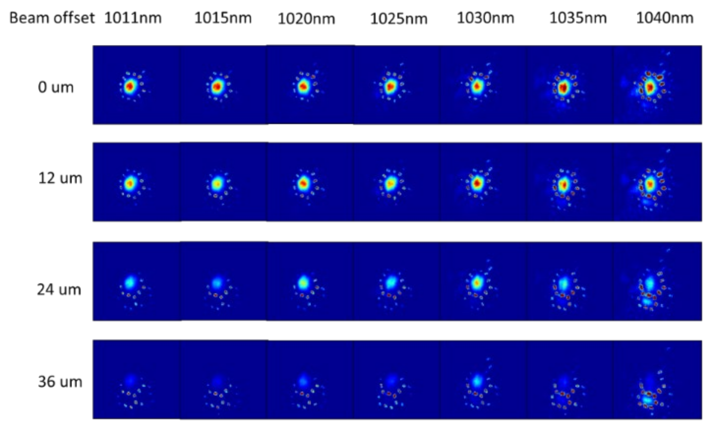

Figure 32 Measured output modes at various launch condition. The number at the left shows the offset of launch position from optimum.

3.1.6 Investigation of the physics of mode instability

Mode instability is a major limit to average power scaling at this point. It is therefore critical to understand the underlying physics better in order to mitigate it. We have initiated an effort to investigate this. In a first experimentation (see setup in figure 33), we have measured for the first time the predicted stimulated thermal Rayleigh scattering gain. The main difficulty has been to control and separate powers from the two modes. This is resolved by using polarization modes. The second difficulty is to tune the differential frequency of two optical waves at hertz level precision. This is resolved by the differential scanning technique used. The measured gain (see figure 33) shows clearly the predicted gain and loss near the zero relative frequency and the predicted response curve.

We have observed and studied mode coupling, i.e. frequency-dependent STRS gain or loss, for the first time using two polarization modes in a polarization-maintaining (PM) fiber amplifier and a pump-probe technique. The choice of the polarization modes allows us to monitor input and output of a mode easily using polarization beam splitters. The sensitive pump-probe technique allows us to perform this experiment at low powers of sub-watt levels instead of hundreds of watts, making it significantly easier. Since the interesting range of frequency difference between the two optical waves is in the several kHz (determined by transverse thermal diffusion rate), the pump and probe waves are generated from the output of a single-frequency laser with kHz linewidth by two acousto-optic modulators (AOM) driven by two ~40MHz RF wave phase-locked to a master oscillator. We can control the relative frequencies of the two RF waves down to Hz level accuracy. To our knowledge, this is the first direct measurement of frequency-dependent STRS gain. Our work firmly establishes that STRS plays a significant role in mode coupling in fiber lasers at high powers.

Assuming the powers of two modes are represented respectively by $P_1(z)$ and $P_2(z)$ and the fiber amplifier gains are independent of propagation distance z, represented respectively by g_1 and g_2, the following coupled nonlinear equations can be written for STRS power coupling between the two modes if the background loss is ignored

$$\frac{\partial P_1^N(z)}{\partial z} = -g_1 \chi\, e^{g_2 z}\, P_1^N(z) P_2^N(z) \quad \textbf{(1a)}$$

$$\frac{\partial P_2^N(z)}{\partial z} = g_1 \chi\, e^{g_1 z}\, P_1^N(z) P_2^N(z) \quad \textbf{(1b)}$$

χ is the nonlinear coupling coefficient for STRS. The normalized powers are defined as

$$P_1^N(z) = P_1(z) e^{-g_1 z} \quad \textbf{(2a)}$$

$$P_2^N(z) = P_2(z) e^{-g_2 z} \quad \textbf{(2b)}$$

The power in mode 2 can be obtained analytically for a fiber amplifier with a length of L in this case,

$$P_2(z) = P_2(0) e^{g_2 L}\, e^{g_1 \chi \int_0^L P_1(z) dz} \quad \textbf{(3)}$$

The first exponential on the right-hand side of the equation is gain due to the amplification and the second exponential term is gain due to mode coupling by STRS. If we can ignore power depletion in mode 1 due to mode coupling and the amplifier gain is sufficiently large, i.e. g_1>>1, we can simplify equation (3) to,

$$P_2(z) = P_2(0) e^{g_2 L} e^{\chi P_1(L)} \quad \textbf{(4)}$$

It is interesting to see that the STRS gain is only dependent on the output power of the first mode and the STRS nonlinear coupling coefficient χ in this case.

The choice of polarization modes was due to the ease of mode mux/demux at the input and output of a fiber amplifier using simple polarization beam splitters. This, however, brought some complications due to the nature of the polarization modes. Assuming orthogonally linearly polarized modes and a linearly polarized input, the polarization state in a PM fiber generally goes from linear to elliptical then back to linear twice over a beat length without any intensity modulation. No temperature wave is expected in this case. It is however well known that the gain of a fiber amplifier has a weak dependence on the state of polarization. With a combination of the periodical variation of the local polarization state in a PM fiber amplifier and polarization-dependent gain, a temperature wave can be generated. To enable polarization mode coupling, the temperature wave also needs to perturb the local birefringence axis periodically. In a practical fiber, any asymmetry can lead to a perturbation of the local birefringence axis by a temperature wave. All the elements are therefore in place for polarization mode coupling in a PM fiber amplifier due to STRS.

In addition, it has also been known for some time that polarization modes in highly birefringent fibers are not strictly linearly polarized, with fields in both orthogonal polarizations. The minor field component of the modes is a consequence of the stress variation across the core. This can also lead to polarization mode coupling without a rocking rotator filter.

The fiber used is PM-YDF-5/130, a double-clad PM ytterbium-doped fiber from Nufern. The core has a NA of 0.12, diameter of 5μm, MFD of 6.5μm at 1060nm, and birefringence of 2.5×10^{-4}. The cladding diameter is 130μm with a pump NA of 0.46. The pump absorption is 0.6dB/m at ~915nm. The experimental setup is shown in Fig. 1. The laser used is a Non-Planar Ring Oscillator (NPRO) single frequency laser capable of providing ~100mW with a linewidth less than 5kHz. The laser beam is split into two beams and each goes through an AOM. The two AOMs are driven by two phase-locked RF waves generated from the same master oscillator with one AOM fixed at 40MHz. The relative frequency can be tuned with Hz-level accuracy up to few hundred kHz. The two beams are launched as the seed beam into the slow birefringence axis (see inset in figure 33) and the probe beam into the fast birefringence axis. A fiber length of 4m was used, pumped by a multimode diode at ~915nm. The output powers of the probe and seed beams are measured after being separated by a polarization beam splitter.

There is always a very small amount of power leaked through to the wrong detector at the polarization beam splitters. This leaked power has a different frequency and leads to a sinusoidal amplitude fluctuation at the frequency difference between the two polarization modes. It can be easily taken out from the total measured power by analyzing the measured amplitude fluctuation and average power. This setup has an extremely high stability in the frequency difference (probe frequency – seed frequency) enabling measurement down to kHz frequency separation, limited by the laser linewidth.

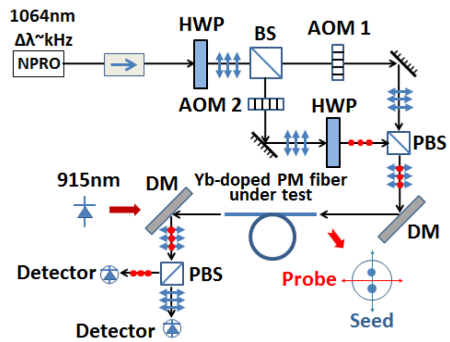

Figure 33 The experimental set up.

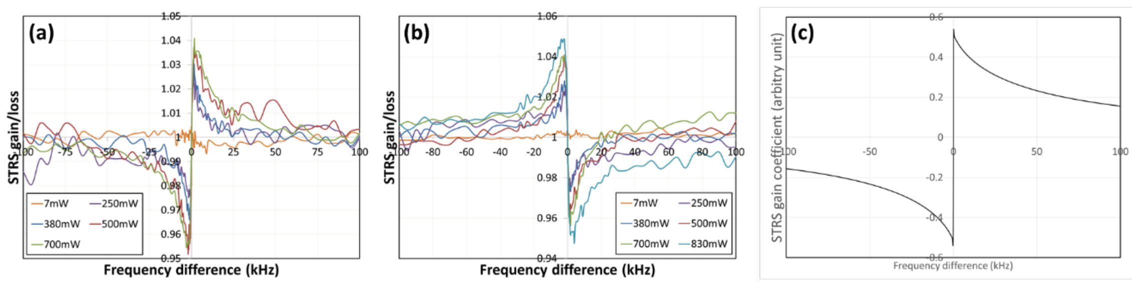

Figure 34 (a) Relative probe gain and (b) relative seed gain for both seed and probe power of 19mW, (c) simulated probe STRS gain coefficient for the PM fiber used in the experiment.

Since there is no mode coupling when the frequency difference is zero. The output power can be normalized against the output at 0Hz frequency difference to obtain gain or loss purely from STRS. With both input probe and seed power being 19mW, the measured STRS gain/loss for the probe and seed beams are shown in figure 34 2a and 2b respectively for various pump powers of 0, 2.5W, 3.3W, 5.6W and 6.5W, to give an output powers at 7mW, 250mW, 380mW, 500mW and 700mW respectively for both seed and probe as shown in the legends. The transfer of power from the seed to the probe beam at a positive frequency difference is clearly shown along with that in the opposite direction for a negative frequency difference.

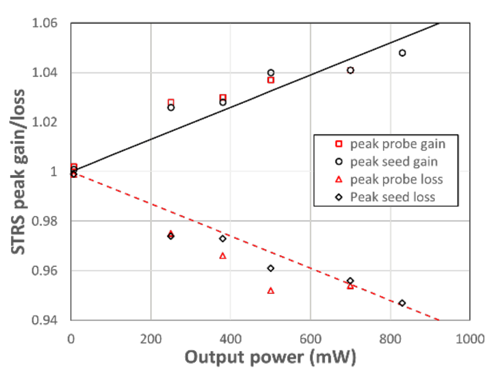

Figure 35 Peak STRS gain and loss versus seed output powers.

It is impossible to simulate the STRS gain coefficient without knowing quantitatively the nature of local heat generation and birefringence perturbation. It is however possible to obtain the shape of the frequency-dependent STRS gain coefficient if the mode distributions are known. This is shown in figure 34 2(c) for the coupling from seed to probe. The STRS gain is zero at 0Hz frequency difference and this is dictated by the phase-matching condition. The decrease in the STRS gain at larger frequency difference is due to the increasing propagation speed of the modal interference, which washes out the temperature wave. It can be seen that the measured gain spectrum is similar to that predicted by the theory.

The peak STRS gain and loss can be obtained from figure 34 and these are plotted against output powers in figure 35. In this low gain regime, the STRS gain and loss are expected to be linear with regard to the output power with a slope of χ from equation (4). The peak χ can be estimated from the linear fits in figure 35 to be ~0.065 ± 0.01 W^{-1}. This is, in fact, close to that expected for the coupling between LP_{01} and LP_{11} modes. i.e. ~0.1 W^{-1}.

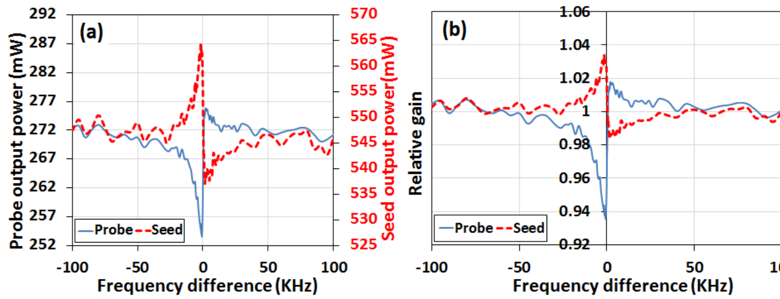

Figure 36 Output powers (a) and STRS gain and loss (b) for seed power of 19mW and probe power of 9.5mW at the amplifier input. The pump power is 3.8W.

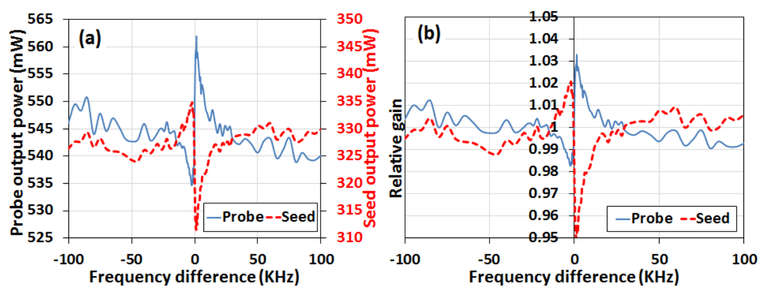

Figure 37 Output powers (a) and STRS gain and loss (b) for seed power of 9.5mW and probe power of 19mW at the amplifier input. The pump power is 3.8W.

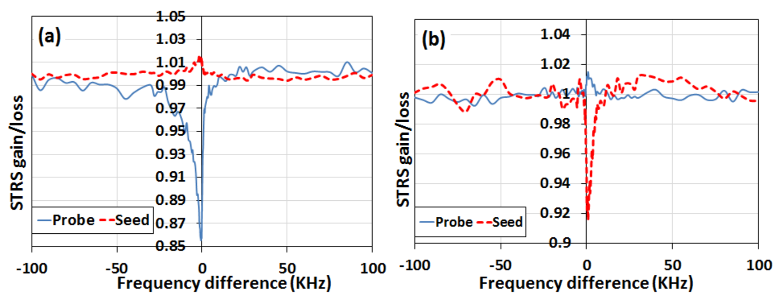

Figure 38 STRS gain and loss for (a) seed power of 19.6mW and probe power of 1.9mW and (b) seed power of 2mW and probe power of 20mW at the amplifier input. The pump power in both cases is 3W.

The mode coupling for seed input power of 19mW and probe input power of 9.5mW was also studied. The output powers of two modes are given in Figure 36 (a) and STRS gain in Figure 36 (b). A similar study was also performed for a seed input power of 9.5mW and a probe input power of 19mW. The results are plotted in Figure 37. From Figure 36 (a) and 37 (a), it can be seen that the power is roughly conserved for the coupling, i.e. the power loss in one mode is gained in the other. This translates into a larger STRS gain or loss for the mode with less power (see Figure 36 (b) and 37 (b)).

It is also interesting to note that, unlike the case when the input powers are equal, the maximum gain and loss at either side of 0Hz frequency difference are no longer roughly equal in amplitude when the two polarization modes have different input powers. Also, the power coupling to the mode with more power is stronger than the other way around.

To verify this asymmetry in coupling, further experiments were performed for seed input of 20mW and probe input of 2mW, and seed input of 19.6mW and probe input of 1.9mW. These are plotted in Figure 38 (a) and (b) respectively. The same trend is confirmed. The power coupling to the mode with more power is significantly stronger. In this case, due to the large difference in the powers of the modes, the weaker coupling, i.e. to the mode with lower power, is hardly visible.

The reasons for the asymmetry in the coupling are not immediately clear. When the powers in the two polarization modes are different, the major axis of the elliptically polarized light in the fiber is closer to the electric field orientation of the mode with more power. This may play a part in the asymmetry, making the coupling to the mode with more power easier.

In order to better understand the polarization-dependent gain, we have conducted experiments in order to characterize this. Linearly polarized light was first passed through a half-wave plate and then launched into the fiber. This allowed the easy change of polarization states. A similar fiber amplifier arrangement as in the STRS gain/loss measurement was used. The maximum polarization-dependent gain was ~0.5dB.

In order to quantitatively simulate the polarization mode coupling in this case, the extent of the perturbation of the birefringence axis also needs to be precisely known. Since this is dependent on a small asymmetry in the transverse temperature distribution relative to the birefringence axis, it is very hard to obtain. In addition, the mode coupling could potentially be influenced by other possible effects such as a minor electric field of the polarization modes. More detailed studies are necessary before a quantitative understanding of the coupling is possible.

We also measured the temporal dynamics of the coupling to provide additional evidence for its origin. In a first experiment, the frequency difference was initially set for maximum coupling at 4kHz. The seed input power was very low at 50mW compared to the probe input power of 1.13W. The probe output power was 2.33W. The amplifier had a linear gain of only ~2. The seed input was then turned off using the AOM. The typical dynamics of the seed output power after turning-off is given in Figure 39 (a). Before turning-off, there was some sinusoidal oscillation at 4kHz in the measured seed output power due to the beating between the amplified seed and the leaked probe at the beam splitter. Turning-off the seed input power caused an initial rapid change in the seed output power and the disappearance of the sinusoidal oscillation. Continued evolution in the seed output power could be clearly seen afterwards before it settled down to a constant value, from the leaked power from the probe. After the turning-off, the temperature wave took some time to disappear due to the finite rate of heat diffusion. A temporary standing refractive index grating existed in the meantime and continued to couple power from the probe to the seed, contributing towards the continued seed power evolution. In this regime, the amplifier dynamics had negligible contribution towards the seed output power.

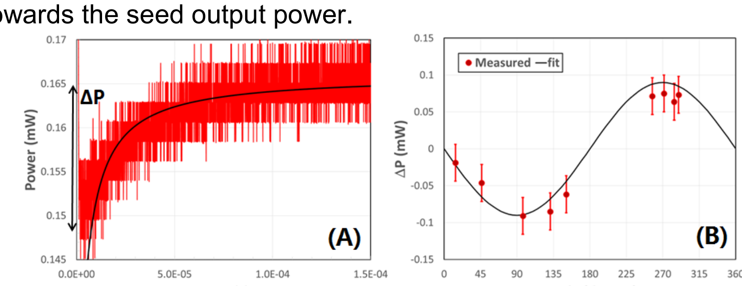

Figure 39 (a) Power evolution after the seed input was turned off (seed input power was 50mW; probe input and output powers were 1.13W and 2.33W respectively; and pump power was 3.5W), and (b) ΔP right after the turning-off versus relative phase of the two modes just before the tuning-off and a sinusoidal fit.

We repeated this experiment several times. Very similar power evolutions were observed. The initial rapid change in the seed power, however, varied. After the seed input was turned off, the total measured seed output power was from coherently combining the leaked probe power and the power coupled from the probe by the temporary grating. It was clearly dependent on the phase between the two components. The phase of the coupled power was determined by the phase of the grating. The grating was formed at the point of turning off a traveling wave and its phase was dependent on when the seed input was turned off. This phase was ultimately determined by the relative phase of the two modes at the time of the turning-off. We could determine this phase from the coherent interference right before the turning-off. The seed power difference between right after the turning-off and when the seed eventually settled down, i.e. ΔP in Figure 39 (a), should be a sinusoidal function of the phase between the two modes at the point of turning-off. This is shown to be largely true in Figure 39 (b).

The decay of the temperature change in the core after turning off a Gaussian-shaped heat source follows $1/(t+r_0^2/(4D))$, where r_0=3.25μm is the mode radius and D=8.46x10^{-7} m^2/s is the thermal diffusivity of silica. A fit based on this (black line) is plotted in Figure 39 (a) along with the measured decay of the mode coupling. The expected decay from the thermal conduction theory is consistent with the measurement.

We also conducted additional experiments in which the seed input at 4kHz frequency difference was turned on. In this case, there was a sinusoidal oscillation in the seed output power after turning-on due to the coherent beating between the leaked power from the probe beam beating with the amplified seed. It could however be subtracted out knowing its amplitude and phase. A similar dynamic as in Figure 39 (a) was observed. The measurement noise was however worse in this case due to the oscillation.

We have measured frequency-dependent STRS gain and loss for the first time, and experimentally confirmed the theoretical understanding of STRS laid out in sixties. This was possible due to innovations in the experiment setup which allow measurements at low powers, at extremely small frequency differences of kHz and with easy separation of modes. This work confirms for the first time that STRS can play significant role in mode coupling in an active fiber. This is also the first direct experimental observation of some of the key features of STRS, e.g. the gain and loss at kHz frequency shifts near the pump, which has been very difficult to measure.

3.1.7 ~ 1 kilowatt Ytterbium-doped all-solid photonic bandgap fiber laser

Despite significant development in fiber laser technology in recent years, there are still great needs to scale powers in fiber lasers for use in a wide range of applications. One promising candidate for high power fiber lasers is the all-solid photonic bandgap fiber, which can mitigate the optical nonlinear effects by scaling the effective mode-area of fibers. Recently, transverse mode instability (TMI) has been recognized as another major limit to average power scaling of single-mode fiber lasers. It is basically a mode-coupling phenomenon driven by quantum defect heating. At high average powers, TMI can develop and the power of fundamental mode in the fiber laser is coupled into higher order modes, leading to significant output beam quality degradation. Threshold in the order of 100-800w has been observed in large-mode-area PCFs. One key to mitigate TMI is to suppress the HOM propagation in the optical fiber.

It is well known that implementing additional cores in the cladding can resonantly couple the HOM from the main core to the surrounding cladding cores, leading to better HOM suppression. In our previous work, we have successfully demonstrated a passive single-mode photonic bandgap fiber operating at the 3rd photonic bandgap with the multiple-cladding-resonant core design to both extend mode areas and effectively suppress HOM in the fiber.

We report an Yb-doped multiple-cladding-resonant all-solid photonic bandgap fiber operating in the 1st photonic bandgap to further suppress TMI for higher power application. The fiber has a ~60μm diameter core and is tested with direct-diode pumping to generate up to 900w laser power which is mainly limited by un-optimized thermal management. No TMI is observed up to this power level. This is a record for single-mode power from a micro-structured fiber laser.

The cross section of the fabricated fiber is shown in Figure 40. The center main core is the active Yb-doped hexagonal core with 56μm flat-to-flat and 64μm corner-to-corner. The pump guide is also hexagonal with 415μm flat-to-flat and 428μm corner-to-corner which is coated with low-index acrylic coating to provide a pump NA of 0.46, suitable for coupling the high power pump light from diode lasers. The measured pump absorption is ~2.3dB/m at 976nm. Surrounding the center main core are some smaller cores in the cladding that are formed by purposefully taking out two and three nodes to create smaller cores in the cladding. The cladding cores and main core diameter ratios are close to 0.6 and 0.5, near the resonant conditions for coupling the major HOMs LP11 and LP21 from the main core into the cladding cores respectively. The use of multiple coupled cladding cores both enhances the coupling with HOMs in the main core and broadens the coupling resonance.

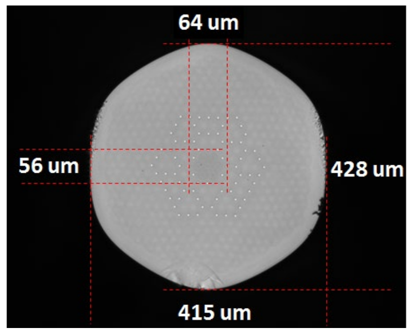

Figure 40 Cross section image of the fabricated fiber.

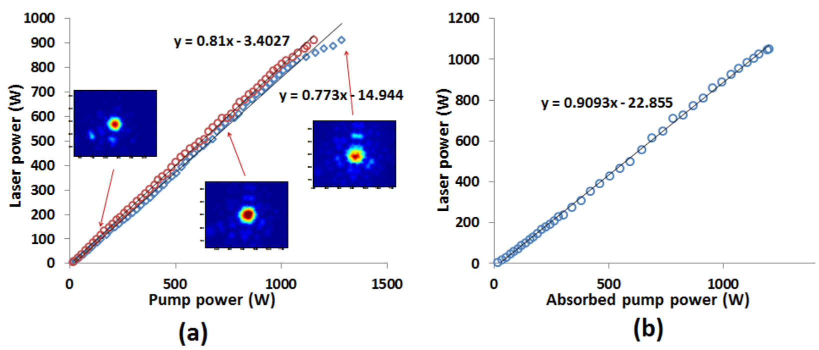

Figure 41 Lasing efficiency measurements for fiber coiled at (a) 60cm and (b) 80cm diameters.

For high power testing experiment, 9m long fiber is coiled at 60cm diameter with both ends right-angle cleaved. Most section of the fiber is submerged under water for cooling purpose and the fiber end sections are cooled by stainless steel plates. The fiber is pumped from one end by a 1.5kw DILAS diode laser emitting at 976nm. Laser is generated from both ends and collected for efficiency calculation. The maximum achieved laser power is 910w with 81% and 77% lasing efficiency corresponding to the absorbed and launched pump power, as shown in Figure 41 (a). Above that, the fiber tip is burned due to the un-optimized thermal management at the very front fiber end. The laser mode patterns are shown in the inserted photos at 130w, 600w and 900w power levels and no TMI is observed up to the maximum power of 910w. However, at 900w level, some light is found in the certain resonant cladding cores composed by removing two nodes. This indicates that certain HOM is generated in the main core and then resonantly coupled into the cladding cores, which helps to further suppress TML.

Another similar high power testing experiment with better thermal management is done on the 8m long fiber coiled at 80cm diameter with laser generated from both ends. The maximum achieved laser power is 1050w, which is limited by pump source. This time, the lasing efficiency is measured as 90% according to the absorbed pump power, as shown in Figure 41 (b). This much increased lasing efficiency may be due to the smaller bending loss at larger fiber coil size. However, the laser beam quality is found to be not as good as the result with 60cm fiber coil size, indicating the fiber bending condition still needs to be optimized.

An Yb-doped all-solid photonic bandgap fiber with a ~60μm diameter core for high power fiber laser is demonstrated. The fiber has a multiple-cladding-resonant design in order to provide better HOM suppression, which helps to better suppress TMI, one of the key limitation for average power scaling of fiber lasers. Maximum laser power of 910w is achieved for a direct diode-pumped fiber laser without TMI. Further power scaling is possible with optimized experiment conditions.

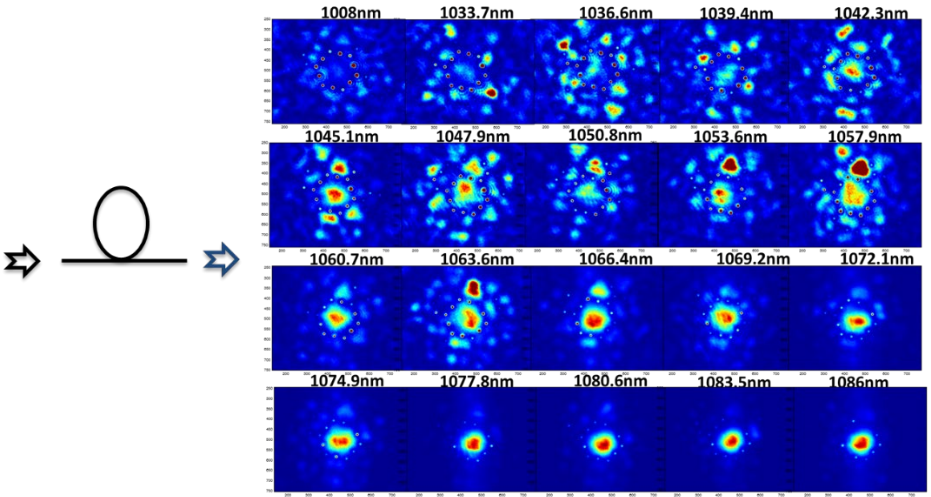

Figure 42 Mode measurement of the 1064nm fiber versus wavelength.

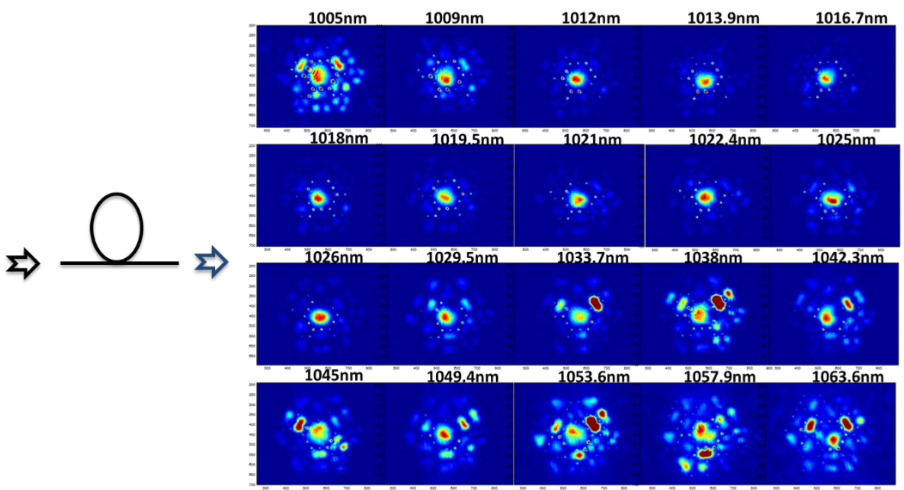

Figure 43 Mode measurement of the 1018nm fiber versus wavelength.

Despite the demonstration, the mode quality at high powers needs to be further improved. To understand what is limiting mode quality in current 1064nm fiber, we conducted mode quality measurement versus wavelength using a tunable laser. The result is shown in figure 42. It is clear that the bandgap is at 1078-1086nm for this fiber for good mode quality. The 1018nm fiber was also measured (see figure 43). The bandgap in this case is at 1014-1026nm for good mode quality. These bandgap size is ~10nm, much smaller than previous all-solid photonic bandgap fibers without multiple cladding resonance. This requires bandgap fine tuning based on measured bandgap for good mode quality. A new 1064nm fiber is drawn based on these studies.

3.1.8 Single-mode low quantum defect Ytterbium-doped all-solid photonic bandgap fiber laser

The interests in high-power fiber lasers at 1018nm is initially due to the need for pumps in tandem pumping configurations. Such tandem pumping configuration uses multimode fiber laser pumps at 1018nm instead of diode pumps at 9xx nm. This reduces heat load of the final stage fiber amplifier in a MOPA by reducing quantum defect and consequently raises TMI threshold. These multimode fiber laser pumps at 1018nm are still pumped by diodes at 9xx nm and tandem pumping configuration can be seen as trading complexity for higher single-mode powers. If high-power single mode fiber lasers at 1018nm can be directly generated using diode pumps at 976nm, this can produce the desired single-mode powers without the complexity of tandem pumps. These fiber lasers have a low quantum defect of 4.1% and is expected to have much improved TMI threshold due to the low heat load.

1018nm ytterbium fiber lasers operate more like a three-level system, where a high population inversion needs to be maintained to achieve adequate gain. This requires high pump power throughout the fiber and leads to a large amount of pump power leaving the fiber. This is not an issue for low output powers, but reduces optical efficiency at high output powers. Population inversion is dependent on both pump and signal intensity in the core. Minimizing signal intensity by using a large core can reduce the necessary pump power needed to maintain the same inversion. This reduces the amount of pump power leaving the fiber and increases the overall efficiency. A large core also leads to multimode operation. This is fine for the tandem pumping scheme. Output powers of multimode 1018nm Yb fiber lasers have been progressively increasing in recent years. One significant drawback of the tandem-pumping scheme is its complexity as large number multimode 1018nm Yb fiber lasers are needed as pumps.

A much simpler approach is to directly obtain single-mode output at 1018nm from an Yb fiber laser and, therefore, eliminate the need for the tandem-pumping scheme all together. Such a single-mode fiber laser is much simpler than a tandem-pumped laser, while a lower quantum defect of 4.1% can still be achieved when pumping with ~976nm diodes. This approach, however, is only possible with a single-mode large-core fiber. All-solid photonic bandgap fibers are excellent candidates for this. In addition, the use of a phosphosilicate host in these fibers also enhances ytterbium gain at 1018nm, leading to a reduction in the required inversion, further increasing efficiency.

In this work, we have demonstrated a record single-mode power of 220W at 1018nm from an Yb all-solid photonic bandgap fiber laser pumped at 976nm. The measured slope efficiency with respect to the launched power is ~62% and with respect to the absorbed pump power is ~77%.

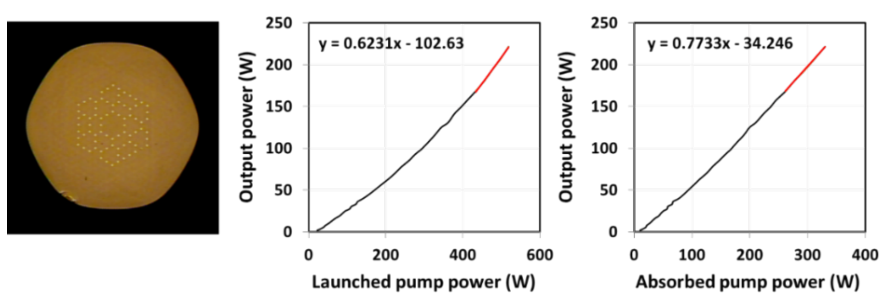

Figure 44 The fiber cross section and measured laser efficiency of the single-mode fiber laser at 1018nm.

The cross section of the fiber is shown in figure 44. It is an Yb-doped multiple-cladding-resonance all-solid photonic bandgap fiber. Multiple-cladding-resonance is incorporated to enhance higher-order-mode suppression by resonant out-coupling. The core diameter is 48μm flat-to-flat and 60μm corner-to-corner, while the cladding diameter is 381μm flat-to-flat and 395μm corner-to-corner. The laser was constructed as an oscillator with a spliced high-reflectivity fiber Bragg grating written in a photosensitive fiber matched to the active fiber and a straight fiber end. The measured efficiency is also shown in figure 44. The laser spectra are shown in figure 45 for pump powers at 80W, 180W and 240W respectively, showing a slight onset of lasing at the gain peak at ~1026nm at high pump powers. The measured mode patterns at 63W, 116W, 180W and 222W are shown in figure 46, showing single-mode operation. The M^2 was measured at 8W to be 1.28 and 1.35 with respective to the x and y axis.

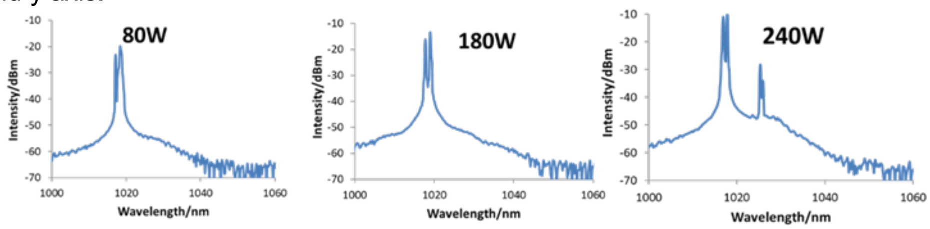

Figure 45 Spectra of the output at 80W, 180W and 240W of the single-mode fiber laser at 1018nm.

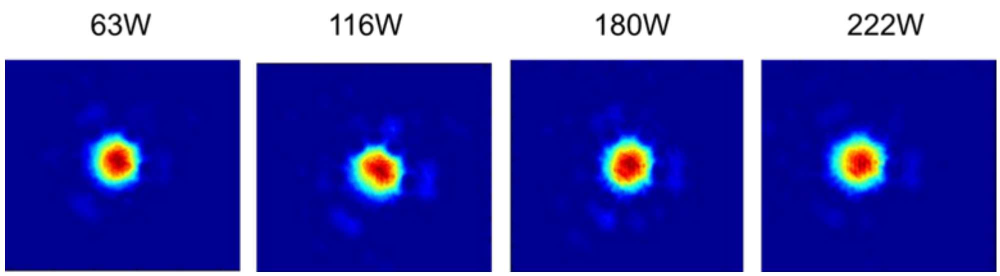

Figure 46 Measured mode pattern at 63W, 116W, 180W and 222W of the single-mode fiber laser at 1018nm.

In conclusion, we have demonstrated record single-mode output power of 220W at 1018nm from an Yb all-solid photonic bandgap fiber laser. The fiber is directly pumped at 976nm with a quantum defect of 4.1%. Compared to a tandem-pumping scheme, this work demonstrates a much simpler approach for power scaling of single-mode fiber lasers with significantly lower quantum defect heating, enabled by the single-mode Yb all-solid photonic bandgap fiber and its phosphosilicate host glass.

3.1.9 Thermal lensing in optical fibers

Average powers from fiber lasers have reached the point that a quantitative understanding of thermal lensing and its impact on transverse mode instability is becoming critical. Although thermal lensing is well known qualitatively, there is a general lack of a simple method for quantitative analysis. In this work, we first conduct a study of thermal lensing in optical fibers based on a perturbation technique. The perturbation technique becomes increasingly inaccurate as thermal lensing gets stronger. It, however, provides a basis for determining a normalization factor to use in a more accurate numerical study. A simple thermal lensing threshold condition is developed. The impact of thermal lensing on transverse mode instability is also studied.

The perturbation method used is very similar to that described in [13]. The thermal-optic effect is introduced by

$$n(r) = n_0(r) + k_T \Delta T(r) \qquad (1)$$

where refractive index profile n, initial refractive index profile n_0 and change in temperature ΔT are expressed in cylindrical coordinates, and $k_T = 1.1\times10^{-5}$ K^{-1} is the thermal-optic coefficient for silica. Under the influence of heat load, the guided mode is expected shrink down to a new equilibrium where it would be stable. This is very similar to what happens under nonlinear self-focus [13]. The only difference is in the time taken to reach this new equilibrium. It is expected to be much slower and determined by the thermal diffusion rate perpendicular to the propagation direction. Under very strong thermal lensing, the optical mode can be focused down to a very small size over a distance in the order of the Rayleigh range, similar to that in nonlinear self-focus.

The temperature profile is approximated by the parabolic solution for uniform heating in the core with a heat load of Q_0 (w/m) and we have ignored the temperature change outside the core by setting $\Delta T=0$ for $r>\rho$, where ρ is the core radius. This is reasonable for multimode fibers commonly found in fiber lasers as the optical power is mostly in the core in these cases. It is however not a good approximation for single-mode fibers where there is significant optical power outside the core.

$$\Delta T(r) = \frac{Q_0}{4\pi\kappa\rho^2}\left(\rho^2 - r^2\right) \qquad (2)$$

where $\kappa=1.38$ w/m/K is the thermal conductivity. Details of the perturbation analysis are given in appendix A. It is based on finding a relationship between modes in the fiber perturbed by the heat load and the original unperturbed fiber. With the assumption of a Gaussian mode (see equation A11 in appendix A), we can obtain an equation for the relative mode size $\gamma=w/w_0$, where w is the spot size of the mode in the perturbed fiber and w_0 in the unperturbed fiber. Spot size is half of the MFD for a Gaussian mode (see equation A11 in appendix A for a detailed definition).

$$\frac{1}{2}\xi Q_0 w_0^2 \gamma^6 + \left(U^2 + 3\xi Q_0 \rho^2 + \frac{9}{2}\xi Q_0 w_0^2\right)\gamma^4 + 3\xi Q_0 \rho^2 \gamma^2 - U^2 = 0 \qquad (3)$$

where U is the core parameter as normally defined for optical fiber, and

$$\xi = \frac{k_T k_0^2 n_{co}^2}{4\pi\kappa} \qquad (4)$$

where k_0 is the vacuum wave number and n_{co} is the core refractive index. Equation (3) can be solved numerically and the result is shown in Fig. 47 for V=3-8.

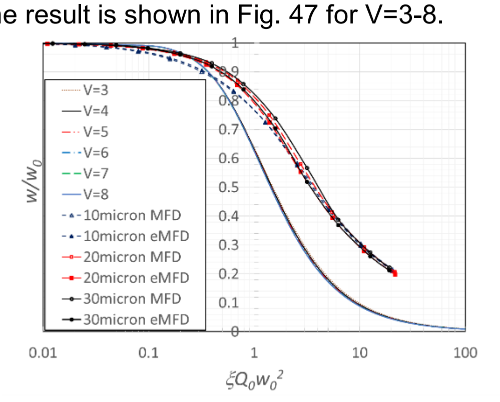

Figure 47. Mode collapse under the influence of thermal lensing. Equation (3) is evaluated for normalized frequency V=3-8. A numerical simulation is also performed for comparison for fibers with core diameters of 10μm, 20μm and 30μm and NA of 0.06. The results are plotted as MFD for near-field MFD and eMFD for effective MFD, i.e. $2(A_{eff}/\pi)^{½}$.

The relative mode size is plotted against the normalized thermal lensing parameter $\xi Q_0 w_0^2$ in Fig. 47. It can be seen that the rate of change in the relative mode size is slow at small $\xi Q_0 w_0^2$, but accelerates at larger $\xi Q_0 w_0^2$. There is very little difference in the curves for different V values. The relative mode size can collapse to small values at high heat load and the rate of change slows down when $\xi Q_0 w_0^2>2$. The most interesting observation is the fact that the effect of thermal lensing is fully characterized by the normalized thermal lensing parameter $\xi Q_0 w_0^2$, where ξ is fully determined by material properties and laser wavelength. This normalized thermal lensing parameter scales linearly with heat load Q_0 and also scales quadratically with MFD. Since the total effect of thermal lensing is determined by the integrated effect seen by the entire mode, it is reasonable to expect it to scale with the mode area, i.e. w_0^2.

For a more accurate study of the impact of thermal lensing, we need to conduct a numerical study. We will focus on the regime where the fundamental mode dominates and ignore any mode distortion due to bending. Since we are only dealing with optical modes with a cylindrical symmetry in this case, we will use an optical mode solver for an arbitrary refractive index profile with a cylindrical symmetry.

We also need to deal with the temperature profile resulting from the heat load from an optical mode with cylindrical symmetry. In our analysis, we have assumed that heat load is proportional to the local mode intensity; consequently we have ignored the effect of gain saturation. Gain saturation will lead to a flattening out of heat load in the center of the core and therefore slightly weaken the effect of thermal lensing.

Since a simple parabolic solution exists for the temperature profile in the case of a spatially uniform heat load in a cylinder, it has been used in many previous thermal analysis of fiber lasers. We need to have a more accurate numerical model for the temperature profile in a cylinder given an arbitrary cylindrical heat load profile. We start by dividing the area with the heat source into many fine layers so that we can assume each layer has a uniform heat load and we can then use the parabolic solution over each layer. This approach, however, does not have enough free parameters to ensure the solution has both continuity and continuity in the 1st order derivative at the boundary between layers, both required for a rigorous solution. We subsequently devised a scheme where we first divide the area with the heat load into many fine layers with equal thickness. We then divide each layer into two sub-layers, one sub-layer with the total heat load for the layer and one sub-layer without source. We can then use the known parabolic solution over the sub-layer with the source and the known logarithmic solution for the sub-layer without source. The relative thickness of the sub-layers can be determined by the continuity condition at the boundary between layers. This new scheme allows us to find an accurate solution while ensuring necessary continuities at all the boundaries. A detailed derivation is provided in appendix B. In the simulations in this work, the region with the heat load is typically divided into 100-200 layers. This is found to be sufficient for a stable solution.

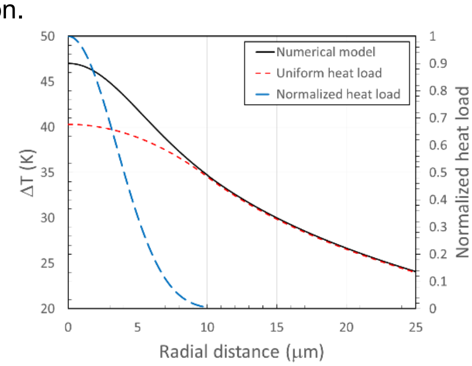

Figure 48. Comparison of the temperature profile from the numerical method used in this work and the parabolic solution for a uniform heat load. ΔT is set to be 0K at the cladding boundary. Core diameter is 20μm; cladding diameter is 400μm and NA is 0.06. The total heat load is 64w/m in both cases. The laser wavelength is at 1.03μm. The normalized heat load profile, i.e. normalized mode intensity profile, is also shown.

A comparison of the temperature profiles from the numerical model used in this study and the uniform heat load is shown in Fig. 48. The fiber has a NA of 0.06 and a core diameter of

20μm, operated at 1.03μm. We use a cladding diameter of 400μm throughout this study. The total heat load in the core is 64w/m in both cases and there is no heat load outside the core. The normalized heat load profile, i.e. the normalized mode intensity profile, is also shown. The numerical model used an iteration process described in the next paragraph to find the optical mode under heat load. It can be seen clearly that the solution in the cladding is the same for both cases and the uniform heat load model underestimates the temperature in the core. This is due to the fact that more heat is deposited near the core center than that accounted in the uniform heat load model.

In the following analysis of thermal lensing in an optical fiber, we first find the fundamental optical mode in the fiber without any heat load. We then apply one Mth of the heat load with a heat load profile equaling the fundamental optical mode intensity. The temperature profile is then calculated, which is then used to calculate the refractive index profile of the new fiber. The fundamental mode is then found for this new fiber. Two Mth of the heat load is then used with a heat load profile equaling the new fundamental mode intensity for the next iteration. This is repeated until total heat load is applied. This slow increase of heat load over many iterations is essential to keep the change in optical mode profile to a minimal for each iteration. Otherwise it can lead to numerical instabilities especially at large heat loads. We found M=30 to be adequate to ensure stability and convergence for our analysis. This is used throughout this study.

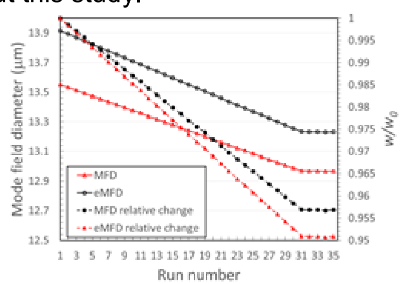

Figure 49. Typical run for the case in Fig. 2. Core diameter is 20μm and NA is 0.06. The total heat load is 64w/m. The laser wavelength is at 1.03μm. Relative changes are shown on the vertical axis on the right. The heat load is gradually increased over 30 steps.

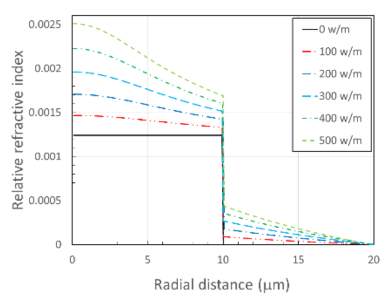

Figure 50. Refractive index profiles under various heat loads. Core diameter is 20μm and NA is 0.06. The laser wavelength is at 1.03μm.

The evolution of MFD (near-field MFD) and eMFD (effective MFD obtained from effective mode area) over the gradual increase of heat load for the case in Fig. 48 is shown in Fig. 49. The relative change in MFD and eMFD is shown on the right vertical axis. The reduction of mode size due to thermal lensing when heat load is gradually increased can be clearly seen. Also can be seen is that the mode size stabilizes at a constant value after the 31st run when the heat load is no longer increased. This demonstrates the convergence of the solution and stability of the numerical process.

The refractive index profiles obtained by the numerical model for the 20μm-core fiber are shown in Fig. 50 for various total heat loads. The refractive index profile is truncated at a radius 20μm, i.e. twice the core radius in this case. In our following analysis of optical mode, we are only concerned with the part of the waveguide seen by the optical mode of interest. We typically truncate the refractive index profile to 2 to 5 times of the core radius depending on guiding strength of the waveguide. Using an unnecessarily large cladding radius in the analysis can lead to poor numerical stability in the optical mode solver in addition to longer computation time. Care is taken in each case to ensure that the truncation does not compromise accuracy.

We then proceed to study the impact of thermal lensing on mode size for three fibers with core diameters of 10μm, 20μm and 30μm. All fibers have a NA of 0.06 and a cladding diameter of 400μm. This study is conducted for a wavelength of 1.06μm. The respective V values are 1.778, 3.557, and 5.335. The 10μm-core fiber is in the single-mode regime and the other two fibers are in the multimode regime. The results are shown in Fig. 47 for both MFD and eMFD (see figure caption for detailed definition). It can be seen that the results from the perturbation method are reasonable for a small normalized thermal lensing parameter, but overestimate the effect of thermal lensing when $\xi Q_0 w_0^2>0.1$. The results for the three fibers at $\xi Q_0 w_0^2>2$ are very close. In this regime, wave guidance is almost entirely from the effect of thermal lensing and the original waveguide plays a very small part. At smaller $\xi Q_0 w_0^2$, the single-mode fiber suffers slightly more mode size reduction. The mode is much larger than the core in the single-mode regime and this enhances the impact of thermal lensing on mode size. MFD and eMFD follows each other fairly closely. A convenient place to set the thermal lensing threshold is $\xi Q_0 w_0^2=0.5$, where the mode size is reduced by ~10% and the effective mode area by ~20%. This study is able to quantify the change in mode size for this condition for the first time; the mode size is reduced by ~4% and the effective mode area by ~8% at $\xi Q_0 w_0^2=0.18$.

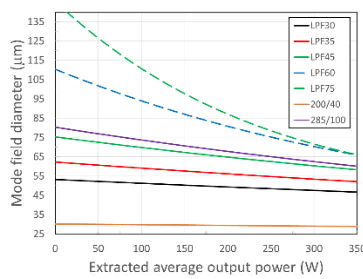

Figure 51. Simulated MFD for the fibers in [9]. Quantum defect heating is used to convert heat load to extracted power. Average heat load is used.

Using the numerical study shown in Fig. 47, we can also provide a theoretical mode size change for the experimental work in [9]. Quantum defect heating is used to convert heat load to extracted power. The average heat load over the amplifier is used, since this can be easily found in the paper but not the more relevant peak heat load. This will underestimate the effect of thermal lensing in this case. This is shown in Fig. 51. For three fibers with smallest MFDs, the predicted MFDs are very close to those measured (within few percent). The divergence becomes large for the fibers with large MFD (>80μm). The measured data for those fibers are highly scattered, indicating much larger measurement errors in this regime. This model does not consider effects such as anti-crossings with modes originated in the cladding and photo-darkening, which are known to take place in some of these fibers. It nevertheless provides a reasonable qualitative agreement with the measurements even for fibers with large MFD.

There is a strong interest in understanding the impact of thermal lensing on TMI. TMI can be quantified by the TMI nonlinear coefficient χ. TMI threshold is inverse proportional to χ and also dependent on input higher-order-mode power and amplifier configuration. Since we can easily evaluate the refractive index profile of the fiber under thermal loading, we just need to find the fundamental and higher-order modes to evaluate χ under the influence of thermal lensing. We have assumed that the fundamental mode is dominating in this case and conducted this study for the LP_{11} mode. Our cylindrical optical vector cannot directly find the LP_{11} mode, but can find its constituent TE_{01} and HE_{21} modes. These modes have the same radial intensity profile as LP_{11}. We therefore found the radial mode intensity profile for the HE_{21} mode and used this for our study.

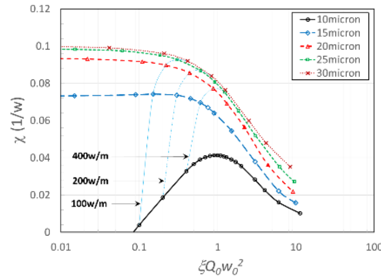

Figure 52. Simulated TMI nonlinear coupling coefficient for fibers with core diameters of 10μm, 15μm, 20μm, 25μm and 30μm respectively. The fiber NA is 0.06 and cladding diameter is 400μm. This study is conducted at a wavelength of 1.06μm. Contour lines indicate constant thermal load.

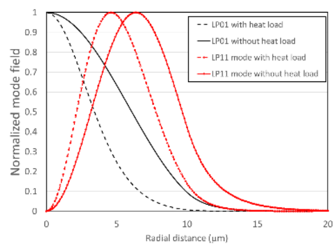

Figure 53. The LP_{01} and LP_{11} modes at 1.06μm in a fiber with a NA of 0.06 and a core diameter of 20μm without heat load and with a heat load of 1000w/m, i.e. $\xi Q_0 w_0^2 = 2.19$. The cladding diameter is 400μm.

We studied 5 fibers with core diameters of 10μm, 15μm, 20μm, 25μm and 30μm respectively. The fiber NA is 0.06 and cladding diameter is 400μm. This study is conducted at a wavelength 1.06μm. The V values are respectively 1.778, 2.667, 3.557, 4.446, and 5.335. The results are shown in Fig. 52. The 10μm-core fiber is single mode at low heat load, but the LP_{11} mode is guided when $\xi Q_0 w_0^2 > 0.084$. Its TMI nonlinear coupling coefficient χ increases until $\xi Q_0 w_0^2 = \sim 1$ as the LP_{11} mode is increasingly guided. When $\xi Q_0 w_0^2 > 1$, thermal lensing becomes significant and χ starts to decrease. Thermal lensing pulls all modes to the core center, but this is more significant for the fundamental mode (see Fig. 53). This lowers the overlap between the LP_{01} and LP_{11} modes, consequently leading to a reduction in χ. A similar trend can be seen for the 15μm-core fiber. Since the LP_{11} is already well guided in this fiber with heat load, the initial increase in χ at low heat load is less pronounced. χ starts to decrease when $\xi Q_0 w_0^2 > 0.3$. The remaining fibers have similar χ at low heat load; this is due to that fact that χ changes very slowly at large V. For these fibers, χ starts to decrease significantly when $\xi Q_0 w_0^2 > 0.3$. Similar studies were conducted for LP_{02} mode and similar trends were obtained. This reduction of TMI at high thermal load is, however, of limited practical use as the effect of thermal lensing is significant at this point. For most practical fibers, the TMI threshold is also well below this thermal load.

We have studied thermal lensing effects in optical fibers with both a perturbation method and numerical method and have developed a normalized thermal lensing parameter. A simple thermal lensing threshold condition is also developed. We have further studied the impact of thermal lensing on TMI and found that strong thermal lensing leads to a reduction in TMI.

3.1.10 Further increase of TMI threshold by reducing core diameter

TMI threshold is expected to inversely scale as square of core diameter and therefore 4kW TMI threshold is expected if core diameter is reduced from 50μm to 25μm. There is correspond reduction in SBS threshold, but this can be compensated by broadening the laser linewidth. An all solid photonic bandgap fiber with a core diameter of 25μm was fabricated recently (see Fig. 54 for cross section). This fiber has 400μm cladding diameter with a pump NA of 0.46. The pump absorption was measured to be 0.8dB/m at 976nm. The estimated SBS threshold at 2GHz linewidth is ~4kW. The fiber can be coiled down to 20cm in diameter (see Fig. 54).

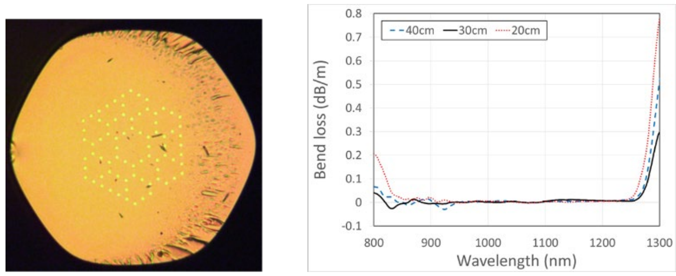

Figure 54 Cross section of the 25/400 fiber and its measured bend loss.

Thrust 2

3.2.1 Brillouin gain characterization system

Previously, we have demonstrated the effectiveness of the proposed technique. The fiber was measured for its Brillouin gain spectrum. The setup is shown in figure 55. It is effectively a pump and probe measurement with counter-propagating pump and probe beams. Pump and probe beams are from two NPRO single frequency lasers capable of providing ~100mW with a line width less than 5kHz. Two isolators are used to prevent feed backs into the NPRO lasers (JDSU). Both pump and probe beams propagate in the same polarization in the PM fiber. The pump is amplified further by an ytterbium-doped fiber amplifier to increase sensitivity of the system so that Brillouin gain spectrum can be measured for centimeter long fibers. A Faraday rotator combined with a Polarizing beam splitter is used to separate the amplified probe beam from the pump for spectrum measurement. The probe frequency is tuned over 16 GHz by thermally tuning the crystal in the NPRO generating the probe beam. A RF spectrum analyzer is used to measure the frequency separation between the pump and probe beams. The key motivation of using the configuration in figure 55 is its high sensitivity in measuring Brillouin gain. This enables that our Brillouin gain spectrum is measured in the low-gain spontaneous Brillouin regime with minimum bandwidth narrowing from any stimulated effects.

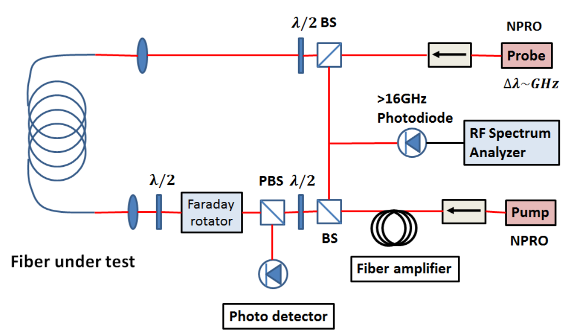

Figure 55 Setup for Brillouin gain measurement.

3.2.2 Fiber treatments

The fiber used in this experiment is a Thorlabs Panda polarization-maintaining (PM) fiber with a NA of 0.12 and MFD of 6.6μm at 980nm (PM980-XP). The cladding diameter is

125μm and coating diameter is 245μm with dual acrylate coating. Second mode cut-off wavelength is 920±50nm. Nominal polarization mode cross talk is less than -30dB at 100m.

The fiber is kept in hydrogen cell for typically well over a week at a pressure of ~150Bar. For the first set of the experiment, the fiber was stripped of coating and exposed to UV light from the side straight after being removed from the hydrogen cell. The laser used is a diode-pumped frequency quadrupled YAG laser at 266nm from Newport Corporation (Hippo 266-2C), which is capable of providing an average power of 2W at 50kHz repetition rate. Pulse width is 11ns. The beam was moved by a mirror mounted on a translation stage to scan along the fiber. The beam was focused with a cylindrical lens onto the fiber. Minimum of 10cm length of the fiber is uniformly exposed. A transmission measurement was then performed to characterize the OH peak at ~1.4μm. The absorption coefficient of OH at ~1.4μm was given to be 50.4dB/km/ppm by Keck et al, 61.9dB/km/ppm by Elliott et al and 60.6dB/km/ppm by Clasen et al. Incorporated OH level was calculated using the coefficient of 50.4dB/km/ppm given by Keck in this work. Using the second order mode cut-off wavelength of 920nm, we could calculate the V value at 1.4μm is ~1.58. The fraction of power of the fundamental mode in the core can then be estimated to be ~44%. Assuming the OH is in the core, OH level was then calculated considering this overlap factor.

3.2.3 Brillouin gain characterizations

The measured Brillouin gain spectrum of the original fiber is shown figure 56(a), showing a single peak at 15.88GHz and a FWHM of 50MHz. The measured Brillouin gain spectrum of a 0.7m long fiber with 0.3m treated is shown in figure 56(b). The measured OH level is 4150 wt ppm in the treated section in this case. The Brillouin gain spectrum shows two peaks. The peak at 15.88GHz is from the untreated section of the fiber. The Brillouin frequency shift is lowered by 140MHz in the treated fibers. Figure 56(c) shows the case where 0.1m of a 0.46m fiber was subject to longer UV exposure time. The measured OH level is 5600 wt ppm with corresponding Brillouin frequency shift lowered by 180MHz. The UV exposure in Figure 56(d) was further increased. The Brillouin frequency shift over the treated 0.1m section with measured OH level at 12500 wt ppm is lowered by 276MHz.

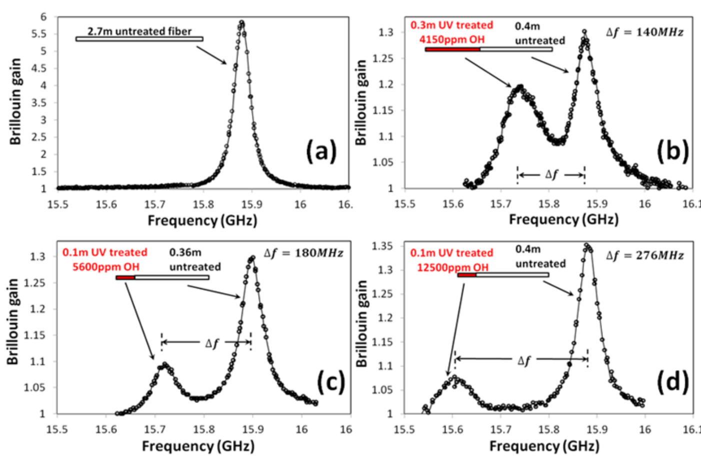

Figure 56 Measured Brillouin gain spectrum for (a) 2.7m original fiber, (b) 0.3m treated fiber with 4150 wt ppm OH and 0.4m untreated fiber, (c) 0.1m treated fiber with 5600 wt ppm OH and 0.36m untreated fiber and (d) 0.1m treated fiber with 12500 wt ppm OH and 0.4m untreated fiber.

The measured change in Brillouin frequency shift versus measured OH level in the treated fiber is shown in figure 57(a). The slope is around -2% per wt% of OH. If we can ignore the changes in the modal index n and bulk modulus E, the relative density change $\Delta\rho/\rho$ required for the observed -2% change in $\Delta f_B/f_B$ is -4%. If all the hydrogen molecules are incorporated in the glass in the form of OH, we can estimate the density change from the addition of hydrogen atoms in the glass. The measured OH level is 12500 wt ppm for the -2% change in $\Delta f_B/f_B$. Considering that the oxygen atoms are already in the glass prior to the treatment, 12500 wt ppm OH corresponds to a density change of 0.074% in density. This is far too small to account for the required 4% change in density.

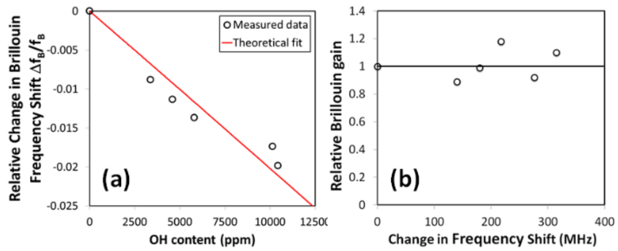

Figure 57 Measured change in relative Brillouin frequency shift due to treatment versus measured OH level in the treated fiber, red solid line is from Eq. 3 assuming $\Delta E/E$ changing at -4% per wt% of OH, and (b) Ratio of Brillouin gain per unit length in the treated fiber over that of the original fiber versus measured change in Brillouin frequency shift.

Changes in modal index n and bulk modulus E must therefore be considered in this case. From the works on photosensitivity, we know the refractive index will increase as a result of the hydrogen treatment. The relative increase in modal index is expected to be much less than 1%. This increase of refractive index will lead to an increase of f_B, and partial cancellation of the observed reductions in f_B. Bulk modulus was, however, observed to change by -12% per wt% OH in silica glass. Ignoring any changes in mode index and density ρ, this along can lead to $\Delta f_B/f_B$ change by -6% per wt% OH. Using ultrasonic micro-spectroscopy, longitudinal acoustic velocity was measured to change by ~-3% per wt% OH, corresponding to a bulk modulus change of ~-6% per wt% OH. Using a bulk modulus change of ~-4% per wt% of OH, a good fit to the measured data (see red solid line in figure 57(a)) is achieved. This bulk modulus change is slightly higher if we consider any positive change in modal index n. Density change can be neglected in our case. This level of change in bulk modulus is consistent with what was reported and sufficient to explain the large change in f_B observed in this work. We, therefore, believe that the significant change in bulk modulus at higher OH levels is largely responsible for the observed significant change in Brillouin frequency shift. The reduction of bulk modulus may arise as a result of the breaking up of closed SiO_2 tetrahedral network by the forming of the dangling OH bonds.

In order to quantify any change in the Brillouin gain in the treated fiber, we plotted the ratio of Brillouin gain per unit length over that of the original fiber as relative Brillouin gain in figure 57(b). The ratio stays essentially around 1, indicating there is no measurable change in the level of Brillouin gain in the treated fibers.

3.2.4 Tailoring acoustic velocity along the fiber

Once we have established that a significant change in Brillouin frequency shift can be achieved using this technique, we investigated the feasibility of UV exposure from one end of the fiber. A 1.9m fiber was first loaded with hydrogen and then exposed to UV by launching the UV light into the first end of the fiber. The output from the second end was monitored and used to optimize launching condition. The fiber was exposed for 5hrs. The long exposure was to ensure saturation. The Brillouin gain spectrum was measured by launching the probe beam into the first end of the fiber. The fiber was then successively cut back from the second end. Brillouin gain spectrum was measured after each cut-back. The measured Brillouin gain spectra are normalized to the peak gain and plotted in figure 58(a). A curve fitting is performed for each of the Brillouin gain spectra by iteratively guessing the local Brillouin frequency shift while minimizing fitting error. Since we expect the slope in the Brillouin frequency shift distribution along the fiber is high towards the UV launching end, i.e. the first end, we expect the Brillouin gain spectrum is dominated by the part of the fiber where the Brillouin frequency shift changes slowly along the fiber, i.e. towards the second end. This can be clearly seen in figure 58(a). For the longer fiber length, the measured Brillouin gain spectrum is getting narrower and getting more and more like the Brillouin gain spectrum of the original fiber. Consequently, we expect a larger error in the obtained local Brillouin frequency shift towards the UV launching end by this method, i.e. the first end. This is especially true for longer fiber lengths. We therefore discarded the Brillouin frequency shift data obtained from the curve fitting over the half of the fiber towards the UV launching end. We only keep the entire data for the shortest three fiber lengths, i.e. 50cm, 60cm and 70cm. The Brillouin frequency shift along the fiber obtained by the curve fitting are shown in figure 58(b) for each of the fiber length measured. Also plotted is an exponential fit in solid black line. It can be seen that the measured Brillouin frequency shift distribution is fairly close to the expected exponential. The maximum change in Brillouin frequency shift is ~150MHz in this case. UV absorption is determined from the exponential fit to be ~1.3dB/cm at the UV laser wavelength of 266nm.

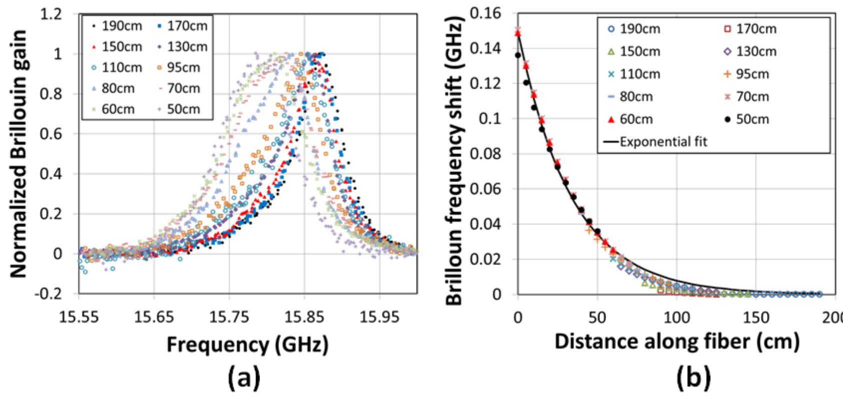

Figure 58 (a) Normalized measured Brillouin gain spectra of a fiber UV-exposed by launching UV light into the first end of the fiber. The fiber was 1.9m long. It was then successively cut-back from the second end to shorter lengths. Brillouin gain was measured for each length of fiber by launching probe into the first end of the fiber. The fiber lengths are shown. (b) The Brillouin frequency shift along the length of fiber obtained by curve fitting the measured Brillouin gain spectrum for each length of fiber. An exponential fit is also shown in solid black line.

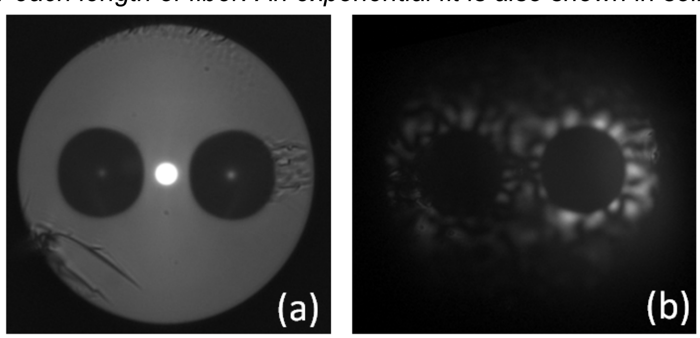

Figure 59. (a) Cross section of the fiber. (b) Image of UV light at the output of the 1.9m fiber.

The loss of pure silica core Schott fiber was measured to be ~0.5dB/cm[21]. In germanium-doped fibers, the loss is much higher due the presence of absorption peaks at ~240nm due to GODC. The loss of a 3mol% germanium-doped optical fiber (Telecom Fiber) and a 10mol% germanium-doped optical fiber (AT&T Tethered Vehicle Fiber) were measured to be ~30dB/cm and ~100dB/cm at ~266nm respectively[22]. Since our measured UV loss is close to that of the silica than germanium-doped silica glass, we took the image of the output ends with a CCD camera during the UV exposure. This is shown in figure 59(b), along with the cross section of the fiber when illuminated by a white light source in figure 59(a). It is interesting to see that the UV light is mostly guided around the two stress elements in the silica cladding glass. Stress elements are typically made of boron-doped silica with much higher thermal expansion coefficient than that of the surround silica glass. Once the stress elements and the surround silica cladding solidify during the draw, the boundary between the two materials is fixed. The silica glass will try to restrain any further contraction of stress elements during the subsequent cooling process. This can put the surround silica glass under strong compression once the fiber is cooled down to the room temperature. This compression can raise the refractive index of the silica cladding around the stress elements and forms waveguides.

3.2.5 Pressure increase with liquid nitrogen cooling

For further improving SBS suppression, higher level of hydrogen is required. We are limited by the bottle pressure from our commercial supplier. We have implemented a setup which allows the immersion of the pressure cell in liquid nitrogen. The hydrogen bottle is connected to the pressure cell when the cell reaches liquid nitrogen temperature. The cell is then closed and allowed to return to room temperature. Pressure is increased by a factor of 3 to 450bar. This allows SBS frequency shift of 1GHz, corresponding to SBS suppression of 13dB.

3.2.6 SBS suppression in fiber amplifiers

Our focus has been on SBS suppression in fiber amplifiers to demonstrate the effectiveness of the technique in a practical system. The successful passive fiber tests so far used fibers with germanium doping in the core. Germanium doping leads to a strong absorption band at ~240nmm arising from oxygen-deficient centers (ODC). The ODC band has sufficient absorption at 266nm, which is critical for the UV exposure at 266nm using an in-house frequency quadrupled YAG laser (see red line figure 52). The active fibers used in ytterbium-doped fiber amplifiers do not have germanium, but has aluminum and phosphor. Both lead to low absorption at 266nm (figure 60). Short wavelength source is required to cause the desired effect. KrF excimer laser 248nm was tested in this period without success. A UV laser at 213nm (see blue line in figure 60) has been located. Fibers are prepared for testing at 213nm currently.

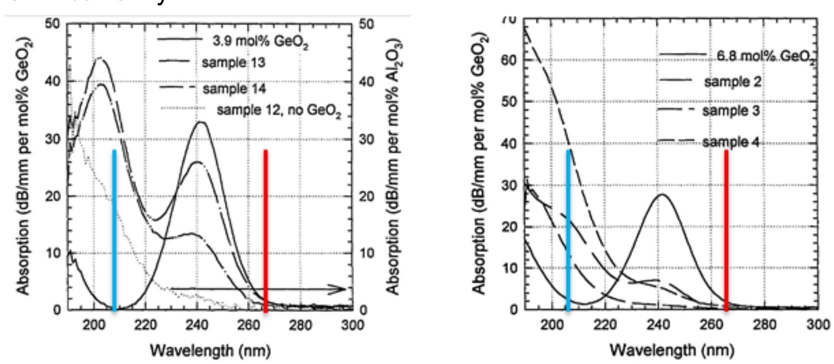

Figure 60 (left) Effect of germanium and aluminum doping in silica on UV absorption, and (right) effect of phosphor doping in silica on UV absorption.

4. Project highlights

Trust 1

1. Established PCF/PBF fabrication processes
2. Set up S^2 mode characterization system
3. Passive 50μm core fiber fully verified in design, fabrication and optical performance.
4. 1st iteration ytterbium active core glass failed, index= $\sim -10\times10^{-4}$.
5. 2nd iteration ytterbium active core glass works for 50μm core fiber, index= $\sim -2\times10^{-4}$
6. 3rd iteration ytterbium active core glass, index = $\sim 2.3\times10^{-4}$
7. Demonstrated active 50μm core fibers
8. Investigating designs for 100μm core
9. Established a quasi-analytic mode for mode instability
10. Successfully demonstrate passive 100μm core

11. Demonstration of multimode 600W from 50μm-core all-solid photonic bandgap fiber
12. Demonstration of 400W single-mode single-frequency from 50μm-core fiber
13. Demonstration of polarizing ytterbium-doped 50μm-core photonic bandgap fiber
14. First to measure stimulated thermal Rayleigh scattering gain
15. Record ~1kW single-mode output from a micro-structured fiber laser
16. Analysis of thermal lensing in optical fibers
17. Fabrication of 25/400 all solid photonic bandgap fiber with potential TMI threshold of ~4kW

Trust II

1. Set up hydrogen loading
2. Set up SBS characterization system
3. Demonstrate a factor of ~13dB SBS suppression by H_2/UV treatment.
4. Identified large change in bulk modulus due to bond breakages
5. Demonstration of desired exponential distribution of Brillouin frequency
6. Investigate SBS suppression in fiber amplifiers

5. Conclusions

In the first thrust, major breakthrough has been made by demonstrating highly efficient and robust single-mode 50μm-core all-solid photonic bandgap fibers in both laser and amplifier configurations with slope efficiency well over 80% for launched pump powers and well over 90% for absorbed pump powers in the more recent results. The effective mode area is 4 times over previous demonstration in all-solid photonic bandgap fibers. The slope efficiency also set new record. The demonstration of 600W output in one of our all-solid photonic bandgap fibers at AFRL is 5 times higher than the previous record. The demonstration of 400W of single-frequency and single-mode output is also a record.

This feat was enabled by the fabrication of ytterbium-doped glass with highly uniform and accurate refractive index control achieved in the second iteration of active core glass fabrication completed in June 2013. The tests result indicates that the refractive index is ~2×10^{-4} below silica. This is sufficient for 50μm-core fibers, but not for 100μm-core fibers. The 4th iteration of active core glass fabrication has been completed in March 2016, aiming at further improving refractive index control.

We have also investigated designs of 100μm-core all-solid photonic bandgap fibers and successfully demonstrated passive record-breaking 100μm-core all-solid photonic bandgap fibers with robust single-mode operation using an innovative multiple resonant design.

We have focused on further HOM suppression in all-solid photonic bandgap fibers to further improve mode instability threshold in this period. Multiple resonant cladding design has been incorporated into 50μm core active all-solid photonic bandgap fibers. We have achieved record near kW single-mode output from this new fiber, a record for micro-structured fibers and LMA fibers at this core diameter. We have also directly measured mode-coupling due to stimulated thermal Rayleigh scattering, providing first direct evidence for its role in mode instability. Recently, a 25/400 all solid photonic bandgap fiber was fabricated with a potential TMI threshold of ~4kW. The fiber is tested at AFRL.

6. References

1. M.E. Fermann, “Single mode excitation of multimode fibers with ultra-short pulses,” Optics Letters, pp.52-54, 1988.
2. J.P. koplow, D.A.V. Kliner and L. Goldberg, “Single-mode operation of a coiled multimode fiber amplifier,” Optics Letters, vol.25, pp.442-444, 2000.
3. M.J. Li, X. Chen, A. Liu, S. Gray, J. Wang, D.T. Donnell and L.A. Zenteno, “Limit of effective area for single-mode operation in step-index large mode area laser fibers, ” Journal of Lightwave Technology, vol.27, pp.3010-3016, 2009.

4. D. Guertin, N. Jacobsen, K. Tankala, and A. Galvanauskas, “33μm core effectively single-mode chirally-coupled-core fiber laser at 1064nm, ” Optical Fiber Communications Conference, paper OWU2, 2008.
5. A. Siegman, “gain-guided, index-anti-guided fiber lasers,” Journal of Optical Society of America B, vol.24, pp.1677-1682, 2007.
6. C.D. Brooks and F. Teodoro, “Multi-MW peak-power, single-transverse-mode operation of a 100μm core diameter, Yb-doped rodlike photonic crystal fiber amplifier,” Applied Physics, vol.89, pp.111119, 2006.
7. J. Limpert, O. Schmidt, J. Rothhardt, F. Röser, T. Schreiber, and A. Tünnermann, “Extended single-mode photonic crystal fiber, ” Optics Express, vol.14, pp.2715-2720, 2006.
8. S. Ramachandra, J.W. Nicholson, S. Ghalmi, M.F. Yan, P. Wisk, E. Monberg, and F.V. Dimarcello, “Light propagation with ultra-large modal areas in optical fibers, ” Optics Letters, vol.31, pp.1797-1799, 2006.
9. L. Dong, X. Peng and J. Li: “Leakage channel optical fibers with large effective area”, Journal of Optical Society of America B, 24, pp.1689-1697, 2007.
10. L. Dong, T.W. Wu, H.A. McKay, L. Fu, J. Li and H.G. Winful, "All-glass large core leakage channel fibers, " IEEE Journal of Selected Topics in Quantum Electronics, vol.14, *invited paper*, 47-53, 2009.
11. L. Dong, H.A. Mckay, A. Marcinkevicius, L. Fu, J. Li, B.K. Thomas, and M.E. Fermann, " Extending Effective Area of Fundamental Mode in Optical Fibers, " IEEE Journal of Lightwave Technology, 27, *invited paper*, 1565-1570, 2009.
12. L. Dong, H.A. Mckay, L. Fu, M. Ohta, A. Marcinkevicius, S. Suzuki, and M.E. Fermann, "Ytterbium-doped all glass leakage channel fibers with highly fluorine-doped silica pump cladding, " Optical Express, vol.17, 8962-8969, 2009.
13. D. Taverner, D.J. Richardson, L. Dong, J.E. Caplen, K. Williams, R.V. Penty: “158 μJ pulses from a single transverse mode, large mode-area EDFA, ” Optics Letters, vol. 22, pp.378-380, 1997.
14. P. Laperle, C. Paré, H. Zheng, A. Croteau and Y. Taillon, “Yb-doped LMA triple-clad fiber laser, ” Proceeding of SPIE, vol.6343, pp.63430, 2006.
15. J.M. Fini, “Design of solid and microstructured fibers for suppression of higher order modes, ” Optics Express, vol.13, pp.3477-3490, 2005.
16. S. Ramachandran, J.W. Nicholson, S. Ghalmi, M.F. Yan, P. Wisk, E. Monberg, and F.V. Dimarcello, “Light propagation with ultra large modal areas in optical fibers, ” Optics Letters, vol.31, pp.1797-1799, 2006.
17. O. Humbach, H. Fabian, U. Grzesik, U. Haken, and W. Heitmann, “Analysis of OH absorption bands in synthetic silica,” J. non-crystal. Sol., 203, 19-26 (1996).
18. R.M. Atkins, V. Mizrahi, and P.J. Lemaire, “Enhanced photo-induced refractive index changes in optical fibers via low temperature hydrogen loading,” Conference on Lasers and Electro-Optics, paper CPD20, (1993).
19. R. Le Parc, C. Levelut, J. Pelous, V. Martinez, and B. Champagnon, “”Influence of fictive temepraure and composition of silica glass on anomalous elastic behavior,” J. Phys.: Condens. Matter, 18, 7507-7527 (2006).
20. J. Kushibiki, T.C. Wei, Y. Ohashi, and A. Tada, “Ultrasonic microspectroscopy characterization of silica glass,” J. App. Phys., 87, 3113-3121 (2000).
21. M.D. Gallagher and U.L. Osterberg, “”Ultraviolet absorption measurements in single-mode optical glass fibers,” Appl. Phys. Lett., 60, 1791-1793 (1992).
22. R.M. Atkins, “Measurement of the ultraviolet absorption spectrum of optical fibers,” Opt. Lett., 17, 469-471 (1992).
23. A. Shirakawa, H. Maruyama, K. Ueda, C. B. Olausson, J. K. Lyngsø, and J. Broeng, "High-power Yb-doped photonic bandgap fiber amplifier at 1150-1200 nm," Opt. Express 17, 447 (2009).
24. M. J. F. Digonnet, H. K. Kim, G. S. Kino, and S. Fan, "Understanding Air-Core Photonic-Bandgap Fibers: Analogy to Conventional Fibers," J. Light. Technol. 23, 4169– (2005).